The Thesis Committee for Mohit Soni
Certifies that this is the approved version of the following thesis:

# Dynamic Response Analysis of an Offshore Wind Turbine Supported by a Moored Semi-Submersible Platform

**APPROVED BY**
**SUPERVISING COMMITTEE:**

Lance Manuel, Supervisor

Loukas F. Kallivokas

# Dynamic Response Analysis of an Offshore Wind Turbine Supported by a Moored Semi-Submersible Platform

**by**

**Mohit Soni, B.Tech.**

**THESIS**

Presented to the Faculty of the Graduate School of

The University of Texas at Austin

in Partial Fulfillment

of the Requirements

for the Degree of

**Master of Science in Engineering**

THE UNIVERSITY OF TEXAS AT AUSTIN

August 2014

Dedicated to my parents, sister and brother-in-law

# Acknowledgments

First and foremost, I sincerely thank my advisor, Dr. Lance Manuel, for giving me an opportunity to work on such an interesting project, and for his encouragement, guidance and contribution of time for this research. His insights and suggestions throughout the project are gratefully acknowledged.

I would like to thank Dr. Loukas F. Kallivokas for serving on my committee. My colleague, Ms. Watsamon Sahasakkul, has been immensely helpful and patient while we worked on the project. I thank Dr. Jason Jonkman for National Renewable Energy Laboratory for the simulation tools that were used in this study. I also thank Mr. Eungsoo Kim, Mr. Dilnei Schmidt and Mr. Jinsong Liu for their help regarding solving several problems.

I am grateful to Dr. Matthew Barone, Dr. Todd (Daniel) Griffith and Ms. Kelley Ruehl of Sandia National laboratories for providing necessary models and tools, and for discussions throughout the project. The financial support from Sandia National Laboratories by way of Contract No. 1307455 is acknowledged.

No words are enough to thank my parents, my sister and brother-in-law; without their motivation and support, I could not finish this work.

# Abstract

## Dynamic Response Analysis of an Offshore Wind Turbine Supported by a Moored Semi-Submersible Platform

Mohit Soni, M.S.E.
The University of Texas at Austin, 2014

Supervisor: Lance Manuel

Wind energy, the fastest growing source of renewable energy, is a promising resource for power generation. Offshore wind energy, in particular, offers favorable conditions for power generation—high winds with low turbulence, minimal visual impacts and high generation capacities. Offshore wind turbines mounted on floating platforms are the most economical and viable solution for deep water sites. A semi-submersible platform is an appropriate floating platform for a deep water site, providing stability through high water-plane area.

In the wind energy industry, there has been continuing interest in developing larger turbines. At Sandia National Laboratories (SNL), efforts have led to the development of a 13.2 MW wind turbine model with blades

100 meters in length, significantly larger than commercially available blades at present. Such a large wind turbine needs to be carefully analyzed and studied before it can be considered suitable for commercial purposes.

The dynamic analysis of the SNL 13.2 MW wind turbine mounted on a moored semi-submersible platform is the subject of this study. This integrated 13.2 MW wind turbine system has been developed and its various physical properties have been studied in this and another associated study. The semi-submersible platform is developed using various modeling tools. For the wind turbine-platform system model developed, dynamic analyses are performed using simulation tools to understand the coupled behavior of the wind turbine and the platform. A reference site is chosen to define the environmental conditions, based on which the short-term extreme response of the offshore wind turbine is estimated. The system is loaded with selected combinations of winds and waves to assess controlling combinations of wind speeds and wave heights that influence the response. The influence of changes in model parameters on overall response is also studied.

# Table of Contents

# List of Tables

# List of Figures

# Chapter 1

# Introduction

## 1.1 Background

Over the past few decades, wind energy has been the fastest growing renewable energy worldwide [1]. According to the latest data, global wind power capacity reached a total of 158 GW recently [2]. In 2013, installed wind power capacity in the European Union (EU) reached a total of 117.3 GW (gigawatts): 110.7 GW onshore and 6.6 GW offshore, enough to cover 8% of the EU's electricity consumption [3]. The European Wind Energy Association (EWEA) estimates that 230 GW of wind capacity will be installed in Europe by 2020, of which about 25% will be offshore; that number is expected to increase to 400 GW by 2030, with about 40% from offshore [4]. In the United States of America, installed wind power capacity now exceeds 61 GW [5]. The National Renewable Energy Laboratory (NREL) reported that the U.S. has 4,150 GW of potential offshore wind power capacity [6]. In U.S. Department of Energy (DOE) planning, wind energy is projected to provide 20% of the nation's energy needs by 2030; this represents a total of 305 GW, of which offshore wind is expected to contribute 54 GW [7]. Evidently, offshore wind energy is rapidly becoming a significant part of the overall power production industry in the U.S. as well as elsewhere.

Offshore wind energy has many advantages over conventional onshore wind energy. Offshore sites have stronger and more sustained winds, with reduced turbulence, which leads to increased power production, reduced noise and visual impacts on population centers, and utilization of larger turbines to bring down power production costs. The estimation of structural loads, however, is a major challenge for offshore wind turbines; this estimation becomes more difficult due to the consideration of wave forces along with high winds. There is also the added requirement of designing platforms to support the wind turbines.

Offshore wind turbines installed around the world have been almost exclusively bottom-supported foundations, that extend to the sea bed. Such offshore wind turbines have been confined to shallow water areas and are typically found close to coastlines. Offshore sites farther out to the sea provide added advantages of higher winds and lower turbulence levels. Such sites are suitable for wind turbines mounted on floating platforms, which are more economical solutions in deep water. Different configurations of floating platforms are being considered and developed in the wind energy industry, differing in the way they provide stability to the overall wind turbine-platform system as they sustain wind and wave loads. One type of platform that is being considered for deeper waters is a semi-submersible. In research studies, a model of a floating semi-submersible platform, designed to support a 5 MW wind turbine has been developed [8]. Researchers at Sandia National Laboratories have developed a model for a 13.2 MW wind turbine

with 100-m blades [9–11]. The present study seeks to study how a semi-submersible platform model that is being developed for this large-scale turbine [12] performs under various wind and wave inputs. The goal of this study is to evaluate the overall response of the 13.2 MW offshore wind turbine integrated system with a semi-submersible floating platform and moored by catenary lines in 200 meters of water.

## 1.2 Research Objectives and Methodology

This research study is focused on three main objectives: (1) to develop the SNL 13.2 MW offshore wind turbine and semi-submersible platform model; (2) to investigate the extreme response (loads and motions) for different environmental conditions of the 13.2 MW offshore wind turbine system and explain the physical behavior; and (3) to assess the dynamic performance of the 13.2 MW offshore wind turbine system against other established offshore wind turbine models and as a function of changes in various model parameters. A summary of the tasks undertaken in this study are presented below.

### 1.2.1 Development of Wind Turbine Model and Semi-Submersible Platform Model

We utilize the 100-meter long SNL100 blades along with a tower model with a hub height of 146 meters to develop the 13.2 MW wind turbine model, which is mounted on the semi-submersible floating platform. These

100-m blades are significantly longer than the longest commercially available blades today [11]. A semi-submersible model, based on the OC4 semi-submersible platform [8], is developed to support this large-scale wind turbine. The platform is modeled by scaling up the OC4 semi-submersible model [12]. A mooring system is also developed for the overall wind turbine system.

Various physical properties of the wind turbine and semi-submersible platform, such as the blade and tower structural properties are presented in this study along with a discussion of the steady-state response and the system natural frequencies.

### 1.2.2 Extreme Response

For a selected offshore site, we discuss in-depth analyses undertaken of the offshore wind turbine system to assess the short-term extreme response (loads and motions) and understand the behavior of the wind turbine system for different combinations of winds and waves.

### 1.2.3 Influence of Changes in Model Parameters

We assess the dynamic response of the turbine system against other established wind turbine models. The 13.2 MW wind turbine system is compared to that of a land-based equivalent system. We also study the effect of scaling relative to the OC4 semi-submersible system with a 5 MW turbine and the effect of turbine control on overall performance. We also evaluate the

response of the system for somewhat larger waves than at the reference site.

## 1.3 Limitations

This study is focused on gaining a preliminary understanding of the behavior of a large-scale offshore wind turbine supported by a moored semi-submersible platform. We address the development of the wind turbine and the platform; further refinements to the model are still possible. To understand the overall system behavior, the offshore wind turbine has been analyzed for a few sea states at a selected reference site and some interpretations of the results are presented. This study is one of the first aimed at establishing and understanding the behavior of an offshore wind turbine system with this particular large SNL 13.2 MW rotor. The environmental conditions selected are simplified—stochastic winds are simulated in a similar manner to what is used in onshore design guidelines; waves are assumed to be aligned with the wind. Our interpretations of the results and our related discussions should be seen in light of the above limitations, keeping in mind that there might be additional model refinements that need to be made before the overall wind turbine system is deemed satisfactory for use.

## 1.4 Organization of Thesis

Chapter 2 describes floating wind turbine concepts in general and model development for the 13.2 MW wind turbine, the semi-submersible platform, and the mooring lines. Various simulation models and tools used in this study

are also briefly discussed.

In Chapter 3, we discuss the selected reference site and results of the dynamic analysis of the selected system that are summarized using time series, response statistics, and power spectra of turbine loads and platform motions.

Chapter 4 addresses the influence of changes in model parameters that help understand the behavior of the floating offshore wind turbine in comparison with other established models. We compare the performance against land-based units, an OC4 system, equivalent systems without control, and the influence of larger waves than are seen at the reference site.

Finally, in Chapter 5, we summarize conclusions from this research study.

# Chapter 2

# Model Development for the Wind Turbine and Floating Platform

## 2.1 Introduction

Over the last few decades, there has been a considerable amount of research and development in the field of offshore floating platforms, mainly in the offshore oil and gas industry. It has been demonstrated that offshore floating platforms are suitable options for deepwater sites. Currently, there is a growing interest in establishing offshore wind farms at deepwater sites. Due to the unique nature of the dynamics involved, wind turbines mounted on offshore floating platforms pose challenging problems. The platform must be able to support not only the weight of the turbine, but it must also be able to withstand associated deflections and loads, within acceptable limits, for the design to be sustainable in long term.

In an offshore wind turbine on a floating platform system, stability is often achieved largely through provision of high waterplane area; this is the case with barges and semi-submersible platforms. Ballasting provides vertical separation of the center of gravity of the system below its center of buoyancy, while a mooring system is required for station-keeping purposes. In the

following sections, we present the models, properties, and tools used for the wind turbine, platform, and simulations in this study.

## 2.2 Floating Wind Turbine Concepts

For sites with water depths greater than 50 meters, a floating wind turbine can be the most economical solution for wind energy generation. Bottom-supported offshore wind turbines are mostly used in shallow water. A few floating platform concepts have been studied to date for wind turbines in deep waters. The concepts are based on those developed in the oil and gas industry. Classification of a floating wind turbine is usually done based on the means by which it achieves stability. Different arrangements of moorings, tanks, and ballast provide different means of achieving this stability. The National Renewable Energy Laboratory (NREL) has classified offshore floating wind turbines into three broad groups as indicated in Figure 2.1 [13]. The classification is as follows:

1. **Ballast Stabilized**: These platforms achieve stability by ballast weights below a central buoyancy tank and have a deep draft to offset heave motions. The central buoyancy tank creates a high inertial resistance to pitch and roll. The mooring lines have drag embedded anchors. Spar buoys are examples of ballast-stabilized floating platforms.

2. **Mooring-lines Stabilized**: These platforms achieve stability through high mooring line tension. they rely on the mooring lines for resistance

to platform motions. Tension leg platforms (TLPs) are examples of mooring-lines stabilized floating platforms.

3. **Buoyancy Stabilized**: These platforms achieve stability through high waterplane area and through the use of distributed buoyancy. The mooring lines in this kind of platform are for station-keeping purposes only. Examples include barges and semi-submersible platforms.

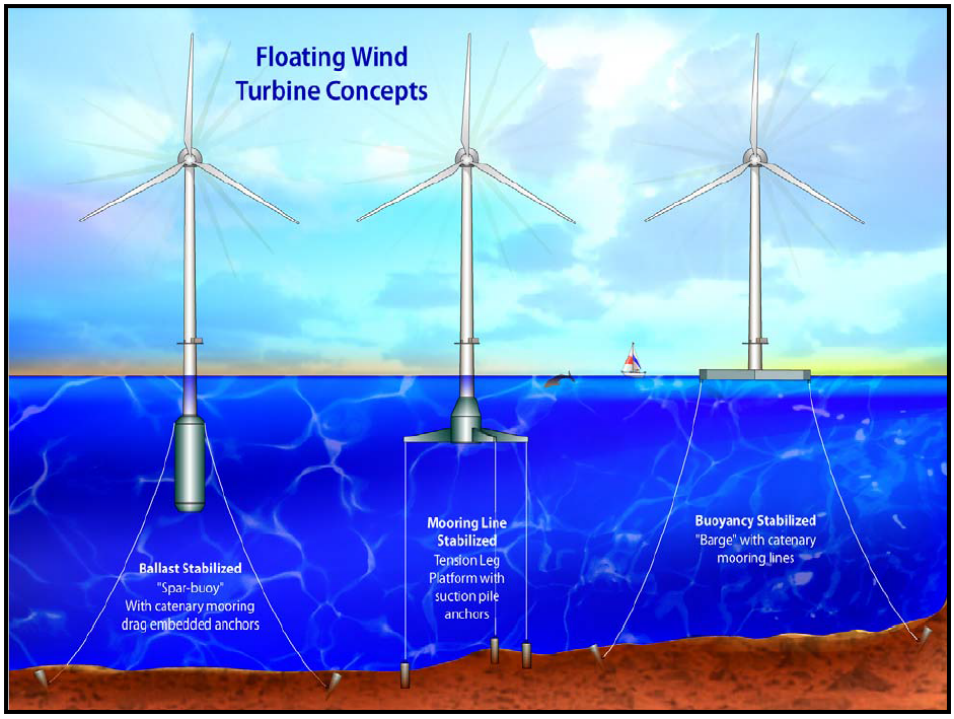


Figure 2.1: Floating wind turbine concepts [13].

A floating offshore platform supporting a wind turbine could be constructed based on practice in the oil and gas industry; however, the

design philosophy for wind turbines is somewhat different. In the oil and gas industry, heavy lifting of materials from the sea floor is often required; hence, oil rigs experience large vertical loading, along with some loads due to winds, waves, and currents. An offshore floating wind turbine, on the other hand, must be designed to withstand winds that can cause large lateral loads. Such platforms should be able to sustain extreme wind loads as well as wave loads, while keeping the displacements within a safe limit.

## 2.3 Wind Turbine Model

The 13.2 MW wind turbine model developed by researchers at Sandia National Laboratories has an extremely large-scale rotor by today's standards. It is significantly larger than commercially available wind turbines [11]. This model continues to undergo refinement; the various properties and overall response of the system need to be studied and understood. As a first step toward model development for offshore use, various physical properties of the wind turbine need to be studied as if sited on land. By analyzing land-based use of this turbine, it may be possible to understand the overall behavior of such a large rotor without additional complications from the wave loading and a floating platform and mooring system.

The SNL13.2-00 land turbine model is developed for analysis of the 13.2 MW wind turbine on land [9, 10]. It does not include any integrated platform in the overall system. The wind turbine has a rotor radius of 102.5 meters. The hub height is chosen to be 146 meters above the ground. This

implies a 43.5-meter clearance between the blade tip at its lowest point and the ground, when the wind turbine is undeflected. The rated wind speed for this machine is 11.3 m/s and the rated rotor speed of 7.44 rpm; these rated quantities are associated with a power output of 13.2 MW. Additional properties of the 13.2 MW turbine are presented in Table 2.1.

Table 2.1: Properties of the 13.2 MW Land-based Turbine.

| | |
|---|---|
| Rated Generator Power | 13.2 MW |
| Rotor Orientation, Configuration | Upwind, 3 Blades |
| Rotor, Hub Diameter | 205 m, 5 m |
| Hub Height | 146 m |
| Cut-In, Rated, Cut-Out Wind Speeds | 3 m/s, 11.3 m/s, 25 m/s |
| Rated Tip Speed | 80 m/s |
| Cut-in, Rated Rotor Speeds | 4.34 rpm, 7.44 rpm |
| Rated Rotor Power | 13.983 MW |
| Generator Efficiency | 94.4% |
| Overhang, Shaft Tilt, Precone | 8.16 m, 5 deg., 2.5 deg. |
| Nacelle Mass | 1,030,000 kg |
| Tower Mass | 1,532,937 kg |
| Tower CM Location | 63.7 m |
| Tower Damping Ratio | 1% |

### 2.3.1 Blade and Tower Structural Properties

The 13.2 MW wind turbine model was developed by up-scaling the baseline NREL 5 MW wind turbine. Various turbine parameters and tower properties were scaled up, while the controller was adapted based on performance considerations. The SNL 100-meter baseline design blades were used with this model [11]. Blade properties were obtained from the input

files in the SNL100-00 land-based wind turbine model [10].

Three views of the selected blade are presented in Figure 2.2. Figure 2.3 shows the variation of mass density and stiffness in two directions along the blade's length. It can be seen that the blade has a very high mass and stiffness at its root which decreases towards the tip. The first 2.5-meter portion of the length represents the rotor hub at the nacelle, which has a relatively high mass density. The root of the blade starts at 2.5 meters, with a mass density of about 3,000 kg/m. As we move outward along the length of the blade, the mass density decreases due to the aerodynamic shape of the blade [11]. The flapwise stiffness (Figure 2.2) decreases monotonically from the root to the tip; the edgewise stiffness, on the other hand, shows a slight increase out to about $1/5^{\text{th}}$ of the length from the root, due to a transition in the blade geometry.

Along with the geometry and airfoil design of the blades, mode shapes of the blades are needed as input to FAST to carry out dynamic analyses. The first five mode shapes for flapwise and edgewise bending are presented in Figure 2.4.

The mass density and stiffness of the tower for the 13.2 MW wind turbine were scaled up by factors of 2.65 and 7.01, respectively, from the NREL 5 MW tower model. The tower mass density and stiffness are plotted as a function of the normalized tower height in Figure 2.5. The tower is symmetric about the fore-aft and side-to-side directions; hence, the fore-aft and side-to-side stiffnesses are identical. An eigenvalue analysis assuming a cantilevered tower can be carried out to determine the mode shapes. The first

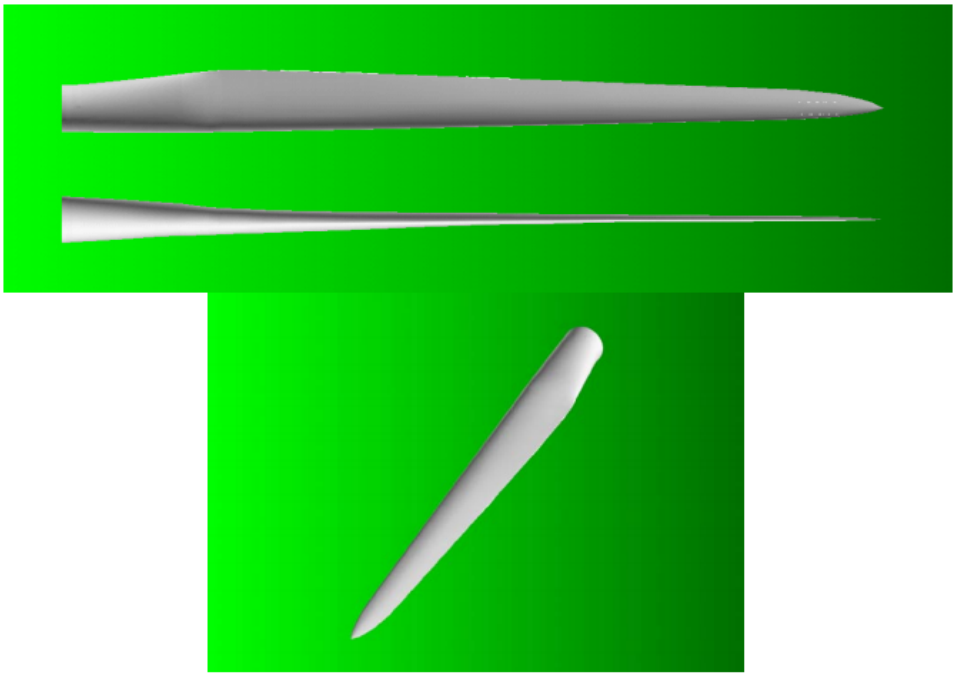

Figure 2.2: Three views of blade surface geometry: flapwise, edgewise and isometric [11].

two tower mode shapes are presented in Figure 2.6, assuming a fixed base.

### 2.3.2 Steady-State Response to Uniform Non-Turbulent Wind

The steady-state response of the land-based 13.2 MW wind turbine is studied by running aeroelastic simulations in FAST under uniform non-turbulent winds. The simulations were run for a long enough duration so that any transients present died out. Figure 2.7 shows the steady state response of the wind turbine as a function of the hub-height wind speed. GenPwr and RotPwr represent the generator (output) power and rotor (input) power, respectively; Blade Pitch represents the pitch angle of Blade 1

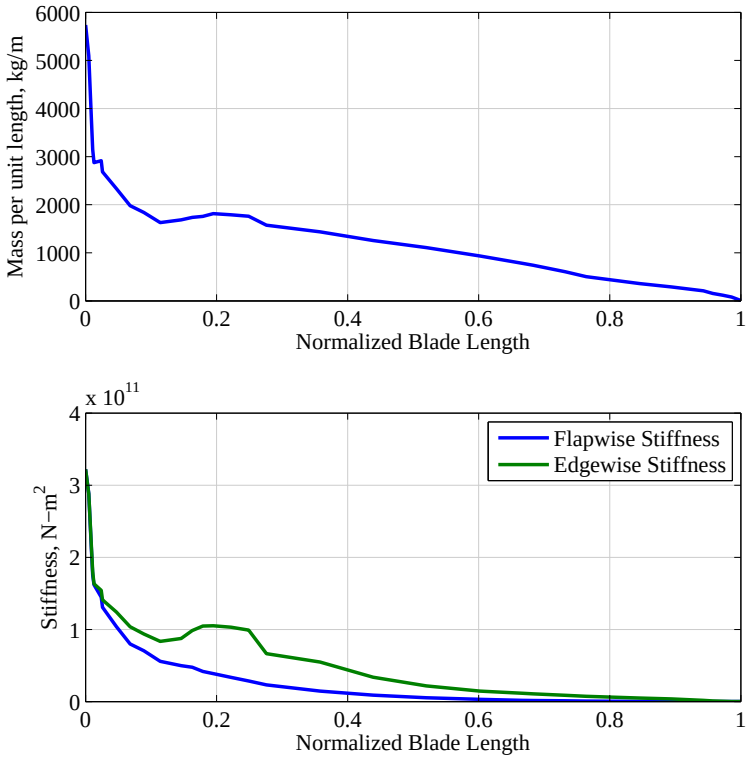


Figure 2.3: Variation of mass density and stiffness along the length of the blade.

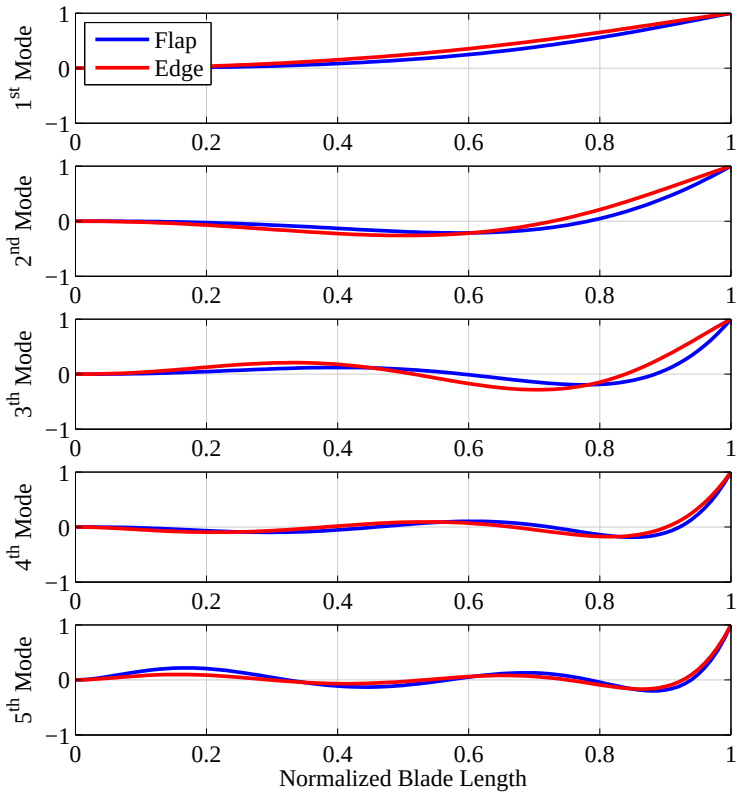


Figure 2.4: Flapwise and edgewise blade mode shapes.

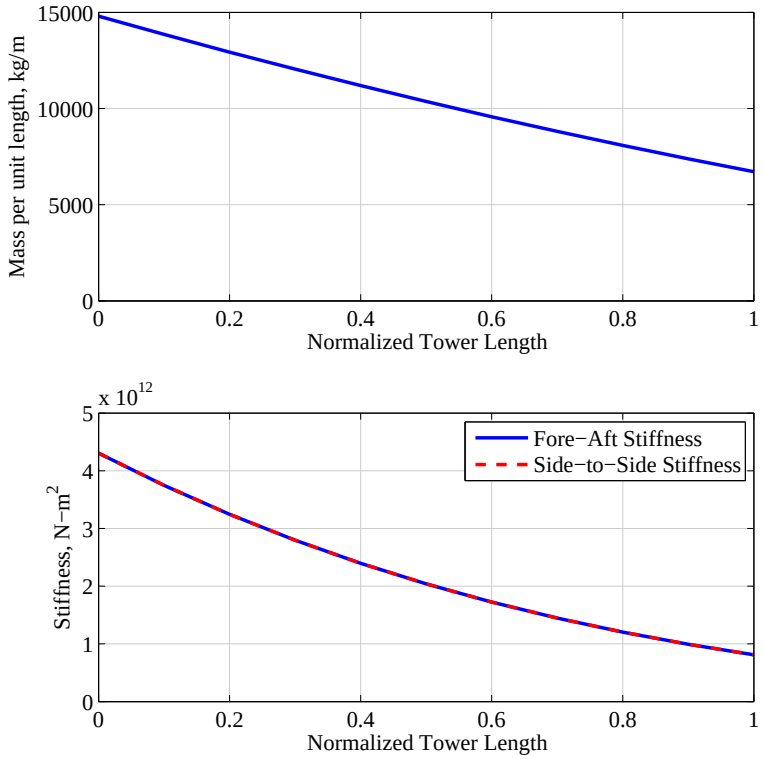


Figure 2.5: Variation of mass density and stiffness along the height of the tower.

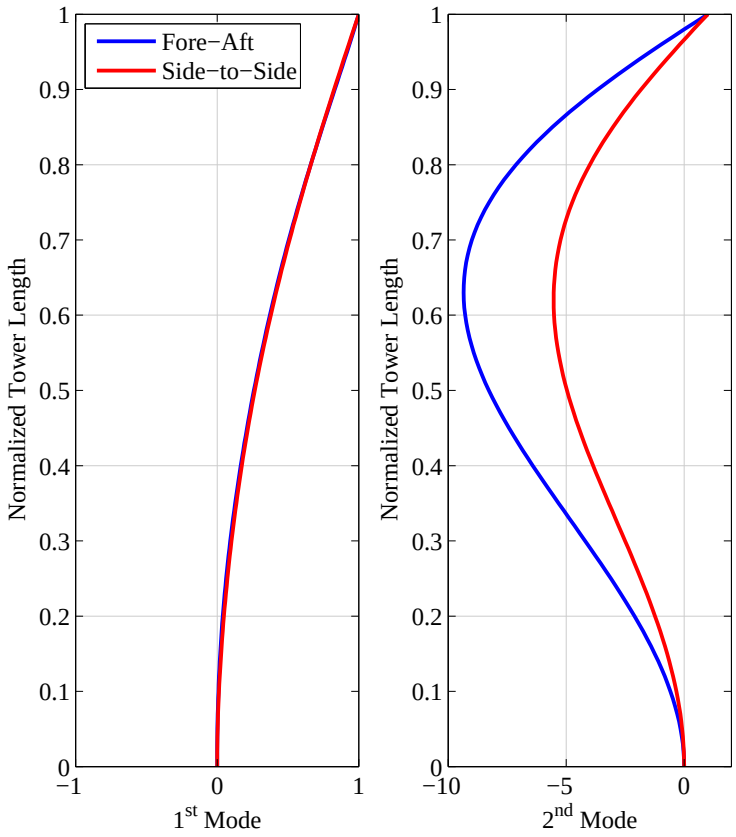


Figure 2.6: Fore-aft and side-to-side tower mode shapes.

(selected arbitrarily).

It can be seen from Figure 2.7(a) that both the rotor and generator power increase with wind speed up to the rated wind speed, after which the generator power remains constant at 13.2 MW, the rated power of the turbine, while the rotor power is constant at 13.98 MW. The difference between the rotor power and generator power is due to losses in efficiency; for this turbine, the efficiency loss is about 5.6%.

Figure 2.7(b) shows that the blade pitch angle remains zero below the rated wind speed. After the rated wind speed is exceeded, the blade pitch angle increases monotonically with increasing wind speed; this is done to alleviate structural loads on the wind turbine while providing the rated power. This is achieved by the use of a blade pitch control algorithm that is enforced when the wind speed exceeds the rated wind speed of the turbine.

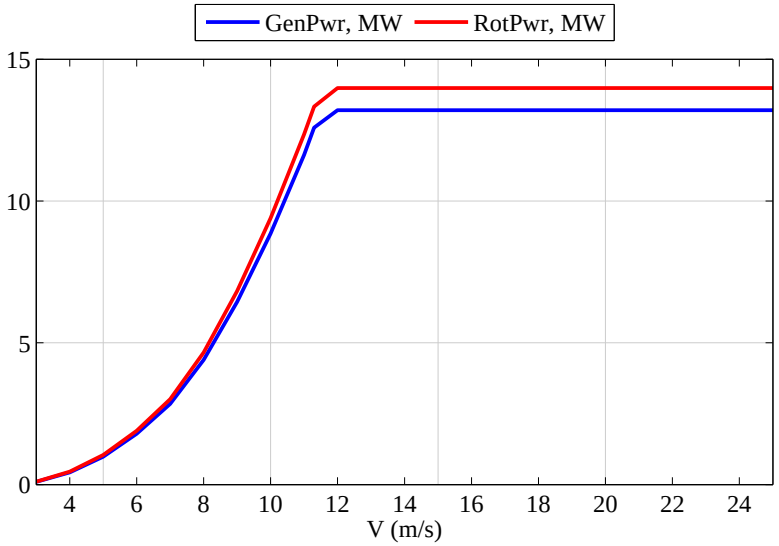


(a) Generator and Rotor Power.

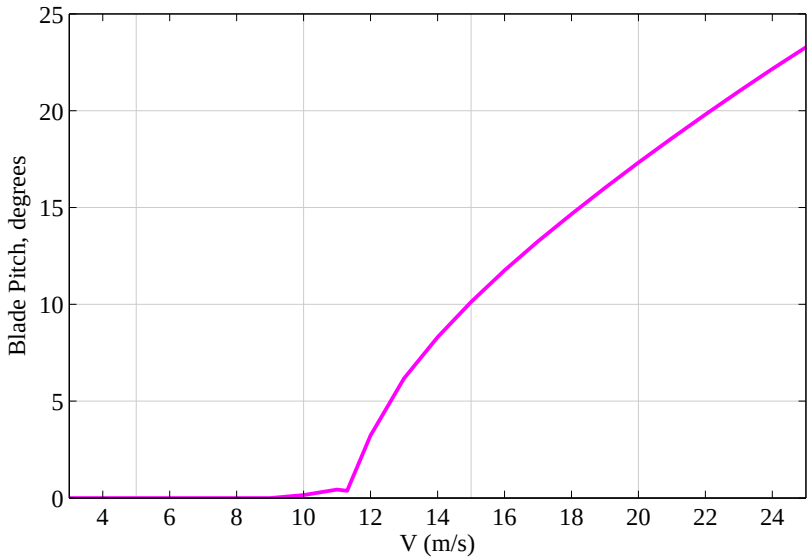


(b) Blade Pitch.

Figure 2.7: Steady-state response of the 13.2 MW wind turbine as a function of hub-height wind speed.

### 2.3.3 Natural Frequencies of the System

The response of the land-based 13.2 MW wind turbine subjected to wind loads is of interest. Incident wind fields with different mean components and turbulence levels need to be simulated in order to assess the behavior of the turbine under operating conditions. Before stochastic simulations of the turbine response are performed using FAST [14] and TurbSim [15], it is instructive to discuss system natural frequencies of the land-based turbine system.

In FAST, the natural frequencies of the turbine system may be obtained by performing an eigenvalue analysis resulting from a linearization analysis [16]. As described in the FAST user's guide [14], the eigenvalue analysis may be carried out using a MATLAB script provided by NREL [17]. A Campbell Diagram is used here to identify natural frequencies with specific modes of vibration. An Excel workbook (see Jonkman [18]) makes this calculation possible. Table 2.2 lists important natural frequencies of the 13.2 MW wind turbine. It may be observed from Table2.2 that both the first tower modes, in the fore-aft and the side-to-side directions, have the same frequencies. This is due to symmetry. The blades, however, show some difference in the flapwise and edgewise bending natural frequencies. The 1P (1-per-rev) rotor rate at the rated wind speed is presented for reference.

Table 2.2: Various natural frequencies of the land-based 13.2 MW wind turbine.

| Description of Modes | Frequency, Hz |
|---|---|
| 1st Tower Fore-Aft | 0.19 |
| 1st Tower Side-to-Side | 0.19 |
| 1st Blade Flapwise | 0.49 |
| 1st Blade Edgewise | 0.51 |
| 2nd Blade Flapwise | 1.25 |
| 2nd Tower Fore-Aft | 1.80 |
| 2nd Tower Side-to-Side | 1.80 |
| 1P (Rated Rotor Rate) | 0.124 |

System natural frequencies can also be identified from a power spectrum analysis of the stochastic response of the turbine as obtained from FAST. Figure 2.8 shows such identified natural frequencies corresponding to different modes of vibration, for three different hub-height wind speeds. The power spectra are presented for the blade root out-of-plane bending moment (RootMyc1) and the tower-base fore-aft bending moment (TwrBsMyt) processes. The various frequencies indicated at peaks of the spectra are in good agreement with those obtained from the linearization analysis. Important peaks in the power spectra of the loads are seen at 1P (corresponding to the rotor rotation rate which is about 0.12 Hz at and above the rated wind speed) and multiples (2P, 3P), as well as at resonance frequencies associated with flapwise and edgewise modes of blade bending as well as with tower bending modes [19]. The first blade flapwise bending mode frequency (same for edgewise mode) at about 0.50 Hz is evident in the

spectra. The second blade bending mode frequency peak is also seen at about 1.25 Hz. Peaks in the TwrBsMyt power spectra are seen at 0.19 Hz for the first mode and around 1.80 Hz for the second mode.

### 2.3.4 Blade Design Improvements

All of the previous discussion on the properties and analysis of the 13.2 MW wind turbine was for the first blade model (designated SNL100-00) that was developed by researchers at Sandia National Laboratories [11]. Updated 100-meter blade reference models have been developed; these are referred to as SNL100-01 and SNL100-02 [20, 21]. These updated designs are modifications to the baseline SNL100-00 blade design with the same external geometry, but with different component materials. The SNL100-00 blade is an all-glass blade, the SNL100-01 blade has a carbon spar cap, while the SNL100-02 blade was developed with an advanced core material. The SNL100-01 blade has a weight reduction of 35% from the SNL100-00 blade, while the SNL100-02 blade has a weight reduction of 48% relative to SNL100-00. Table 2.3 summarizes the main differences between the three blade models. The aim of the blade design improvement study was to reduce the weight of the blades and to, thus, reduce the total weight of the turbine.

Given the significant weight reduction resulting from the blade design improvement study, it is important to reanalyze the 13.2 MW wind turbine with all three blade models to compare the behavior of the three blades and their effect on the overall response of the system. Table 2.4 summarizes the

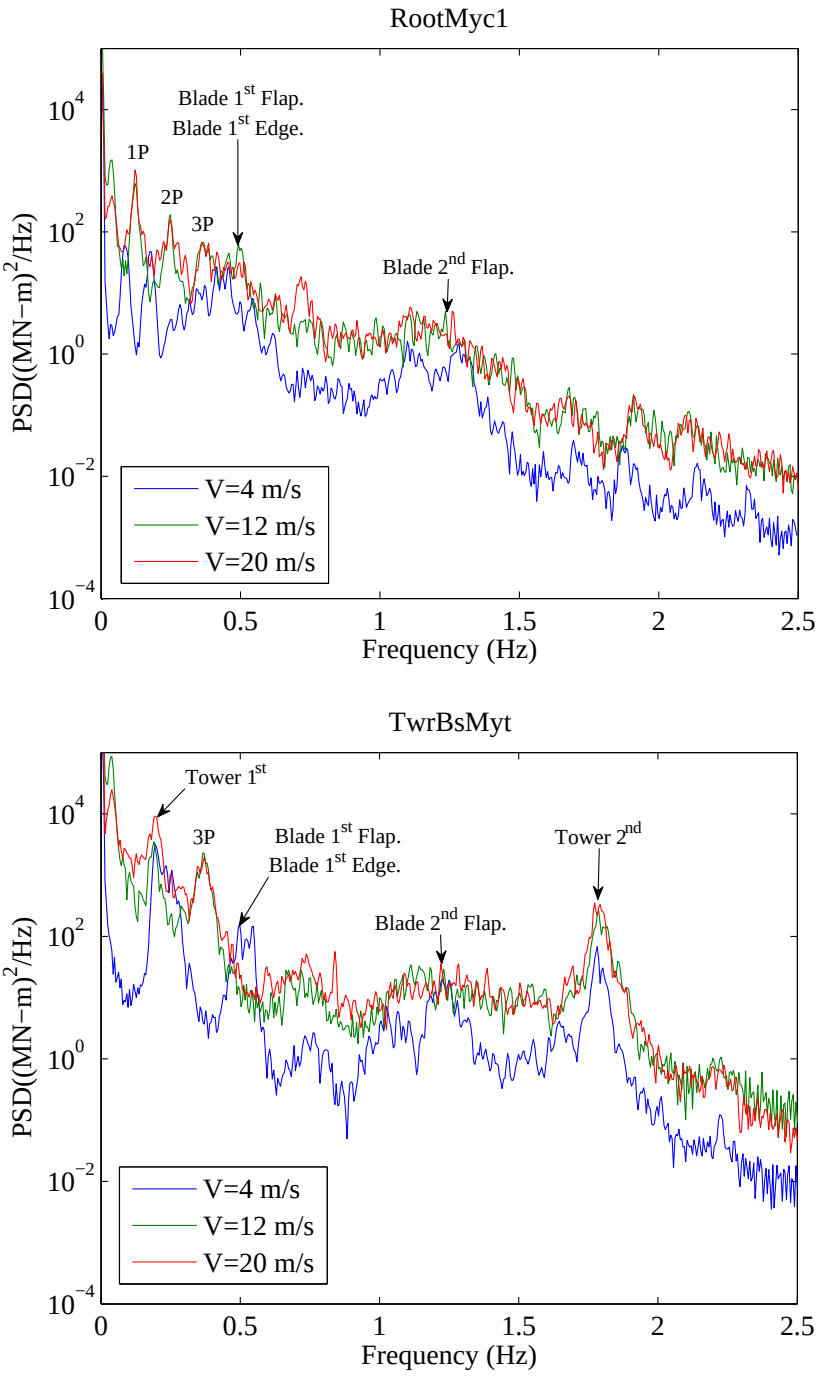


Figure 2.8: Blade root out-of-plane and tower base fore-aft bending moment power spectral density functions for three different hub-height wind speeds.

Table 2.3: Properties of the three 100-meter blade models.

| Parameter | Value | | |
|---|---|---|---|
| Blade Designation | SNL100-00 | SNL100-01 | SNL100-02 |
| Blade Weight (kg) | 114,172 | 73,995 | 59,047 |
| Span-wise CG Location (m) | 33.6 | 33.1 | 31.95 |
| Lowest fixed-base natural frequency (Hz) | 0.42 | 0.49 | 0.55 |
| Blade Damping Ratio | 0.477% | 1.5% | 1.5% |

natural frequencies obtained for various bending modes of vibration for the three different blade models. It can be observed that, in general, as the weight of the blade decreases (from SNL100-00 to SNL100-02), the natural frequencies increase as expected. The first and second blade flapwise natural frequencies show significant increases, while the first edgewise natural frequency shows a relatively small increase. For the three different blade models, Figure 2.9 shows power spectral density plots for blade root out-of-plane and in-plane bending moments. Especially for the second flapwise bending moment, it is clear that the resonant peaks increase noticeably when going from the heaviest SNL100-00 blade to the lightest SNL100-02 blade.

Due to the significant decrease in blade weight in the case of the SNL100-02 blade and the resulting overall reduction in the weight of the turbine, which is extremely important for such a large system, all subsequent analyses are based on use of the 13.2 MW turbine with the SNL100-02 blades.

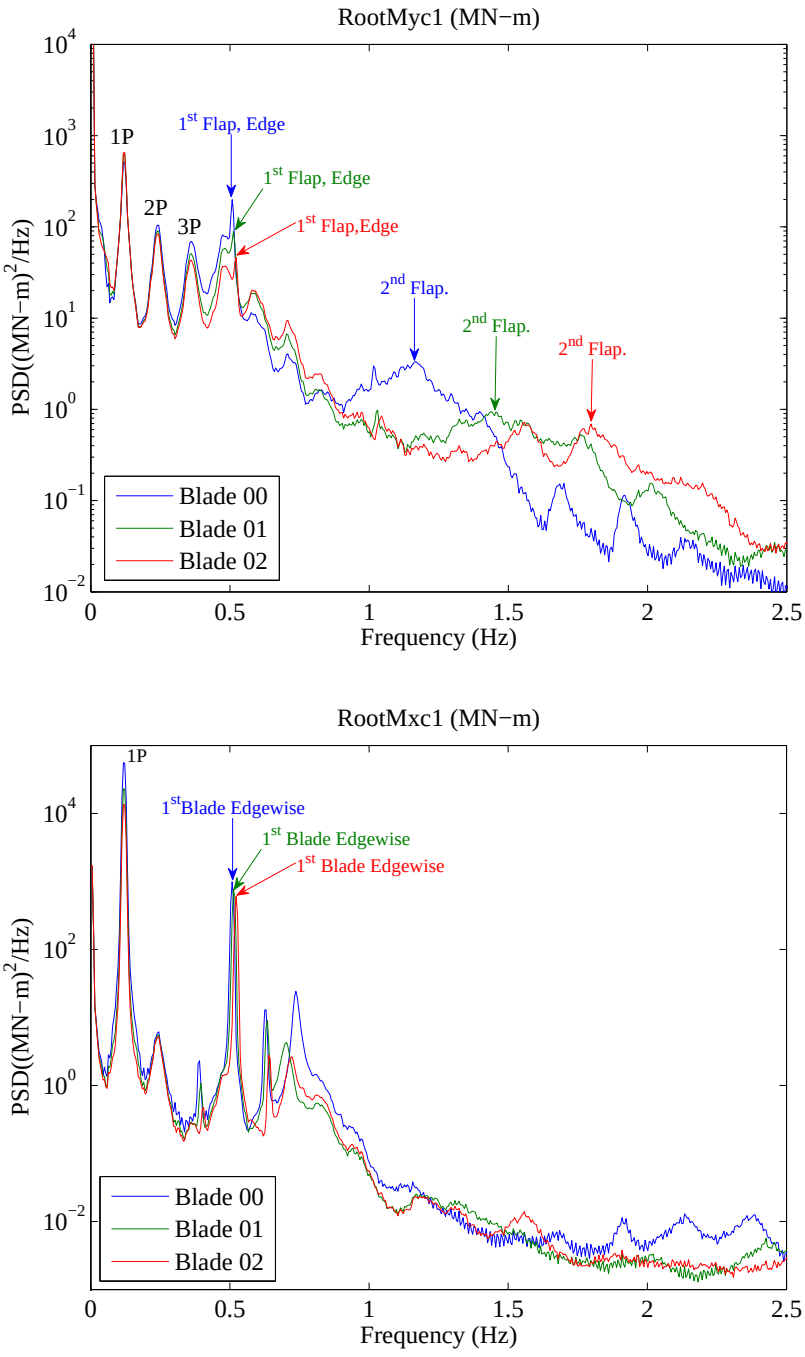


Figure 2.9: Blade root out-of-plane and in-plane bending moment power spectral density functions for the three blade models.

Table 2.4: Natural frequencies in bending modes of vibration for the three blade models.

| Mode | Description | Frequency (Hz) | | |
|---|---|---|---|---|
| | | SNL100-00 | SNL100-01 | SNL100-02 |
| 1 | 1st Blade Flapwise | 0.49 | 0.55 | 0.61 |
| 2 | 1st Blade Edgewise | 0.51 | 0.51 | 0.52 |
| 3 | 2nd Blade Flapwise | 1.25 | 1.55 | 1.74 |

## 2.4 Floating Platform Development

Researchers at the National Renewable Energy Laboratory (NREL) have developed a model for a semi-submersible floating platform to support a 5 MW wind turbine [8]; this was undertaken as part of the Offshore Code Comparison Collaboration Continuation (OC4) study, which was in turn a continuation of the Offshore Code Comparison Collaboration (OC3) study that examined three different bottom-supported wind turbine systems and one floating wind turbine [22]. In the OC4 study, a semi-submersible platform design developed for the DeepCwind project [23] was used. For the SNL 13.2 MW wind turbine which is the subject of the present study, a scaled-up version of the OC4 semi-submersible platform is being used [12]. A scale factor of 1.8 is used, based on consideration of the maximum tower base bending moment that would result. This scaled-up semi-submersible platform is designed to support the 13.2 MW wind turbine and withstand wind and waves associated with a water depth of about 200 meters, while keeping turbine loads and platform motions within safe limits. A mooring

system is also used for station-keeping purposes.

### 2.4.1 Platform Properties

The semi-submersible platform consists of three offset columns connected to a main column by a set of pontoons and cross braces; six pontoons connect the offset columns to each other, while six additional pontoons connect each offset column with the main column, and three cross braces connect the bottom of the main column with the top of the offset columns. The SNL 13.2 MW wind turbine is mounted atop the main column of the semi-submersible platform. The tower is cantilevered at an elevation of 18 meters above the still water level (SWL). The draft of the platform is 36 meters. Figure 2.10 shows the model of the semi-submersible platform selected for this study [8]. There are larger diameter cylinders at the base of each offset column; these are called base columns and their main purpose is to limit heave motions of the platform. The base column and the offset columns are each ballasted with water to maintain equilibrium. Table 2.5 lists platform properties and dimensions of the semi-submersible platform.

The platform mass, including ballast, is $7.86\times10^7$ kg. The center of mass of the platform is located 24.23 m below the SWL and along the platform centerline. The roll and pitch inertias of the floating platform about its CM are each equal to $1.28\times10^{11}$ kg-m$^2$ while the yaw inertia is $2.25\times10^{11}$ kg-m$^2$. Table 2.6 lists the floating platform structural properties.

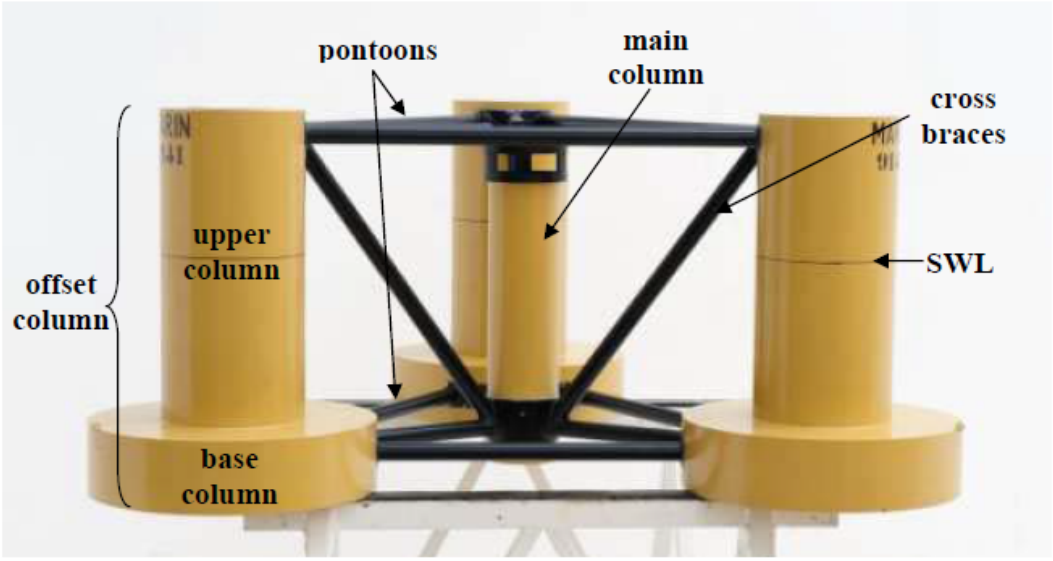


Figure 2.10: The semi-submersible floating platform model [8].

Table 2.6: Platform Structural Properties.

| | |
|---|---|
| Platform mass including ballast (without turbine) | $7.86\times10^7$ kg |
| CM location below SWL | 24.23 m |
| Platform roll inertia about CM | $1.28\times10^{11}$ kg-m$^2$ |
| Platform pitch inertia about CM | $1.28\times10^{11}$ kg-m$^2$ |
| Platform yaw inertia about CM | $2.25\times10^{11}$ kg-m$^2$ |

### 2.4.2 Platform Coordinate System

The semi-submersible floating platform is assumed to behave as a rigid body with six degrees of freedom. The first three degrees of freedom correspond to translational motions of the platform in surge, sway and heave, which describe motions along the $x$, $y$, and $z$ axes, respectively. The next

Table 2.5: Properties and Dimensions of the Semi-Submersible Platform.

| | |
|---|---|
| Distance to platform base from SWL | 36.00 m |
| Distance to top of main column from SWL | 18.00 m |
| Distance to top of offset columns from SWL | 21.60 m |
| Spacing between offset columns | 90.00 m |
| Height of upper columns | 46.80 m |
| Height of base columns | 10.80 m |
| Diameter of main column | 11.70 m |
| Diameter of upper columns | 21.60 m |
| Diameter of base columns | 43.20 m |
| Diameter of pontoons and cross braces | 2.88 m |

three degrees of freedom correspond to rotational motions in roll, pitch, and yaw, which describe rotations about the $x$, $y$, and $z$ axes, respectively. A coordinate system is defined such that $x$=0 and $y$=0 at the center of the floating platform in plan; also, $z$=0 is defined so as to coincide with the still water level (SWL). Figure 2.11 [24] shows the platform coordinate system and the six degrees of freedom that define the platform's motions. An incident non-zero mean wind field is applied along the positive $x$-direction; the turbine's rotor plane is assumed to point in the negative $x$-direction, implying zero yaw misalignment. Waves are assumed to have a heading of zero degrees; thus, they are also incident along the positive $x$-direction. Only aligned wind and waves are, therefore, considered in this study.

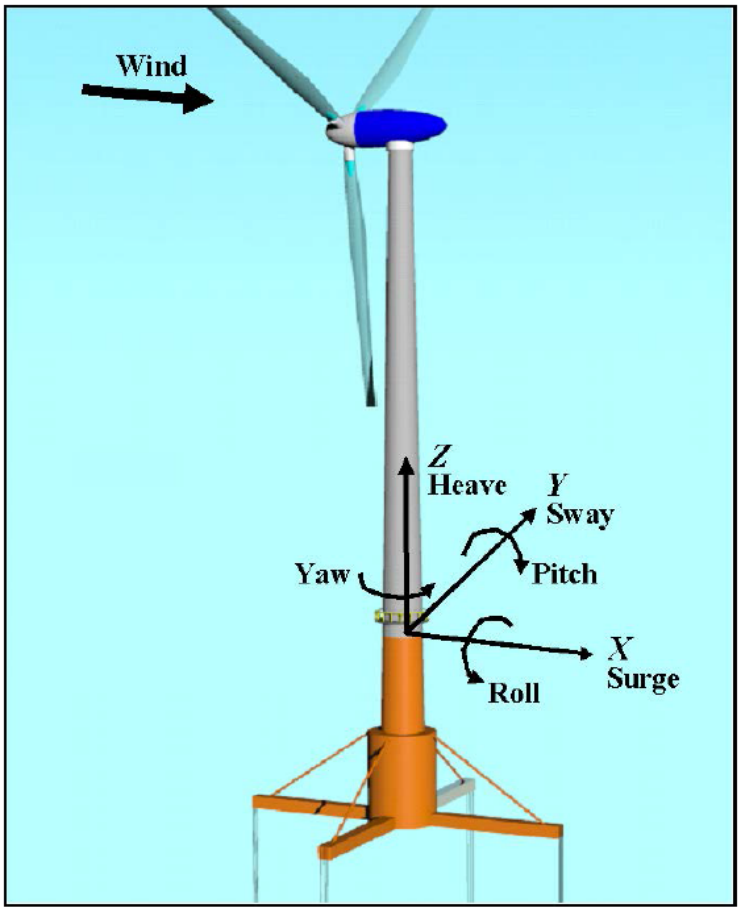


Figure 2.11: Reference coordinate system for the floating platform [24].

### 2.4.3 Platform Hydrodynamic Properties

Understanding the influence of wave loading on a floating platform is important in order to assess the overall platform response in different sea states. Hydrodynamic loads include contributions from linear hydrostatics, linear excitation from incident waves, linear radiation from outgoing waves (generated by the platform motions), and other nonlinear effects [8, 25]. It

is also suggested that, for a semi-submersible platform, non-linear damping effects due to hydrodynamic drag forces are important [26, 27].

The hydrodynamic loads due to excitation from incident waves and radiation from outgoing waves (due to platform motions) occur as a result of flow separation. For this analysis, linear potential flow theory is employed. The computer program, WAMIT [28], is used to solve the linearized potential flow hydrodynamic radiation, diffraction, and hydrostatics problems resulting from the interaction of surface waves with the platform (see Section 2.6.2).

WAMIT uses a panel method for the three-dimensional model and a numerical solution procedure in the frequency domain [12]. The radiation problem relates to the waves generated and radiated outward from the surface of the platform after platform motions due to incident waves have stopped; the forces from the radiation problem result in frequency-dependent added-mass and damping matrices. Added mass refers to the additional component of mass of water that is accelerated together with the platform when it moves; damping is the force that reduces the motion of the platform after the incident wave has passed the platform's surface. The diffraction problem relates to the waves diffracted around the platform when the platform stops moving; this yields forces and moments due to wave excitation and results in frequency-dependent wave excitation forces. The hydrostatic problem takes care of the static restoring coefficients, which are calculated from the water-plane area and the displaced volume of water due to platform buoyancy; this results in a frequency-independent coupled hydrostatic restoring matrix for the platform.

In addition to the linear potential flow theory considerations, non-linear viscous drag forces arising from the relative velocity term in Morison's equation needs to be taken into account to obtain appropriate levels of hydrodynamic damping. For a semi-submersible platform, each member of the platform will experience its own drag forces.

## 2.5 Mooring System

Mooring systems are important for any floating offshore platform. For a floating semi-submersible platform, the mooring lines are important only for station-keeping purposes—i.e., to maintain the position of the platform, without significant drifting, under the action of wind and waves. A mooring system is made up of mooring lines, anchors, and connectors (called fairleads at the platform). A mooring line connects an anchor at the seafloor to the floating structure or platform. It can be made up of synthetic fiber rope, wire, or chain or various combinations of those three. Environmental factors determine the materials that make up the mooring system.

To secure the semi-submersible platform used in this analysis, it is assumed to be moored with three catenary lines spread symmetrically about the $z$-axis of the platform. The mooring system used in this analysis is scaled up from the OC4 Phase II [8] mooring system so as to incorporate the larger platform needed for the 13.2 MW turbine. The fairleads—points on the platform where the mooring lines are attached—are located at the top of the base columns, at a depth of 25.2 meters below the mean sea level (MSL) and

at a radius of 73.56 meters from the platform centerline. The anchors are located at the sea bed, at a water depth of 200 meters below MSL and at a radius of 837.6 meters from the platform centerline. One of the mooring lines is directed along the positive $x$-axis, coincident with the direction of the incident non-zero mean wind and the waves. The two remaining lines are each offset 120° symmetrically with respect to the first. Figure 2.12 shows the layout of the mooring system. Each mooring line has an unstretched length of 835.5 meters, a diameter of 0.13788 meters, an equivalent mass density of 367.25 kg/m, an equivalent apparent mass (in water) of 351.96 kg/m, and an equivalent extensional stiffness of 2,442 MN. The seabed drag coefficient for the mooring lines is assumed to be 1.0. Table 2.7 lists important properties of the mooring lines.

Table 2.7: Mooring System Properties.

| | |
|---|---|
| Number of mooring lines | 3 |
| Angle between adjacent lines | 120° |
| Depth to Anchors below SWL (Water Depth) | 200 m |
| Depth to Fairleads below SWL | 25.2 m |
| Radius to Anchors from Platform Centerline | 837.6 m |
| Radius to Fairleads from Platform Centerline | 73.56 m |
| Unstretched Mooring Line Length | 835.5 m |
| Mooring Line Diameter | 0.13788 m |
| Equivalent Mooring Line Mass Density | 367.25 kg/m |
| Equivalent Mooring Line Apparent Mass in Water | 351.96 kg/m |
| Equivalent Mooring Line Extensional Stiffness | 2442 MN |
| Seabed Drag Coefficient for Mooring Lines | 1.0 |

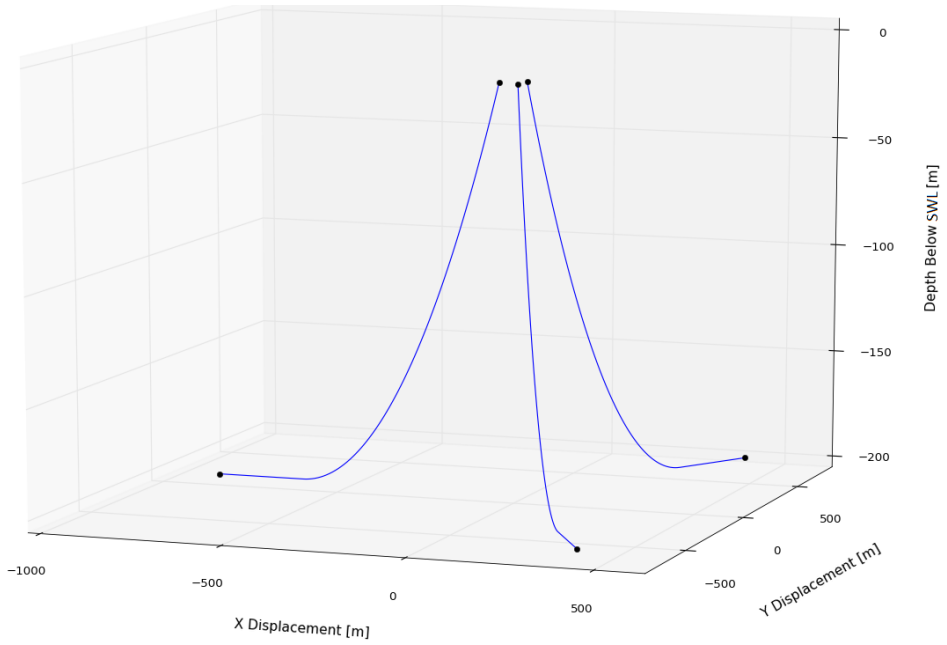


Figure 2.12: Isometric view of the mooring system layout for the semi-submersible platform.

## 2.6 Simulation of Overall Turbine System Response

To carry out dynamic response simulations of the overall wind turbine system, the program, FAST [29], was used. FAST was developed at the National Renewable Energy Laboratory (NREL) [14]. For the turbulent inflow wind field simulations, the program, TurbSim [30], also developed at NREL [15] was used. In the following, we provide some details of how various tools are used in the overall system response simulations.

### 2.6.1 TurbSim - Incident Turbulent Wind Field

To generate incident turbulent wind fields, the program TurbSim [30] is used. TurbSim generates zero-mean longitudinal, lateral, and vertical ($u$, $v$ and $w$) components of turbulence over a two-dimensional grid defined in the TurbSim input file. The grid specified must cover the turbine rotor plane and should extend outward by a sufficient amount to account for turbine rotor deflections that might occur in the course of the simulations. A non-zero mean wind profile (shear) is added to the longitudinal turbulence component; in particular, the mean hub-height longitudinal wind speed is specified along with an assumed wind shear power-law profile. The IEC (International Electrotechnical Commission) turbulence category 'B' [31] is chosen, which corresponds to a turbulence intensity ($I_{ref}$) of 0.14 for a hub-height wind speed of 15 m/s. The actual turbulence intensity that is simulated varies with the hub-height wind speed and the height from the mean water level according to IEC 61400-1 [31].

For simulation of the time series for each of the three wind velocity components, a Kaimal power spectral density function is assumed. IEC 61400-1 [31] defines an exponential coherence model that is used in conjunction with the Kaimal power spectra to account for the spatial correlation structure of the longitudinal velocity component.

### 2.6.2 MultiSurf and WAMIT

MultiSurf [32], developed by AeroHydro Inc., is a computer-aided design (CAD) program that is useful for building models for analysis using WAMIT. In our studies, MultiSurf is used to create WAMIT input files and desired meshes for the selected floating semi-submersible platform.

WAMIT [28], developed by WAMIT Inc. and the Massachusetts Institute of Technology, is a computer program based on potential theory for analyzing floating or submerged bodies in the presence of ocean waves. It uses the boundary integral element method or, equivalently, the panel method to solve for the velocity potential and fluid pressure on the submerged surfaces of the bodies. Separate solutions for the diffraction and radiation problems for each of the prescribed modes of motion of the bodies are used to obtain relevant hydrodynamic parameters including added mass and damping coefficients and exciting forces. For selected wave headings, three hydrodynamic output files from WAMIT are used as input files to FAST. These files include frequency-dependent added mass and damping coefficients and wave excitation forces for the six degrees of freedom. A

hydrostatic file, generated by WAMIT, which has stiffness matrix for the platform, is also used an input to FAST.

### 2.6.3 FAST - Dynamic Analysis

The program, FAST [29, 33], developed at NREL, is used in dynamic analysis of land-based and offshore wind turbines. It models a three-bladed horizontal axis wind turbine as a multi-degree-of-freedom system. The platform is modeled as a rigid body with six degrees of freedom for its translational and rotational motions in three orthogonal directions. The tower is assumed to be flexible; it is modeled using the first two modes of vibration in both the fore-aft and side-to-side directions. The blades are also modeled using a modal representation, with multiple mode shapes defining their dynamic behavior. The 13.2 MW wind turbine has collective blade pitch control which is important for alleviating high structural loads, especially in high winds. When the turbine experiences wind speeds above rated (11.3 m/s), the blades start to pitch to relieve aerodynamic and structural loads on the system, while maintaining constant power output [19, 34].

The program, FAST, has been in use for many years now. The latest version, FAST v8 [33], is greatly improved in terms of modularity. This version integrates several modules for the different physical domains that make up the coupled aero-hydro-servo-elastic solution. Figure 2.13 shows the various programs and modules involved in the simulation of an offshore wind turbine

system using FAST.

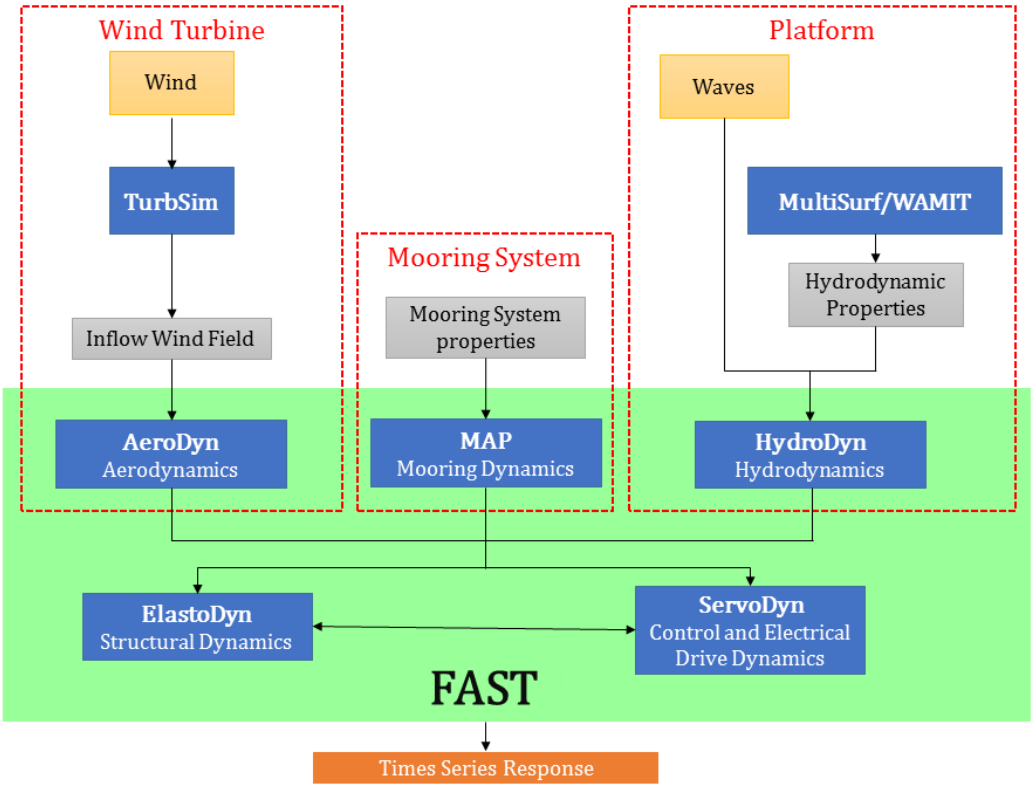


Figure 2.13: Simulation flowchart showing the various programs/modules involved in computation using FAST.

There are several modules integrated into FAST v8. The AeroDyn module computes loads on turbine blades due to steady or unsteady winds; it also computers tower drag loads due to wind. This module uses TurbSim-based simulated incident wind fields as input and uses blade airfoil characteristics to compute rotor aerodynamic loads. The HydroDyn module is the primary module that accepts simulated external wave conditions and

platform hydrodynamic properties from WAMIT to calculate the hydrodynamic loading on the platform. Either regular or irregular waves can be employed. This module also calculates viscous drag forces on the platform by utilizing Morison's equation for the individual members of the semi-submersible platform. The MAP [35] (Mooring Analysis Program) module solves for the response of the system of mooring lines quasi-statically. The ServoDyn module accounts for the blade pitch and variable-speed generator control. Control algorithms are unique to each turbine and are input to ServoDyn. The ElastoDyn module incorporates the structural dynamics characteristics of the entire system, taking into consideration all the degrees of freedom involved in representing the wind turbine and the floating platform. In general, given time series of wind velocities and of waves that are applied as inputs, time series of the response of different components of the wind turbine and platform are produced as output. These can then be studied to assess the overall turbine-platform system behavior.

# Chapter 3

# Short-Term Extreme Response of the 13.2 MW Offshore Wind Turbine System

## 3.1 Introduction

The aim of this study is to estimate extreme loads for the 13.2 MW wind turbine supported by a semi-submersible platform, for which, a preliminary model has been developed [12]. We perform short-term response analyses using stochastic simulations for different environmental conditions, i.e., different combinations of waves and winds. To identify controlling conditions, we study time histories, power spectra and response statistics, for the turbine loads as well as platform motions. This study only addresses short-term loads based on one-hour long simulations. These short-term simulation studies may be combined with metocean wind-wave data to ultimately derive load levels associated with long return periods, which would be important in evaluating the reliability of the integrated turbine system.

## 3.2 The Reference Site and Environmental Conditions

For loads analysis of an offshore wind turbine, the design standard for offshore wind turbines, IEC 61400-3 [36], requires that simulations be carried

out with site-specific external conditions that describe the wind and wave environment. The site selected for our study is close to Half Moon Bay, about 24 nautical miles south-southwest of San Francisco, California. Wind and wave data are available from National Data Buoy Center (NDBC) Station 46012 [37]. The geographical coordinates of this site are 37°21′ N, 122°52′ W. Figure 3.1 shows the location of this site, obtained via Google Maps[1]. The site was selected because it has a water depth of 208.8 meters, close to the 200 meters water depth assumed for the semi-submersible and mooring system model development.

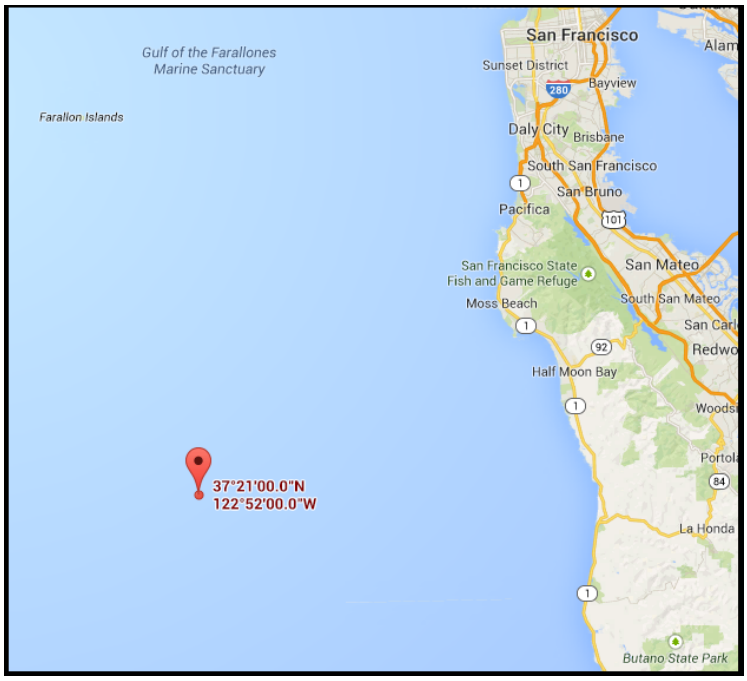


Figure 3.1: Reference Site near San Francisco, California.

[1]Website: http://maps.google.com

About 34 years of data (1980-2013) are available this site, based on a 1-hour reference (averaging) period, yielding a total of about 195,000 data points. The environmental data were provided in tables with the joint probability histograms derived from the raw data. Table 3.1 shows the percent occurrence of different hub-height wind speed and significant wave height bins, and Table 3.2 shows the percent occurrence of different significant wave height and peak spectral wave period bins considering all of the data. The reference elevation for the wind speed data was 5 meters above the mean sea level. As suggested in IEC 61400-3 [36], a vertical power-law shear exponent, $\alpha$, of 0.2 was assumed for extrapolating the wind speed at this reference elevation to the hub height as follows:

$$V_{hub} = V_{ref} \left( \frac{z_{hub}}{z_{ref}} \right)^{\alpha} \tag{3.1}$$

where $V_{hub}$ is the hub-height wind speed, $V_{ref}$ is the wind speed at the reference elevation, $z_{hub}$ is the hub height, $z_{ref}$ is the reference elevation, and $\alpha$ is the power-law exponent (assumed to be equal to 0.2). Figure 3.2 shows the mean wind speed along and the mean $\pm$ 1 standard deviation wind speed at the hub height for the reference site; the variation over the months of the year averaged over 34 years is seen.

Table 3.1: Hub-Height Wind Speed vs Significant Wave Height

| Hub-Height | Significant Wave Height (m) | | | | | | | | | |
|---|---|---|---|---|---|---|---|---|---|---|
| Wind Speed (m/s) | 0-0.5 | 0.5-1.5 | 1.5-2.5 | 2.5-3.5 | 3.5-4.5 | 4.5-5.5 | 5.5-6.5 | >6.5 | Total % | Total No. |
| <1.0 | * | 0.8 | 0.6 | 0.1 | * | * | * | - | 1.6 | 3158 |
| 1 - 3 | * | 4.7 | 4.2 | 1.1 | 0.3 | * | * | * | 10.3 | 20116 |
| 3 - 6 | * | 7.8 | 8.1 | 2.1 | 0.5 | 0.1 | * | * | 18.7 | 36416 |
| 6 - 10 | * | 8.3 | 12.3 | 3.8 | 0.9 | 0.2 | 0.1 | * | 25.6 | 49941 |
| 10 - 15 | * | 4.5 | 13.0 | 5.5 | 1.3 | 0.3 | 0.1 | * | 24.6 | 48104 |
| 15 - 20 | - | 0.5 | 4.7 | 4.6 | 1.5 | 0.3 | 0.1 | * | 11.8 | 22948 |
| 20 - 24 | - | * | 0.6 | 1.9 | 1.1 | 0.2 | * | * | 3.9 | 7614 |
| 24 - 33 | - | * | 0.1 | 0.6 | 0.8 | 0.4 | 0.1 | * | 1.9 | 3772 |
| 33 - 48 | - | - | - | * | * | * | * | * | 0.1 | 151 |
| >48 | - | 0.3 | 0.7 | 0.4 | 0.2 | * | * | - | 1.5 | 2979 |
| Total % | 0.0 | 27.0 | 44.3 | 20.0 | 6.6 | 1.6 | 0.3 | 0.1 | 100.0 | |
| Total No. | 75 | 52762 | 86518 | 39075 | 12802 | 3109 | 659 | 199 | | 195199 |

Note: * represents values $< 0.05$

Table 3.2: Significant Wave Height vs Peak Spectral Wave Period

| Peak Spectral | Significant Wave Height(m) | | | | | | | | | |
|---|---|---|---|---|---|---|---|---|---|---|
| Wave Period (s) | 0-0.5 | 0.5-1.5 | 1.5-2.5 | 2.5-3.5 | 3.5-4.5 | 4.5-5.5 | 5.5-6.5 | >6.5 | Total % | Total No. |
| <3 | * | * | - | - | - | - | - | - | 0.0 | 2 |
| 3 - 4 | * | 0.2 | * | - | - | - | - | - | 0.2 | 386 |
| 4 - 5 | * | 2.4 | 1.0 | * | - | - | - | - | 3.4 | 6569 |
| 5 - 6 | * | 6.2 | 8.2 | 1.0 | * | - | - | - | 15.5 | 30321 |
| 6 - 7 | * | 7.6 | 13.1 | 5.4 | 0.8 | * | * | - | 27.0 | 52663 |
| 7 - 8 | - | 5.9 | 10.0 | 5 | 1.9 | 0.4 | * | * | 23.2 | 45222 |
| 8 - 9 | - | 3.0 | 6.3 | 3.7 | 1.3 | 0.4 | 0.1 | * | 14.9 | 29036 |
| 9 - 10 | - | 1.2 | 3.3 | 2.7 | 1.1 | 0.3 | 0.1 | * | 8.7 | 17069 |
| 10 - 11 | - | 0.4 | 1.6 | 1.4 | 0.8 | 0.3 | 0.1 | * | 4.6 | 8895 |
| >11 | - | 0.1 | 0.8 | 0.8 | 0.5 | 0.2 | 0.1 | * | 2.5 | 4949 |
| Total % | 0 | 27.0 | 44.3 | 20.0 | 6.6 | 1.6 | 0.3 | 0.1 | 100.0 | |
| Total No. | 55 | 52762 | 86503 | 39037 | 12790 | 3107 | 659 | 199 | | 195112 |

Note: * represents values $< 0.05$

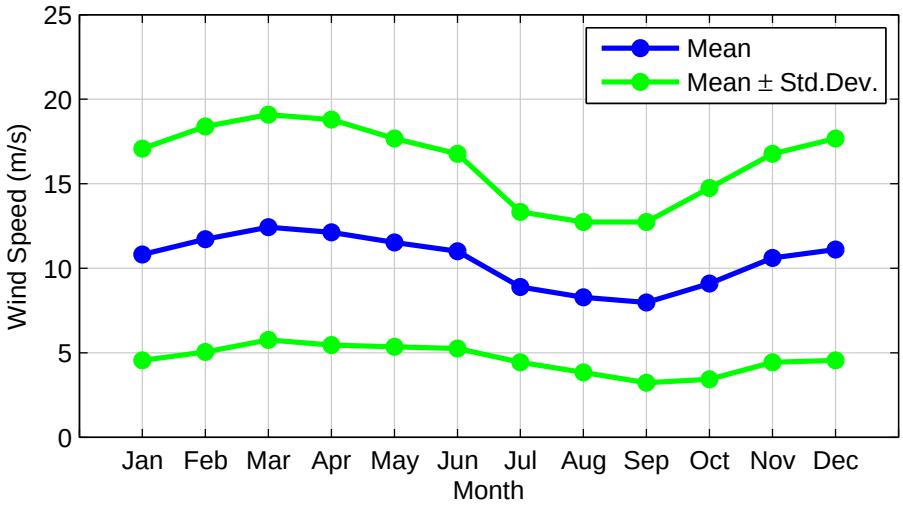


Figure 3.2: Hub-Height Wind Speed: Mean and Mean $\pm$ 1 Standard Deviation

The joint distribution of the 1-hour average hub-height wind speed, $V$, the significant wave height, $H_s$, and the wave peak spectral period, $T_p$, are useful for understanding important and more frequently occurring combinations of these environmental parameters. Figure 3.3 shows the joint $H_s$-$V$ and $H_s$-$T_p$ distributions, based on 34 years of data.

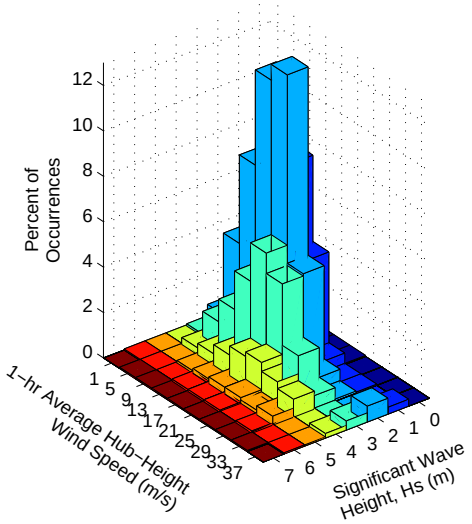


(a) Hub-Height Wind Speed vs Significant Wave Height

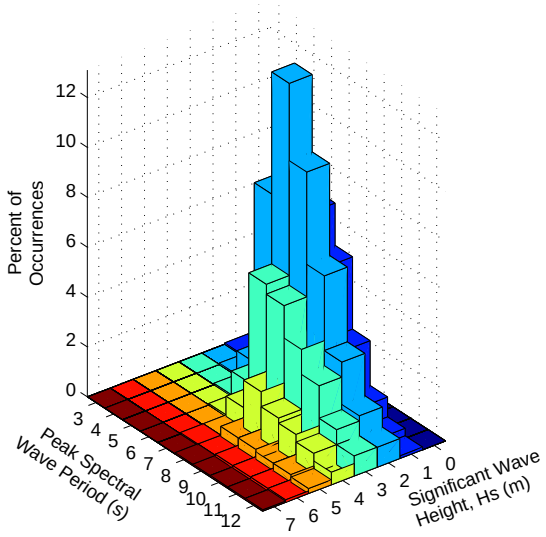


(b) Significant Wave Height vs Wave Peak Spectral Period

Figure 3.3: Joint $H_s$-$V$ and $H_s$-$T_p$ Distributions for the Reference Site.

Based on these joint probability distributions, important sea states can be selected based on probability mass or likelihood of occurrence. These sea

states were selected by first choosing six different values of the hub-height mean wind speed, $V$, over the operating range of the wind turbine from cut-in to cut-out ($V_{in} = 3$ m/s $< V < V_{out} = 25$ m/s). For each selected wind speed, based on the $H_s$-$V$ joint distribution, three different significant wave heights were chosen, representing low, medium, and high waves at the reference site. Then, for the selected wave heights, a wave peak spectral period was selected (close to the conditional mean $T_p$ given $H_s$) based on the $H_s$-$T_p$ joint distribution. A total of 18 sea states were selected that represent the range of wind speeds and wave heights and account for more likely environmental conditions at the site. Table 3.3 lists the selected sea states where it should be noted that the actual values used for the environmental variables, $V$, $H_s$, and $T_p$, were considered with a small number of significant digits for convenience.

Table 3.3: Selected sea states for short-term response analysis.

| V (m/s) | Low Wave Height | | Medium Wave Height | | High Wave Height | |
|---|---|---|---|---|---|---|
| | $H_s$ (m) | $T_p$ (s) | $H_s$ (m) | $T_p$ (s) | $H_s$ (m) | $T_p$ (s) |
| 5 | 1.0 | 8.0 | 2.5 | 9.0 | 4.0 | 10.5 |
| 9 | 1.0 | 7.0 | 2.5 | 8.0 | 4.0 | 9.5 |
| 12 | 1.0 | 6.0 | 2.5 | 7.0 | 4.0 | 8.5 |
| 16 | 2.0 | 8.0 | 3.5 | 8.5 | 5.0 | 10.5 |
| 19 | 2.0 | 7.0 | 3.5 | 7.5 | 5.0 | 9.0 |
| 23 | 2.5 | 6.5 | 1.0 | 7.5 | 5.5 | 11.0 |

From Tables 3.1 and 3.2, it can be observed that, within a $\pm 1$ m/s range for wind speed, a $\pm 1$ m range for significant wave height, and a $\pm 1$ second

range for wave peak spectral period, the 18 selected sea states account for about 80% of all the data. This suggests that the selected sea states represent the environmental conditions at the site quite well.

Standard values of 1,025 kg/m$^3$ for the water density and 1.225 kg/m$^3$ for the air density were assumed for the site. An IEC turbulence category B [31] was assumed for the analysis. Also, for the sea surface elevation simulations, a JONSWAP (Joint North Sea Wave Atmosphere Program) spectrum [38] was assumed.

## 3.3 Stochastic Response Simulations

For each of the selected sea states in Table 3.3, fifteen one-hour simulations are carried out. The wind velocity field is generated using TurbSim, platform hydrodynamic properties were obtained using WAMIT; both of these are used as inputs to FAST for simulating the response of the integrated turbine-platform-mooring system. A time step of 0.02 sec is employed in FAST for the response simulations. Response statistics studied include the 1-hour maximum, mean, standard deviation, peak factor (defined as the [max-mean] divided by standard deviation), skewness, kurtosis, and mean upcrossing rate. The response variables studied in detail include the blade tip out-of-plane deflection, the tower-top out-of-plane deflection, the blade root out-of-plane and in-plane bending moments, the tower base fore-aft and side-to-side bending moments, and the platform surge and pitch motions.

## 3.4 Numerical Studies

### 3.4.1 Time Series

Figure 3.4 shows representative time series (200-second segments taken out of a full hour-long simulation) of various system responses, normalized with respect to their maximum values over 200 seconds. Figure 3.5 shows these same response time series for the whole one hour. Time series are shown for the hub-height longitudinal wind speed (WindVxi) and the sea surface elevation (WaveElev), which describe the external conditions; also shown are the blade pitch angle (BldPitch1) where controller actions are evident, the blade root out-of-plane bending moment (RootMyc1), the tower base fore-aft bending moment (TwrBsMyt), the platform surge motion (PtfmSurge), and platform pitch motion (PtfmPitch). The time series shown in Figures 3.4 and 3.5 correspond to the sea state where $V$=12 m/s, $H_S$=4 m and $T_P$=8.5 sec.

From the time series, it can be observed that the blade pitch angle increases (from zero) when the incident wind exceeds the rated wind speed; this is a property of the controller that seeks to limit high structural loads while maintaining rated power. The blade root out-of-plane bending moment (RootMyc1) shows complex dynamic behavior due to effect mostly of the wind and less so from the waves, along with the pitch control action, and the rotor rotation rate, as well as blade resonance effects. The tower-base fore-aft bending moment (TwrBsMyt) shows a close relationship to the sea surface elevation (WaveElev) and to the platform pitch motion (PtfmPitch). The platform surge process exhibits dominant long-period response related to the

low platform surge resonance frequency. The platform pitch motion also exhibits energy at long periods, though the dominant energy is at somewhat lower periods than is the case for the platform surge motion. The blade root out-of-plane bending moment and tower base fore-aft bending moment show much greater high-frequency response compared to the platform surge and pitch motions.

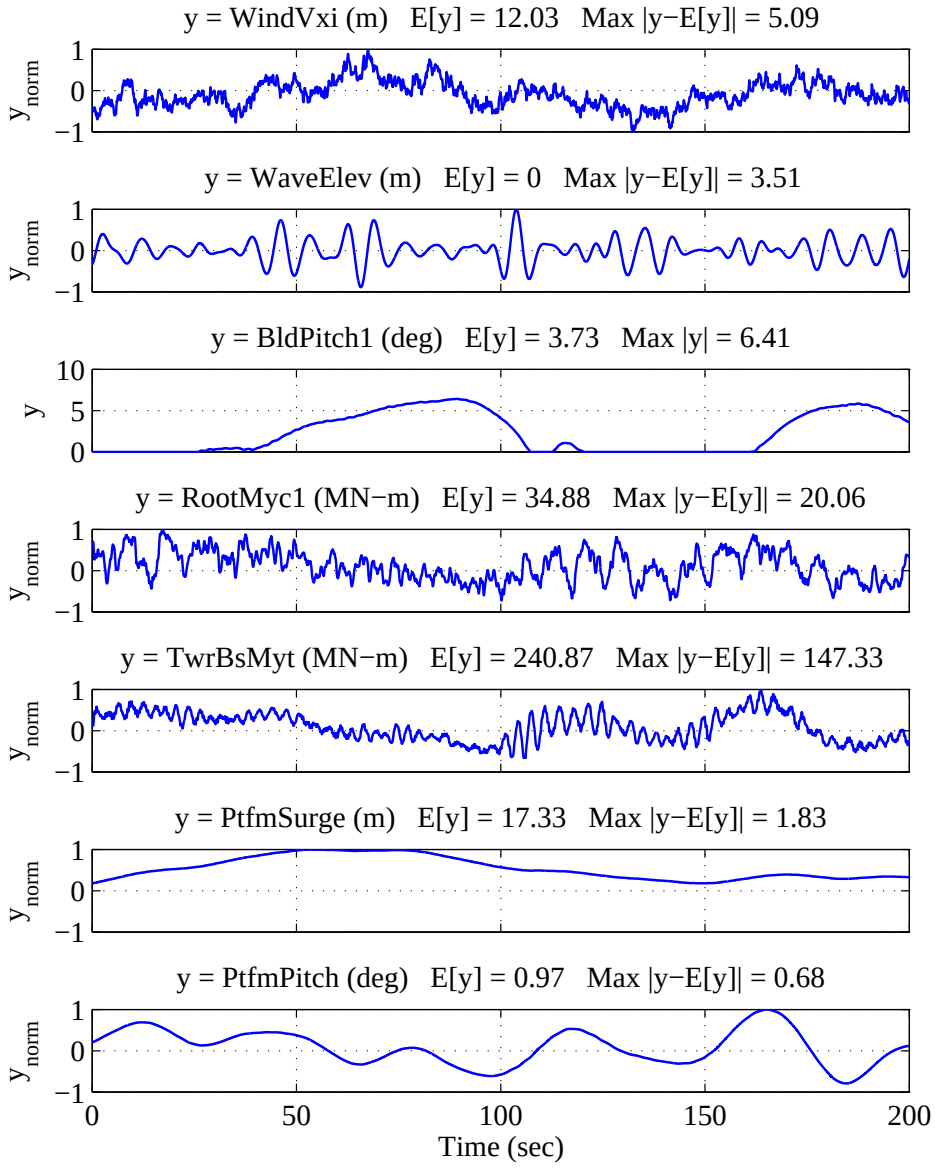


Figure 3.4: Representative 200-second segments from full 1-hour simulated time series of the hub-height longitudinal wind speed, wave elevation, blade pitch angle, out-of-plane bending moment at the blade root, fore-aft bending moment at the tower base, platform surge, and platform pitch at $V$=12 m/s, $H_s$=4 m, $T_p$=8.5 sec.

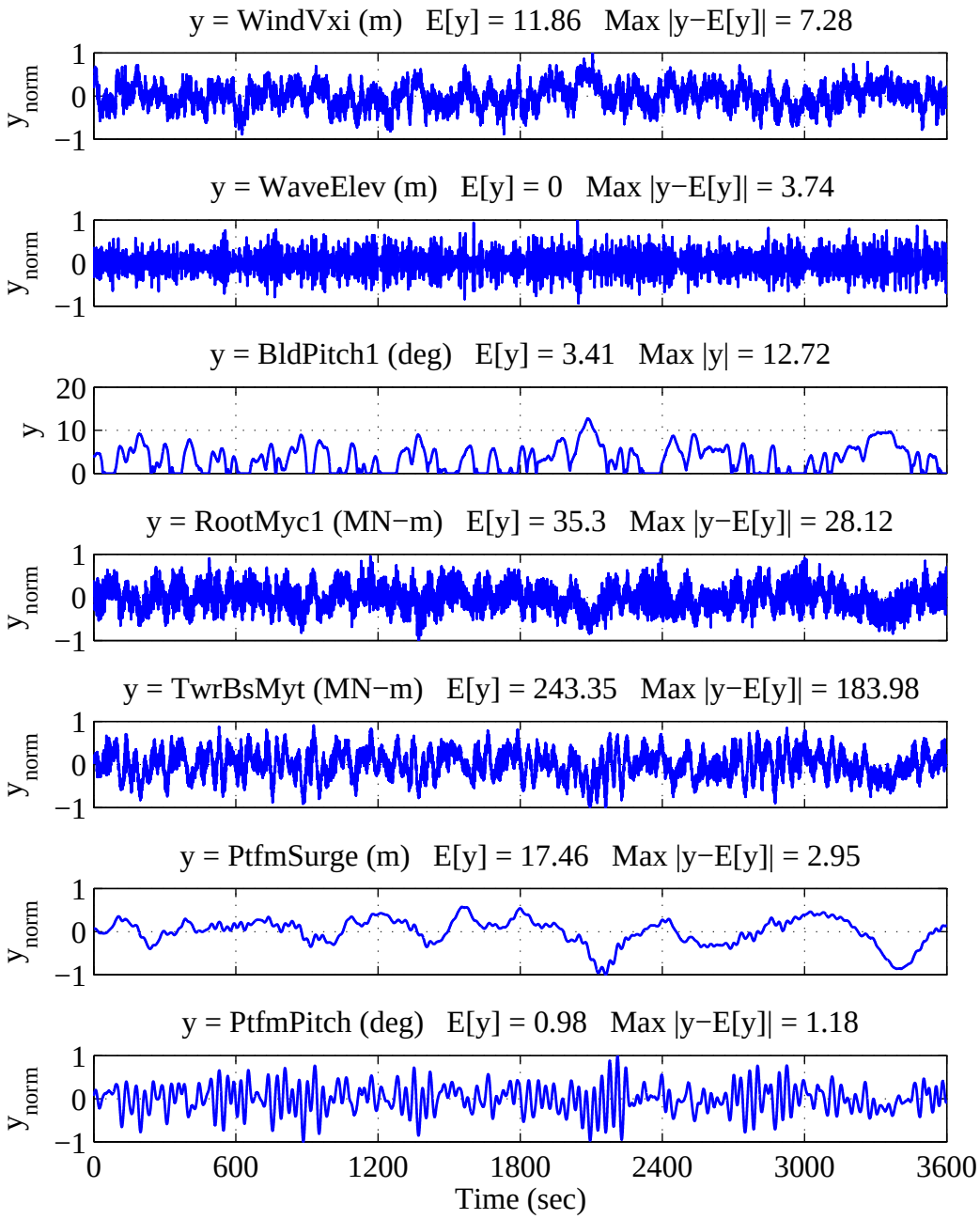


Figure 3.5: One-hour simulated time series of the hub-height longitudinal wind speed, wave elevation, blade pitch angle, out-of-plane bending moment at the blade root, fore-aft bending moment at the tower base, platform surge, and platform pitch at $V$=12 m/s, $H_s$=4 m, $T_p$=8.5 sec.

### 3.4.2 Response Statistics

Different environmental combinations of wind and wave parameters can influence the various turbine-platform-mooring system loads and motions differently. To understand the importance of various environmental conditions, system response statistics are studied as a function of wind speed and wave height using the selected sea states. Response measures with large variability can have a significant effect on extremes, even if the mean levels are not large. Also, if variability is significant, extrapolated response extremes associated with long return periods can be large.

Extreme loads and motions of a turbine-platform-mooring system are of great interest for design against ultimate limit states. The maxima of different response variables estimated from one-hour simulations can be used to study extremes. This one-hour extreme of any response process may be related to other response statistics as follows:

$$Max = Mean + SD \times PF$$

where $Max$ refers to the one-hour extreme, $Mean$ and $SD$ are the mean and standard deviation of the response process, and $PF$ is a peak factor, which is effectively derived once $Max$, $Mean$, and $SD$ are estimated. The peak factor effectively represents the number of standard deviations that separate the one-hour extreme response from the mean response. Each of these response statistics can be helpful in understanding the nature of the response process being studied; in particular, larger peak factors can occur if (i) the mean

upcrossing rate of the process is high which would imply that many response cycles occur in the 1-hour duration; (ii) the response is highly non-Gaussian as indicated by skewness and kurtosis values. Thus, a large 1-hour extreme response can result when one or more of the following is true: the mean is large (often this is a quasi-static effect); the standard deviation is large (often this is driven by fluctuations and variability in the process as with turbulence but it can also arise from stronger dynamic than quasi-static influence); or the peak factor is large (it is convenient to understand this is as resulting from faster response processes or strongly non-Gaussian character).

#### 3.4.2.1 Blade Tip Out-of-Plane Deflection

Figure 3.6 summarizes ensemble statistics (maximum, mean, and standard deviation) from fifteen one-hour simulations of the blade tip out-of-plane deflection for all the selected eighteen sea states. The blade tip deflection increases with mean wind speed from 5 m/s to 12 m/s and then monotonically decreases after that. This occurs due to the blade pitch control that occurs when the wind speeds exceed the rated wind speed of 11.3 m/s and causes structural response levels to be reduced. The largest one-hour extreme is seen at 12 m/s; there is very small variation in the extremes with changes in the wave height. The mean blade tip out-of-plane deflection does not show much variation with the wave height. The standard deviation is not affected greatly by the blade pitch control; it increases slightly with wind speed but shows very little variation with wave height.

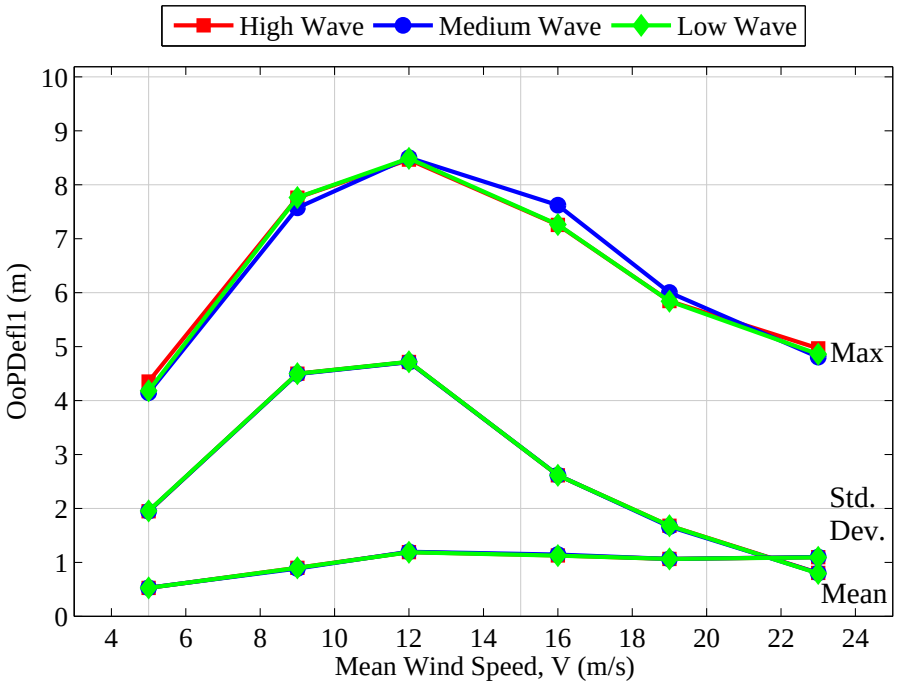


Figure 3.6: Ensemble one-hour statistics for the blade tip out-of-plane deflection in eighteen sea states.

Table 3.4 summarizes various response statistics (including the maximum, mean, standard deviation, peak factor, skewness, kurtosis, and mean upcrossing rate) from fifteen one-hour simulations of the blade tip out-of-plane deflection for the five most critical sea states out of the eighteen studied (in this discussion and others related to the different response measures studied, the five most critical sea states are those for which the five largest 1-hour extreme responses occurred from among all the eighteen considered). The mean blade tip out-of-plane deflection increases with wind

speed up to 12 m/s, after which it starts to decrease due to pitching of the blades. The higher sea state ($V$=16 m/s, $H_s$=3.5 m) shows a decrease in the mean of about 50% compared to the lower sea state ($V$=12 m/s, $H_s$=4 m). There is insignificant increase in the mean deflections with increasing wave height, for a given wind speed. The maximum of the blade tip deflection occurs at 12 m/s, which is close to the rated wind speed of the turbine. The standard deviation of the blade tip out-of-plane deflection increases with wind speed up to the rated wind speed but remains almost constant thereafter.

The peak factor for the one-hour simulations increases considerably especially at the highest wind speed. This is because the skewness increases significantly there (when $V$=16 m/s). The mean upcrossing rate is fairly constant for the four higher sea states. Overall, it is mainly the larger mean value when $V$=12 m/s that causes the largest response extremes for those sea states where $V$=12 m/s.

#### 3.4.2.2 Tower-Top Fore-Aft Deflection

Figure 3.7 summarizes ensemble statistics (maximum, mean, and standard deviation) from fifteen one-hour simulations of the tower-top fore-aft deflection for all the selected eighteen sea states. The mean tower-top deflection shows similar behavior to the blade tip out-of-plane deflection. It increases with increasing wind speed from 5 to 12 m/s, after which it decreases; this is again the effect of blade pitching at wind speeds

Table 3.4: Ensemble statistics of the blade tip out-of-plane deflection from fifteen one-hour simulations for 5 critical sea states.

| V (m/s) | $H_s$ (m) | $T_p$ (sec) | Blade Tip Out-of-Plane Deflection (OoPDefl1) Statistics | | | | | | |
|---|---|---|---|---|---|---|---|---|---|
| | | | Max (m) | Mean (m) | SD (m) | Peak Factor | Skewness | Kurtosis | Mean Upcrossing Rate ($s^{-1}$) |
| 9 | 4.0 | 9.5 | 7.76 | 4.50 | 0.90 | 3.64 | 0.07 | 2.75 | 1.50 |
| 12 | 2.5 | 7.0 | 8.50 | 4.71 | 1.20 | 3.17 | -0.08 | 2.65 | 1.07 |
| 12 | 4.0 | 8.5 | 8.49 | 4.72 | 1.19 | 3.18 | -0.08 | 2.64 | 1.07 |
| 16 | 2.0 | 8.0 | 7.26 | 2.61 | 1.13 | 4.11 | 0.24 | 3.03 | 1.13 |
| 16 | 3.5 | 8.5 | 7.62 | 2.62 | 1.14 | 4.39 | 0.26 | 3.07 | 1.12 |

greater than the rated wind speed of 11.3 m/s. The mean tower-top deflections are largest at winds around the rated wind speed and show relatively little influence of the waves. The maxima show the same trend of increasing with wind speeds up to rated, after which they decrease. The decrease in maximum is less pronounced that the decrease in the mean for above-rated winds. The maximum values show little variation with wave height. The standard deviation of the tower-top fore-aft deflection shows very slight variation with wind speed and wave height. The largest one-hour extremes are seen for wind speeds of 12 m/s, which is close to the rated wind speed. The extremes at $V$=12 m/s and $V$=16 m/s are only slightly different, suggesting that the tower-top deflection extremes are slightly affected by blade pitch control.

Table 3.5 summarizes various response statistics (including the

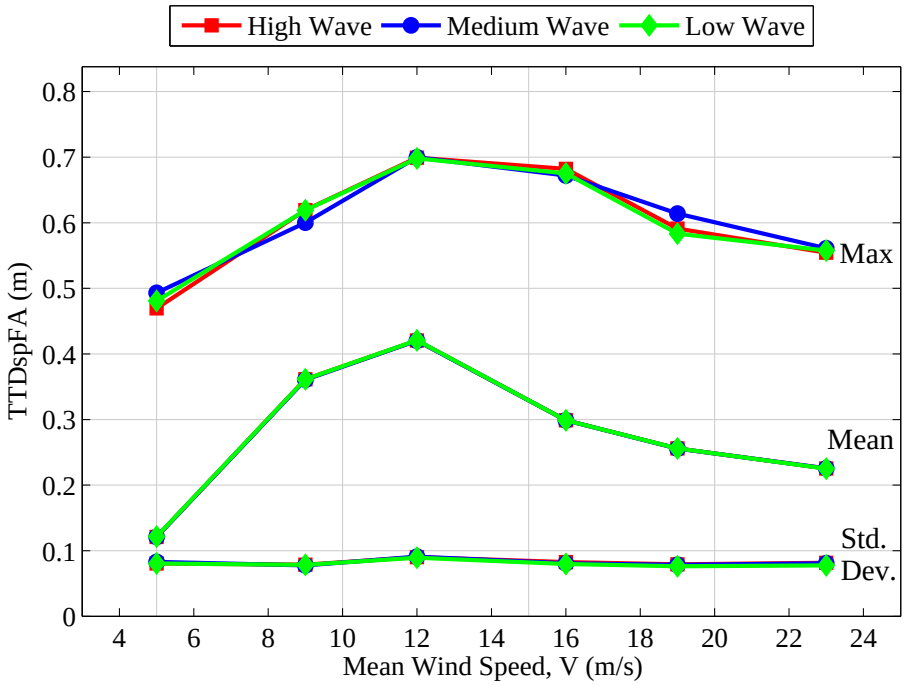


Figure 3.7: Ensemble one-hour statistics for the tower-top fore-aft deflection in eighteen sea states.

maximum, mean, standard deviation, peak factor, skewness, kurtosis, and mean upcrossing rate) from fifteen one-hour simulations of the tower-top fore-aft deflection for the five most critical sea states out of the eighteen studied. The mean tower-top fore-aft deflection increases with increasing wind speed up to 12 m/s, after which is starts to decrease, due to the blade pitching effect. The mean tower-top deflection decreases by about 30% when going from wind speeds of 12 m/s to 16 m/s. There is no significant effect of wave height on the mean tower-top deflections. The maxima of the tower-top

deflections show the same trend as the mean, but the decrease above the rated wind speed is less significant. The standard deviation shows almost no influence of the incident wind speed.

The peak factor for the one-hour simulations increases with increasing wind speed. The skewness increases significantly for high winds ($V$=16 m/s) compared to lower winds ($V$=9, 12 m/s). Mean upcrossing rates show very slight variation with wind speed. The significant change in the peak factor at high winds occurs due to the increase in the skewness of the response process. The product of the standard deviation and peak factor is higher for the higher winds than that for the lower winds. Since the mean of the tower-top deflections is lower for high winds but the product of standard deviation and peak factor is higher, the maximums are more comparable at 12 m/s and 16 m/s. In summary, we see that the highest tower-top fore-aft deflections occurs around and slightly above the rated wind speed ($V$=12 m/s and $V$=16 m/s) and they show slight variation with wave height.

#### 3.4.2.3 Blade Root In-Plane Bending Moment

Figure 3.8 summarizes ensemble statistics (maximum, mean, and standard deviation) from fifteen one-hour simulations of the blade root in-plane bending moment for all the selected eighteen sea states. The maximum blade root in-plane bending moment shows an increasing trend with increasing wind speed. This is expected because the blade in-plane bending moments are not affected as much by pitching of the blades as they

Table 3.5: Ensemble statistics of the tower-top fore-aft deflection from fifteen one-hour simulations for 5 critical sea states

| V (m/s) | $H_s$ (m) | $T_p$ (sec) | Tower-top Fore-Aft Deflection (TTDspFA) Statistics | | | | | | |
|---|---|---|---|---|---|---|---|---|---|
| | | | Max (m) | Mean (m) | SD (m) | Peak Factor | Skewness | Kurtosis | Mean Upcrossing Rate ($s^{-1}$) |
| 9 | 4.0 | 9.5 | 0.62 | 0.36 | 0.08 | 3.31 | -0.05 | 2.92 | 0.94 |
| 12 | 2.5 | 7.0 | 0.70 | 0.42 | 0.09 | 3.08 | -0.07 | 2.55 | 0.76 |
| 12 | 4.0 | 8.5 | 0.70 | 0.42 | 0.09 | 3.11 | -0.06 | 2.59 | 0.76 |
| 16 | 2.0 | 8.0 | 0.68 | 0.30 | 0.08 | 4.64 | 0.40 | 3.57 | 1.07 |
| 16 | 5.0 | 10.5 | 0.68 | 0.30 | 0.08 | 4.72 | 0.43 | 3.65 | 1.11 |

are by gravity. As the wind speed increases, the response in the plane of the rotor increases. It can be observed that the mean of the blade root in-plane bending moment is almost constant at all wind speeds. The mean bending moment is mainly due to the weight of the blade and its rotation rate. The maximum blade root in-plane bending moment increases with wind speed due to the associated increase in turbulence. As the mean hub-height longitudinal wind speed increases, turbulence levels increase to maintain a specified turbulence intensity. This is what causes higher maximum at the higher winds. The standard deviation shows the same variation as the response maxima, with slightly smaller increases with wind speed.

Table 3.6 summarizes various response statistics (including the maximum, mean, standard deviation, peak factor, skewness, kurtosis, and mean upcrossing rate) from fifteen one-hour simulations of the blade root

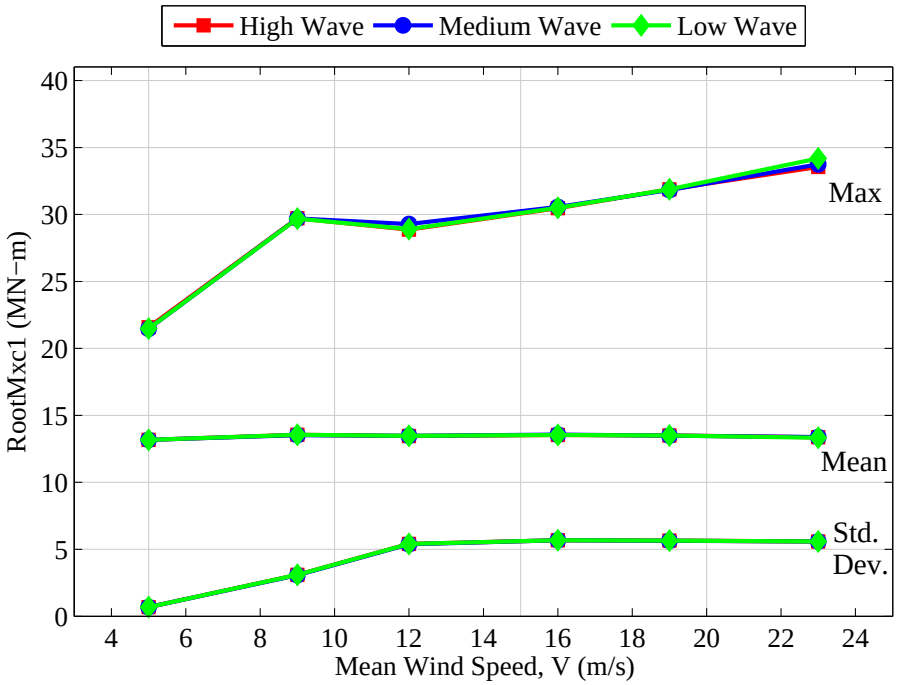


Figure 3.8: Ensemble one-hour statistics for the blade root in-plane bending moment in eighteen sea states.

in-plane bending moment for the five most critical sea states out of the eighteen studied. The mean for all the sea states is almost the same because the mean is mainly affected by the weight of the blade and its rotation rate. The maximum increases with increasing winds from 19 m/s to 23 m/s. Negligible increase in response maxima are seen with changes in the wave height. The standard deviation is almost same for the five critical sea states.

The peak factors for the one-hour simulations are quite comparable for the five critical sea states. The skewness, kurtosis, and mean upcrossing rate

are also comparable for these five sea states and, hence, the peak factor shows slight variation. Overall, the highest blade root in-plane bending moments occurred at the highest wind speeds with highest wave heights. Interestingly, the kurtosis values are far from the Gaussian value of 3.0; this blade root in-plane bending moment is a fairly periodic process and has a kurtosis close to that of a sine wave for which the kurtosis is 1.5.

Table 3.6: Ensemble statistics of the blade root in-plane bending moment from fifteen one-hour simulations for 5 critical sea states

| V | $H_s$ | $T_p$ | Blade Root In-Plane Bending Moment (RootMxc1) Statistics | | | | | | |
|---|---|---|---|---|---|---|---|---|---|
| | | | Max | Mean | SD | Peak Factor | Skew-ness | Kurt-osis | Mean Upcrossing Rate |
| (m/s) | (m) | (sec) | (MN-m) | (MN-m) | (MN-m) | | | | ($s^{-1}$) |
| 19 | 3.5 | 7.5 | 31.83 | 5.64 | 13.49 | 1.94 | 0.01 | 1.57 | 0.74 |
| 19 | 5.0 | 9.0 | 31.87 | 5.65 | 13.50 | 1.94 | 0.01 | 1.57 | 0.74 |
| 23 | 2.5 | 6.5 | 33.55 | 5.59 | 13.37 | 2.09 | 0.00 | 1.62 | 0.75 |
| 23 | 4.0 | 7.5 | 33.75 | 5.59 | 13.38 | 2.10 | 0.00 | 1.62 | 0.75 |
| 23 | 5.5 | 11 | 34.19 | 5.59 | 13.34 | 2.14 | 0.01 | 1.62 | 0.75 |

#### 3.4.2.4 Blade Root Out-of-Plane Bending Moment

Figure 3.9 summarizes ensemble statistics (maximum, mean, and standard deviation) from fifteen one-hour simulations of the blade root out-of-plane bending moment for all the selected eighteen sea states. The mean blade root out-of-plane bending moment shows similar behavior as was seen with the blade tip out-of-plane deflection and the tower top fore-aft

deflection; it increases with increasing wind speeds up to rated and decreases thereafter due to the pitch control characteristics of the wind turbine that take effect above the rated wind speed of 11.3 m/s. The mean blade root out-of-plane bending moment is largest around the rated wind speed. No effect of variations in wave heights is observed in the mean response. The maximum response also follows the same trend as the mean, with largest maximum occurring for wind speeds around rated. Small variations with wave height are seen for the maximum values of blade root out-of-plane bending moment.The standard deviation shows a slight increase with increasing wind speed. Due to this monotonic increase in standard deviation with wind speed, the maximum values show a less significant decrease above the rated wind speed compared to the decrease seen for the mean response.

Table 3.7 summarizes various response statistics (including the maximum, mean, standard deviation, peak factor, skewness, kurtosis, and mean upcrossing rate) from fifteen one-hour simulations of the blade root out-of-plane bending moment for the five most critical sea states out of the eighteen studied. The mean blade root out-of-plane bending moment increases with wind speed and then decreases for above-rated wind speeds. Increasing the wave height has a very small effect on the mean response. Comparing statistics for the third sea state ($V$=12 m/s, $H_s$=2.5 m) with those for the fifth sea state ($V$=16 m/s, $H_s$=3.5 m), we note that the mean decreases by about 35% from the third sea state to the fifth. This occurs due to the blade pitch control. The standard deviation values for these two sea

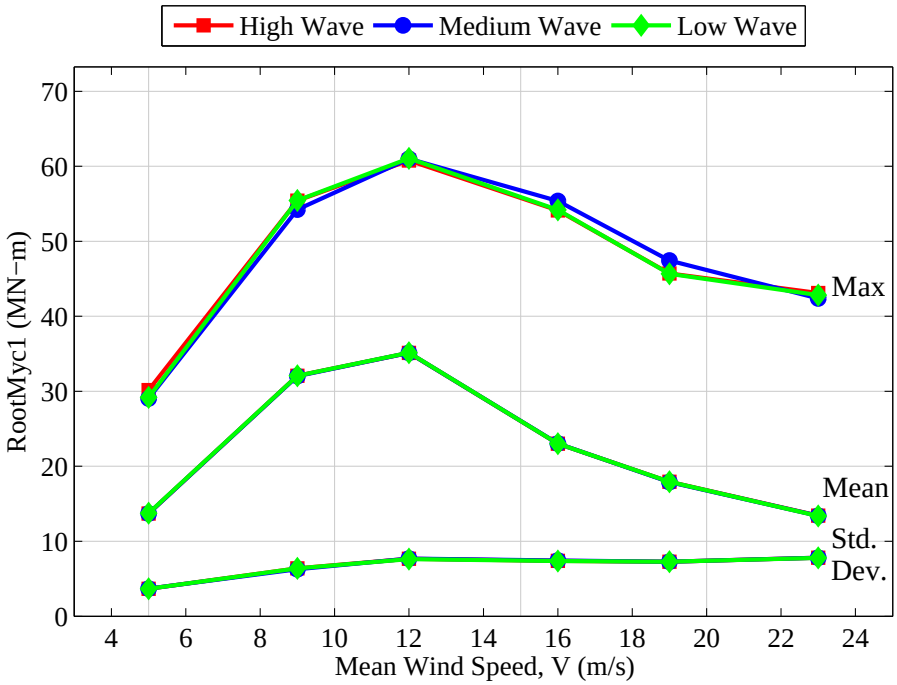


Figure 3.9: Ensemble one-hour statistics for the blade root out-of-plane bending moment in eighteen sea states.

states are comparable.

Even though the mean response decreases significantly, the maximum response decreases by only about 10% from $V$=12 m/s to $V$=16 m/s. This is because the peak factor on the one-hour maximum response is seen to increase by about 30% when we go from $V$=12 m/s to $V$=16 m/s. It is the significantly larger skewness for $V$=16 m/s that causes the peak factor to increase significantly. The mean upcrossing rates are not very different for the different sea states. In summary, the highest blade root out-of-plane

bending moment occurs around the rated wind speed; the extremes show a slight decrease as the wind speeds exceed the rated wind speed.

Table 3.7: Ensemble statistics of the blade root out-of-plane bending moment from fifteen one-hour simulations for 5 critical sea states

| V (m/s) | $H_s$ (m) | $T_p$ (sec) | Blade Root Out-of-Plane Bending Moment (RootMyc1) Statistics | | | | | | |
|---|---|---|---|---|---|---|---|---|---|
| | | | Max (MN-m) | Mean (MN-m) | SD (MN-m) | Peak Factor | Skew-ness | Kurt-osis | Mean Upcrossing Rate ($s^{-1}$) |
| 9 | 4.0 | 9.5 | 55.43 | 32.08 | 6.39 | 3.66 | 0.08 | 2.76 | 1.75 |
| 12 | 1.0 | 6.0 | 60.78 | 35.13 | 7.66 | 3.35 | -0.04 | 2.73 | 1.42 |
| 12 | 2.5 | 7.0 | 61.06 | 35.15 | 7.63 | 3.40 | -0.04 | 2.71 | 1.41 |
| 12 | 4.0 | 8.5 | 61.01 | 35.11 | 7.70 | 3.37 | -0.05 | 2.72 | 1.42 |
| 16 | 3.5 | 8.5 | 55.38 | 23.03 | 7.44 | 4.35 | 0.20 | 3.06 | 1.46 |

#### 3.4.2.5 Tower Base Side-to-Side Bending Moment

Figure 3.10 summarizes ensemble statistics (maximum, mean, and standard deviation) from fifteen one-hour simulations of the tower base side-to-side bending moment for all the selected eighteen sea states. The maximum tower base side-to-side bending moment increases significantly with increasing wind speed. This is expected because the in-plane bending moments are not affected by pitching of the blades. Maximum values show a slight increase with increase in wave height. The mean response also shows an increase with wind speeds, but this increase is not as significant as is the case with the maxima. There seems to be almost no influence of the wave

height on the mean tower base side-to-side bending moment. The standard deviation is almost constant for wind speeds up to 12 m/s, after which it increases with increasing wind speeds. This increase in the standard deviation with wind speed along with the increase in the mean with speed causes the maximum to increase significantly with wind speed. There is only a very small increase in standard deviation values with increasing wave heights.

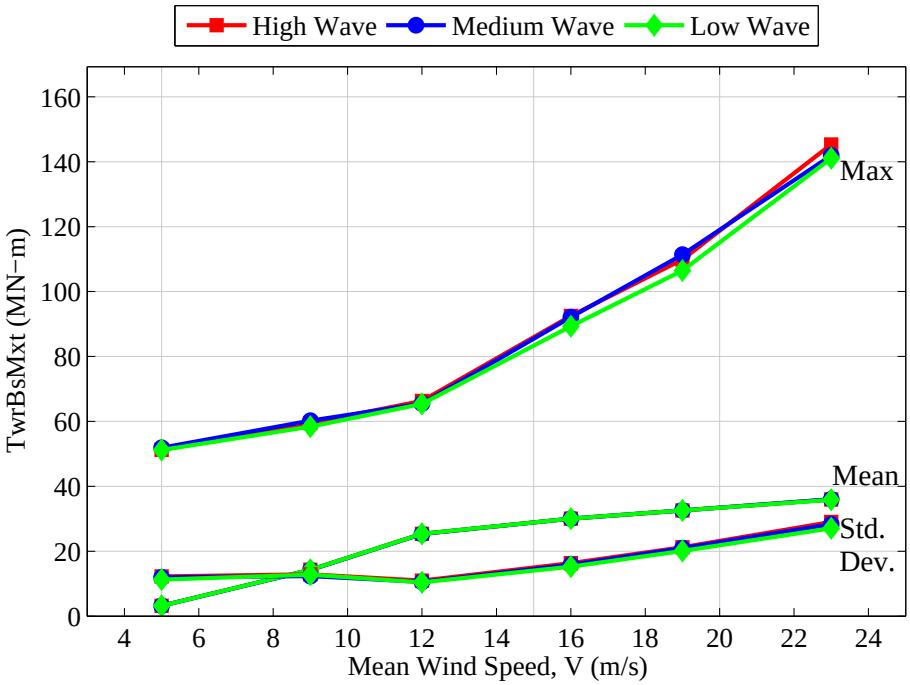


Figure 3.10: Ensemble one-hour statistics for the tower base side-to-side bending moment in eighteen sea states.

Table 3.8 summarizes various response statistics (including the

maximum, mean, standard deviation, peak factor, skewness, kurtosis, and mean upcrossing rate) from fifteen one-hour simulations of the tower base side-to-side bending moment for the five most critical sea states out of the eighteen studied. Comparing the second ($V$=19 m/s, $H_s$=3.5 m) and the fourth ($V$=23 m/s, $H_s$=4.0 m) sea states, the mean response is seen to increase by 8% from 32.59 MN-m to 36.03 MN-m in going from $V$=19 m/s to $V$=23 m/s. The standard deviation values increase by 33% from 20.96 MN-m to 28.31 MN-m in going from $V$=19 m/s to $V$=23 m/s. Together, these two effects cause the maximum value to increase by 22% from 111.37 MN-m to 141.93 MN-m in going from $V$=19 m/s to $V$=23 m/s.

The peak factor on the one-hour extreme response remains comparable for all the sea states. Skewness values are close to zero and kurtosis values are close to 3; this suggests an almost Gaussian response. Mean upcrossing rates are comparable for all five sea states. Overall, the highest tower base side-to-side bending moments occurs at the highest winds (close to cut-out) and with the highest wave heights.

#### 3.4.2.6 Tower Base Fore-Aft Bending Moment

Figure 3.11 summarizes ensemble statistics (maximum, mean, and standard deviation) from fifteen one-hour simulations of the tower base fore-aft bending moment for all the selected eighteen sea states. The mean tower base fore-aft bending moment shows similar behavior to that of the blade tip out-of-plane deflection, the tower top fore-aft deflection, and the

Table 3.8: Ensemble statistics of the tower base side-to-side bending moment from fifteen one-hour simulations for 5 critical sea states

| V (m/s) | $H_s$ (m) | $T_p$ (sec) | Tower Base Side-to-Side Bending Moment (TwrBsMxt) Statistics | | | | | | |
|---|---|---|---|---|---|---|---|---|---|
| | | | Max (MN-m) | Mean (MN-m) | SD (MN-m) | Peak Factor | Skew-ness | Kurt-osis | Mean Upcrossing Rate ($s^{-1}$) |
| 19 | 2.0 | 7.0 | 109.89 | 32.57 | 21.21 | 3.65 | 0.00 | 2.95 | 1.79 |
| 19 | 3.5 | 7.5 | 111.37 | 32.59 | 20.96 | 3.76 | 0.01 | 2.99 | 1.82 |
| 23 | 2.5 | 6.5 | 145.33 | 35.96 | 28.99 | 3.79 | -0.01 | 3.00 | 1.75 |
| 23 | 4.0 | 7.5 | 141.93 | 36.03 | 28.31 | 3.74 | -0.02 | 3.00 | 1.77 |
| 23 | 5.5 | 11 | 141.07 | 35.84 | 27.09 | 3.89 | 0.01 | 3.09 | 1.83 |

blade root out-of-plane bending moment. The mean response increases with wind speed up to the rated wind speed, after which blade pitch control comes into effect which causes a decrease in the tower base bending moment. The mean response is largest around the rated wind speed and shows no variation with wave height. The maximum of the tower base fore-aft bending moment shows the same trend as the mean; the decrease above rated winds is not as significant as is the case for the mean response. There is a slight variation in response maxima with wave height. The standard deviation response is almost constant for all wind speeds and shows very slight variation with wave height. The largest mean and one-hour extreme response occur around the rated wind speed.

Table 3.9 summarizes various response statistics (including the

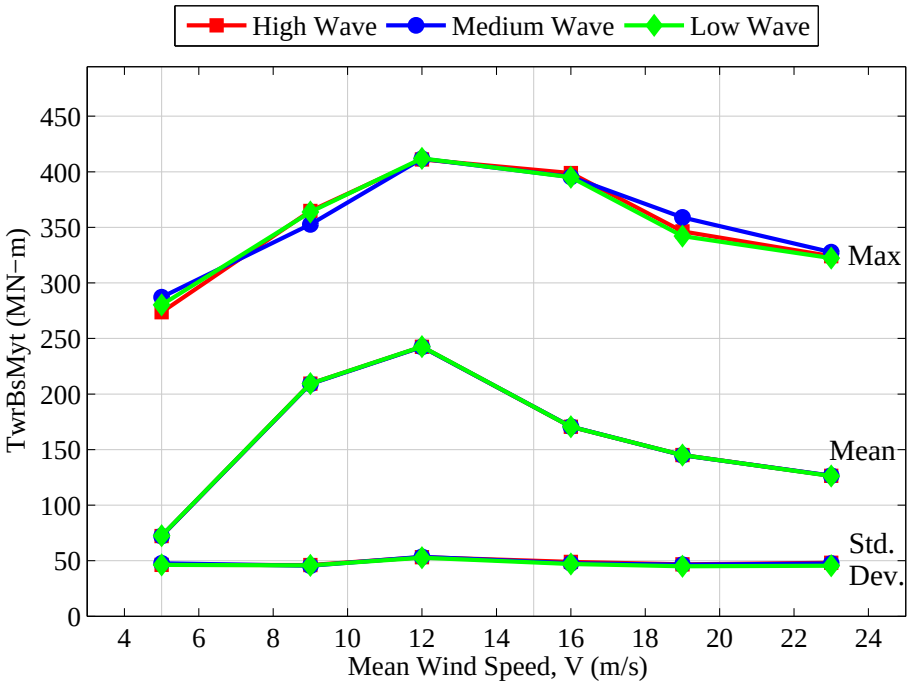


Figure 3.11: Ensemble one-hour statistics for the tower base fore-aft bending moment in eighteen sea states.

maximum, mean, standard deviation, peak factor, skewness, kurtosis, and mean upcrossing rate) from fifteen one-hour simulations of the tower base fore-aft bending moment for the five most critical sea states out of the eighteen studied. The mean is highest at 12 m/s (around the rated wind speed), and decreases significantly at a wind speed of 16 m/s. Comparing response statistics of the fourth sea state ($V$=12 m/s, $H_s$=4.0 m) with the fifth sea state ($V$=16 m/s, $H_s$=5.0 m), the mean decreases by 30% from 242.66 MN-m to 170.63 MN-m in going from $V$=12 m/s to $V$=16 m/s; this is

due to the blade pitch control. The standard deviation decreases by 10% from the fourth to the fifth sea state. The peak factor increases by 50%, due to significant changes in the skewness, kurtosis, and mean upcrossing rate. Even though the standard deviation decreases, the product of the peak factor and the standard deviation is much larger for $V$=16 m/s (224 MN-m) than for $V$=12 m/s (170 MN-m). This results in the total effect of a decrease in response maximum by only 4% compared to a decrease in mean by 30% going from $V$=12 m/s to $V$=16 m/s. In summary, the highest tower base fore-aft bending moment occurs around the rated wind speed with slightly decreasing response maxima with increasing winds.

Table 3.9: Ensemble statistics of the tower base fore-aft bending moment from fifteen one-hour simulations for 5 critical sea states

| V | $H_s$ | $T_p$ | Tower Base Fore-Aft Bending Moment (TwrBsMyt) Statistics | | | | | | |
|---|---|---|---|---|---|---|---|---|---|
| | | | Max | Mean | SD | Peak Factor | Skew-ness | Kurt-osis | Mean Upcrossing Rate |
| (m/s) | (m) | (sec) | (MN-m) | (MN-m) | (MN-m) | | | | ($s^{-1}$) |
| 9 | 1.0 | 7.0 | 364.76 | 209.35 | 46.11 | 3.38 | -0.04 | 2.93 | 1.29 |
| 12 | 1.0 | 6.0 | 411.09 | 242.49 | 53.18 | 3.18 | -0.08 | 2.61 | 1.12 |
| 12 | 2.5 | 7.0 | 411.81 | 242.33 | 53.56 | 3.17 | -0.08 | 2.57 | 1.09 |
| 12 | 4.0 | 8.5 | 412.05 | 242.66 | 52.64 | 3.22 | -0.06 | 2.61 | 1.11 |
| 16 | 5.0 | 10.5 | 395.01 | 170.63 | 47.02 | 4.77 | 0.42 | 3.63 | 1.50 |

#### 3.4.2.7 Platform Surge Motion

Figure 3.12 summarizes ensemble statistics (maximum, mean, and standard deviation) from fifteen one-hour simulations of the platform surge motion for all the selected eighteen sea states. The mean platform surge motion first increases with increasing wind speed up to the rated wind speed of 11.3 m/s; it decreases thereafter due to the blade pitch control effects. The largest response occurs around the rated wind speed of the wind turbine. There is negligible effect of wave height on the mean platform surge. The maximum surge motion follows the same variation with wind speed as the mean surge motion, decreasing significantly above the rated wind speed. There is a very slight variation in the maximum platform surge motion with wave height. The standard deviation is very small in comparison with the mean and maximum response; it decreases slightly with increasing wind speed. The largest extreme response in surge motion occurs around the rated wind speed.

Table 3.10 summarizes various response statistics (including the maximum, mean, standard deviation, peak factor, skewness, kurtosis, and mean upcrossing rate) from fifteen one-hour simulations of the platform surge motion for the five most critical sea states out of the eighteen studied. The mean surge response is highest around 12 m/s and shows negligible variation with wave height. Comparing the fourth ($V$=12 m/s, $H_s$=4.0 m) and fifth ($V$=16 m/s, $H_s$=3.5 m) sea states, the mean surge response is seen to decrease by 25% from 17.43 m to 13.03 m in going from $V$=12 m/s to

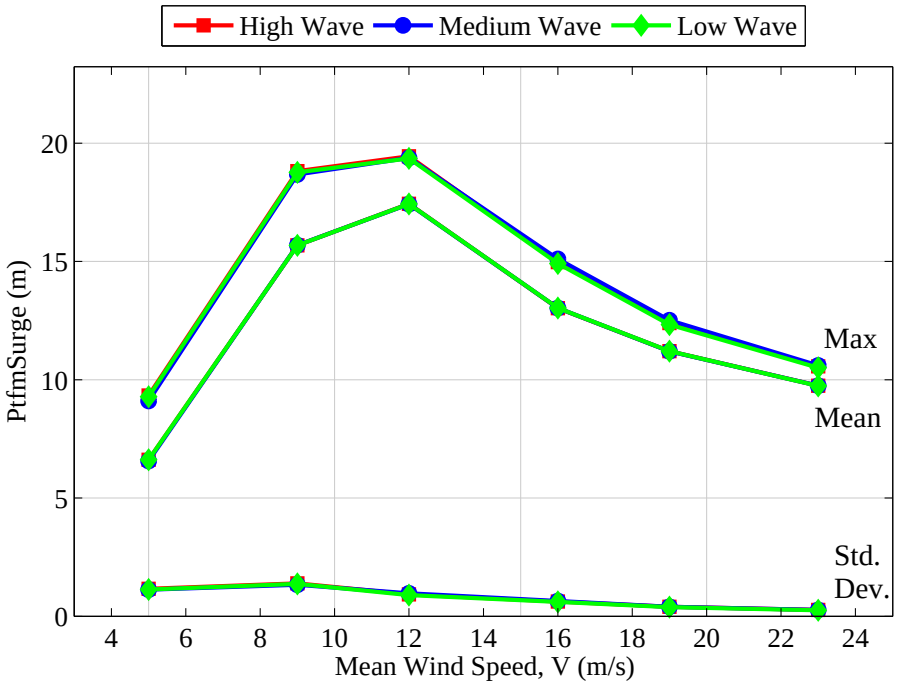


Figure 3.12: Ensemble one-hour statistics for the platform surge motion in eighteen sea states.

$V$=16 m/s. The standard deviation also decreases by 28%. The peak factor, however, increases by about 51% due to the significant increase in skewness, kurtosis, and mean upcrossing rate. The products of the standard deviation and the peak factor for both these sea states are comparable in value; therefore, the overall maximum decrease by 22% from 19.36 m to 15.10 m in going from $V$=12 m/s to $V$=16 m/s. Overall, the platform surge motion is affected by the wind speed; surge motions are highest around the rated wind speed of the wind turbine.

Table 3.10: Ensemble statistics of the platform surge motion from fifteen one-hour simulations for 5 critical sea states

| V (m/s) | $H_s$ (m) | $T_p$ (sec) | Platform Surge Motion (PtfmSurge) Statistics | | | | | | |
|---|---|---|---|---|---|---|---|---|---|
| | | | Max (m) | Mean (m) | SD (m) | Peak Factor | Skew-ness | Kurt-osis | Mean Upcrossing Rate ($s^{-1}$) |
| 9 | 4.0 | 9.5 | 18.77 | 15.68 | 1.37 | 2.29 | -0.03 | 2.49 | 0.01 |
| 12 | 1.0 | 6.0 | 19.44 | 17.43 | 0.93 | 2.21 | -0.25 | 2.57 | 0.03 |
| 12 | 2.5 | 7.0 | 19.38 | 17.42 | 0.97 | 2.06 | -0.23 | 2.38 | 0.02 |
| 12 | 4.0 | 8.5 | 19.36 | 17.43 | 0.90 | 2.16 | -0.31 | 2.71 | 0.02 |
| 16 | 3.5 | 8.5 | 15.10 | 13.03 | 0.65 | 3.27 | 0.57 | 3.77 | 0.04 |

#### 3.4.2.8 Platform Pitch Motion

Figure 3.13 summarizes ensemble statistics (maximum, mean, and standard deviation) from fifteen one-hour simulations of the platform pitch motion for all the selected eighteen sea states. The mean platform pitch motion first increases with wind speed up to the rated wind speed of 11.3 m/s; at higher wind speeds, it decreases due to blade pitch control effects for above-rated wind speeds. Platform pitch motion is largest around the rated wind speed of the wind turbine and shows significant variation with wave height, especially at high wind speeds. The standard deviation increases with wind speed up to rated and remains almost constant thereafter. The standard deviation response shows slight variation with wave height. The largest extreme platform pitch motion occurs, as expected, around the rated wind speed.

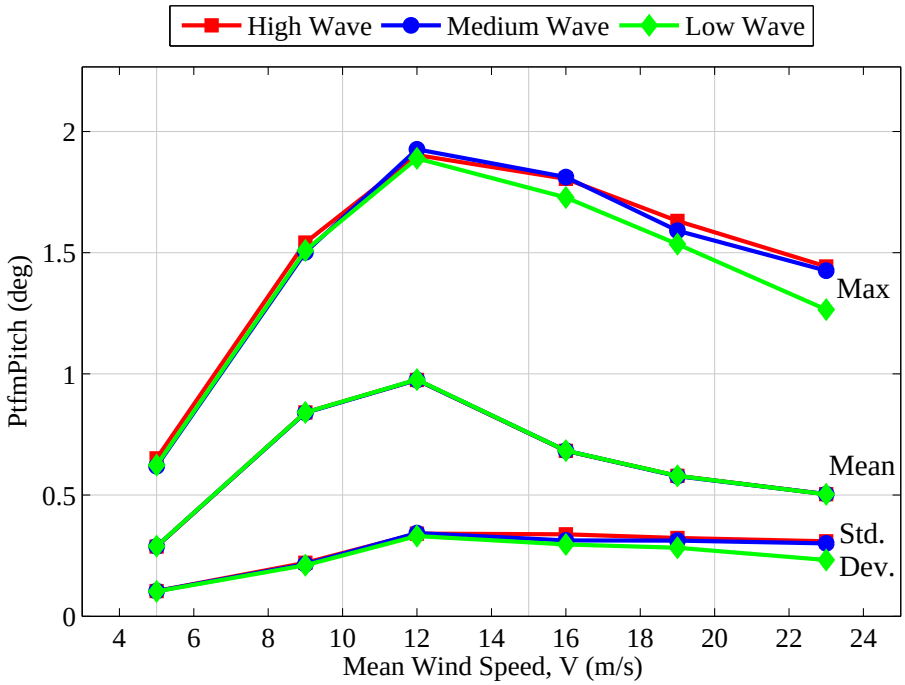


Figure 3.13: Ensemble one-hour statistics for the platform pitch motion in eighteen sea states.

Table 3.11 summarizes various response statistics (including the maximum, mean, standard deviation, peak factor, skewness, kurtosis, and mean upcrossing rate) from fifteen one-hour simulations of the platform pitch motion for the five most critical sea states out of the eighteen studied. The mean platform pitch motion is highest around the rated wind speed. Comparing the fourth ($V$=12 m/s, $H_s$=4.0 m) and fifth ($V$=16 m/s, $H_s$=5.0 m) sea states, the mean pitch motion is seen to decrease by 30% from 0.98 degrees to 0.68 degrees in going from $V$=12 m/s to $V$=16 m/s. The standard

deviation decreases by 10% in going from $V$=12 m/s to $V$=16 m/s. The peak factor on the one-hour extreme response shows a significant increase of 28% in going from $V$=12 m/s to $V$=16 m/s. This is because the skewness changes significantly, while the kurtosis and mean upcrossing rate increase slightly. The product of the standard deviation and the peak factor increases by about 10% in going from $V$=12 m/s to $V$=16 m/s. The maximum, however, decreases by 8% from 1.89 degrees to 1.73 degrees in going from $V$=12 m/s to $V$=16 m/s. In summary, the largest platform pitch motion occurs around the rated wind speed and shows significant variation with wave height.

Table 3.11: Ensemble statistics of the platform pitch motion from fifteen one-hour simulations for 5 critical sea states

| V (m/s) | $H_s$ (m) | $T_p$ (sec) | Platform Pitch Motion (PtfmPitch) Statistics | | | | | | |
|---|---|---|---|---|---|---|---|---|---|
| | | | Max (deg) | Mean (deg) | SD (deg) | Peak Factor | Skew-ness | Kurt-osis | Mean Upcrossing Rate ($s^{-1}$) |
| 9 | 1.0 | 7.0 | 1.54 | 0.84 | 0.22 | 3.18 | 0.09 | 2.86 | 0.12 |
| 12 | 1.0 | 6.0 | 1.90 | 0.98 | 0.34 | 2.73 | -0.20 | 2.87 | 0.15 |
| 12 | 2.5 | 7.0 | 1.93 | 0.97 | 0.34 | 2.78 | -0.18 | 2.81 | 0.15 |
| 12 | 4.0 | 8.5 | 1.89 | 0.98 | 0.33 | 2.76 | -0.22 | 2.86 | 0.14 |
| 16 | 5.0 | 10.5 | 1.73 | 0.68 | 0.30 | 3.52 | 0.19 | 3.23 | 0.17 |

### 3.4.3 Natural Frequencies of the System and Power Spectra

Power spectral density function plots can be useful to identify the natural frequencies of the system. Figures 3.14, 3.15, and 3.16 show power

spectral density function plots for blade root out-of-plane and in-plane bending moments, for tower base fore-aft and side-to-side bending moments, and for platform surge and pitch motions.

Important peaks in the power spectra are seen at 1P (corresponding to the rotor rotation rate of 0.12 Hz) and multiples thereof (see power spectra for the blade root out-of-plane and in-plane bending moments). The first blade flapwise (out-of-plane) mode's natural frequency is 0.5 Hz, which can be seen in the blade and tower bending moment power spectra. A peak at the first blade edgewise (in-plane) natural frequency of 0.70 Hz is also seen in the power spectra. The tower has the same natural frequencies in both the fore-aft (out-of-plane) and side-to-side (in-plane) directions; this is because of symmetry. The tower first and second natural frequencies of 0.27 Hz and 2.36 Hz, respectively, are evident in the two tower base bending moment power spectra.

It can be seen by comparing Table 2.2 and Figures 3.14-3.16 that the natural frequencies of the tower have increased for the system with the semi-submersible offshore floating platform compared to the land-based turbine. This happens because the tower is not fixed at the base any more and is allowed to move, even if it is still connected to the platform. Therefore, the tower moves along with the platform motions and this causes its natural frequencies to change. Blade natural frequencies also change in a similar manner although the differences are quite small because there is a small effect of the platform on the blades. The 1P peaks and multiples thereof are still the same because

the rotor rotation rate for wind speeds above rated is still maintained.

For different response variables studied here, the inflow wind has different contributions. The platform surge and pitch motions, due to the size of the platform, show very slow response compared to the blades and tower. The dominant wave energy is at a frequency of about 0.10 Hz, which is much higher than the low surge natural frequency (around 0.009 Hz) and even the low pitch natural frequency (around 0.03 Hz). It is obvious that for excitation frequencies much higher than a system natural frequency, the response will not be in phase with the excitation. Hence, response levels are low and out of phase with the excitation.

To understand the effects of the inflow wind field on the integrated system response in greater detail, Figure 3.17 compares various response power spectra for different one-hour average hub-height longitudinal wind speeds of 5 m/s, 9 m/s and 12 m/s, while the significant wave height is held constant at 2.5 m. It is evident that the blade and tower loads show an increase in energy, represented by the increased variance or area under the power spectrum curve, with increasing wind speed. The tower load increase in energy is comparatively less than the increase in energy (variance) for the blade loads. The platform motions' power spectra also show significant increases in energy with increasing wind speeds. The platform pitch motion shows very significant increases in energy with increasing wind speeds.

Understanding the effects of changing wave heights on the integrated system response is also useful. Figure 3.18 shows a comparison of various

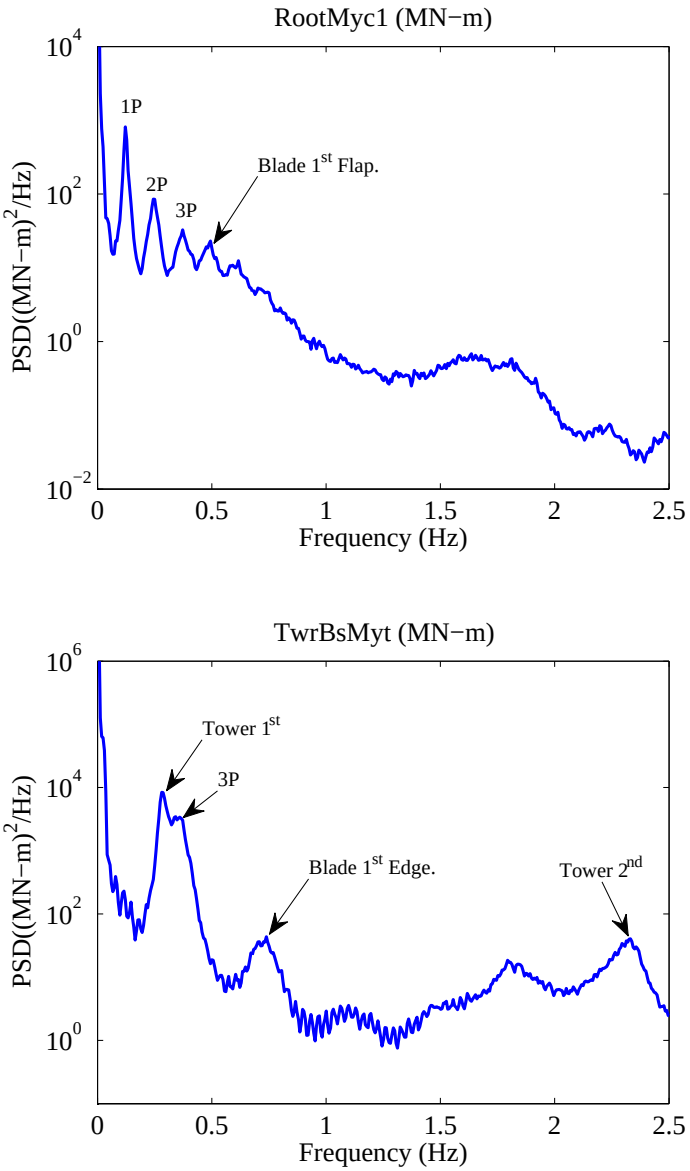


Figure 3.14: Power spectral density functions of the blade root out-of-plane bending moment and the tower base fore-aft bending moment showing identified natural frequencies for a particular sea state ($V$=12 m/s, $H_S$=4.0 m, $T_P$=8.5 sec).

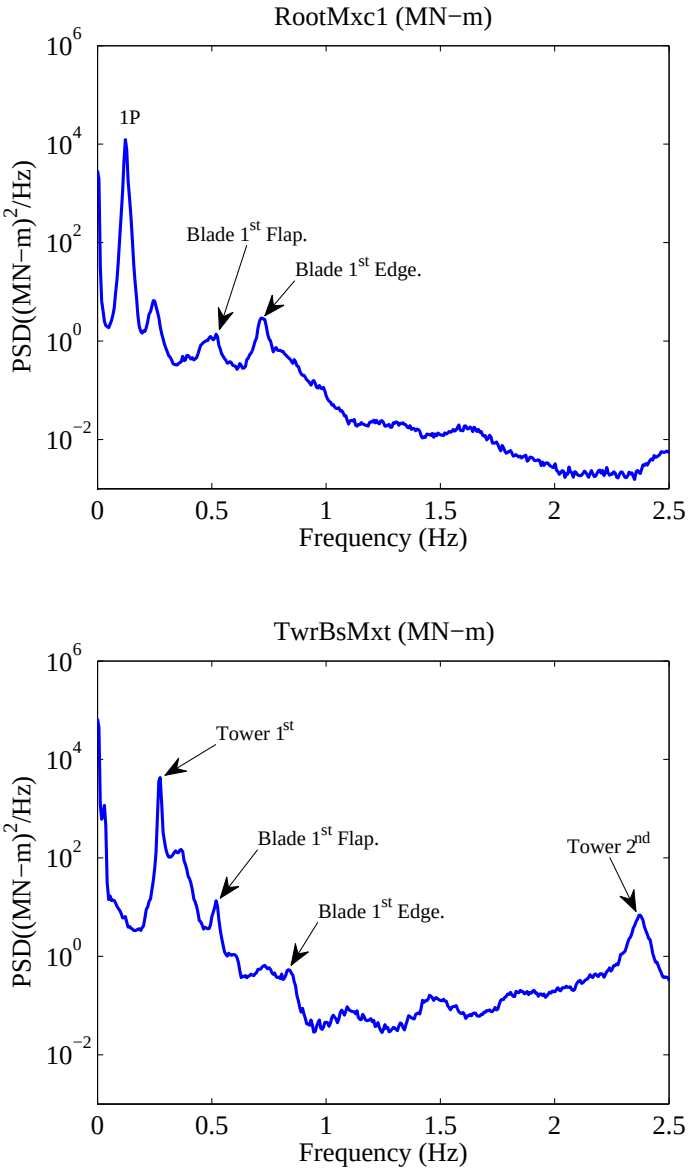


Figure 3.15: Power spectral density functions of the blade root in-plane bending moment and the tower base side-to-side bending moment showing identified natural frequencies for a particular sea state ($V$=12 m/s, $H_S$=4.0 m, $T_P$=8.5 sec).

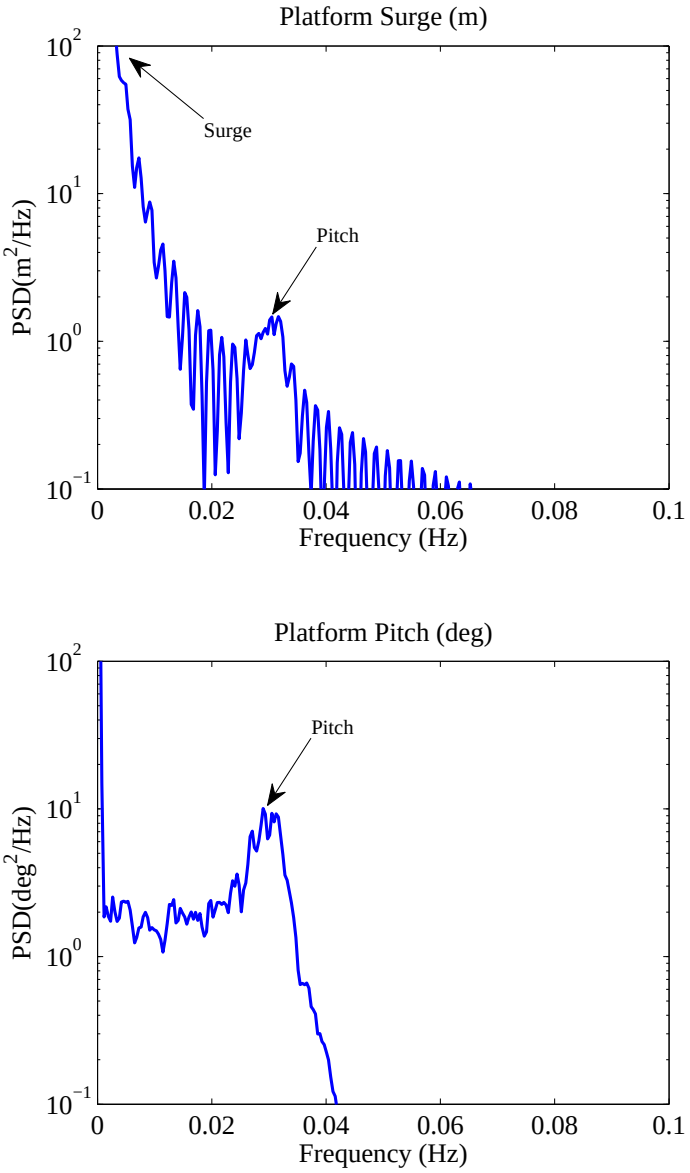


Figure 3.16: Power spectral density functions of the platform surge and pitch motions showing identified natural frequencies for a particular sea state ($V$=12 m/s, $H_S$=4.0 m, $T_P$=8.5 sec).

response power spectra for significant wave heights of 1.0 m, 2.5 m and 4.0 m, while the one-hour average hub-height longitudinal wind speed is kept constant at 12 m/s. As the significant wave height is changed, there are expected changes in the power spectra for the wave elevation. It can be observed, however, that most of the system response power spectra are insensitive to wave height changes. The platform motions, however, show small variations with wave height. If wave heights are increased significantly compared to the levels used here (based on the selected site), it is possible that greater response levels will result.

## 3.5 Summary

In this chapter, we focused on estimating the short-term extreme response for a 13.2 MW offshore wind turbine supported by a semi-submersible floating platform and a mooring system. For the selected site, various response variables of the wind turbine system were studied. We identified important combinations of wind speeds and wave heights that cause extreme response levels for this site. We also identified important natural frequencies of the system and assessed the importance of different wind speeds and different wave heights on the system through time-domain and frequency-domain analysis. By studying these various response statistics and spectra, conclusions can be made regarding design drivers for all the blade and tower loads and for the platform motions.

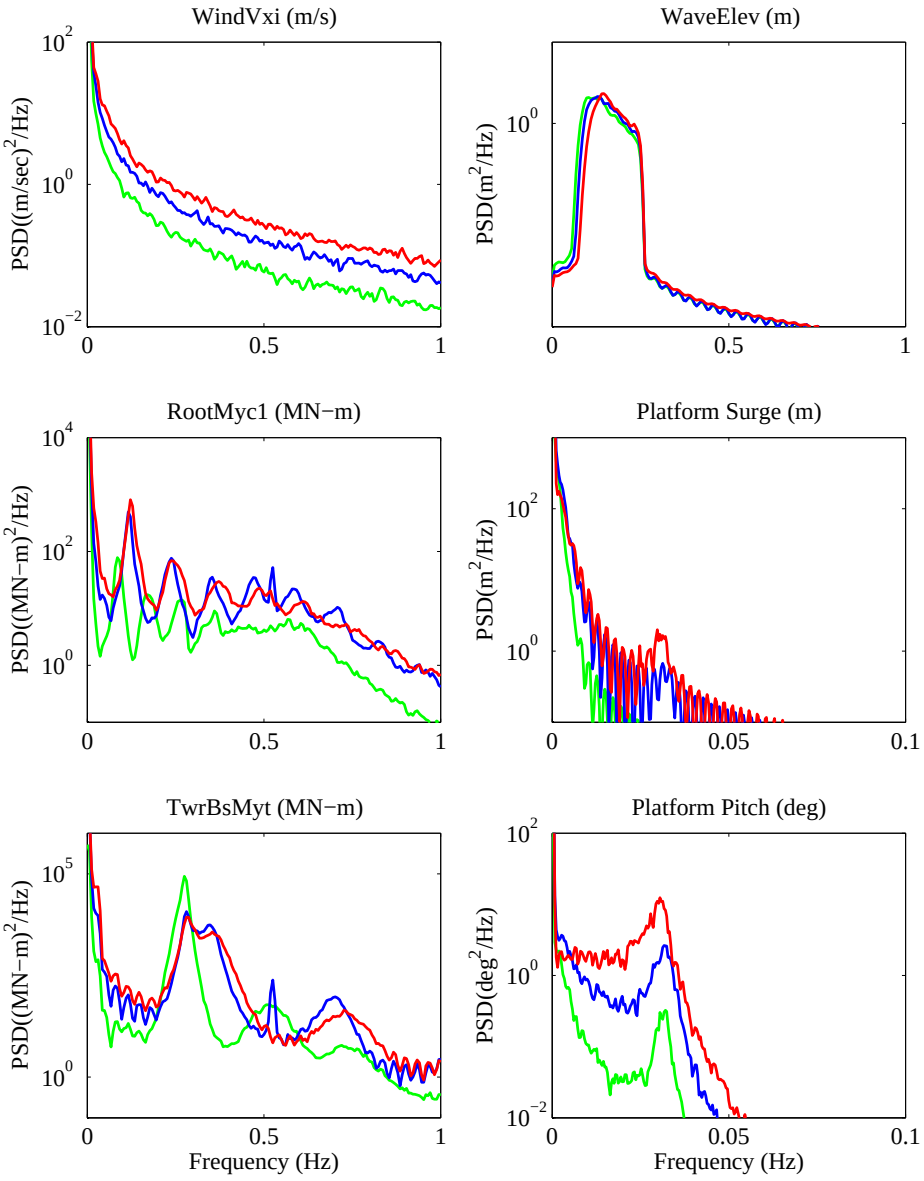


Figure 3.17: Variation in power spectral density functions of the hub-height longitudinal wind speed, wave elevation, and various other system response variables as the one-hour average hub-height longitudinal wind speed is changed for a fixed significant wave height of 2.5 m (green: $V$=5 m/s, blue: $V$=9 m/s, red: $V$=12 m/s).

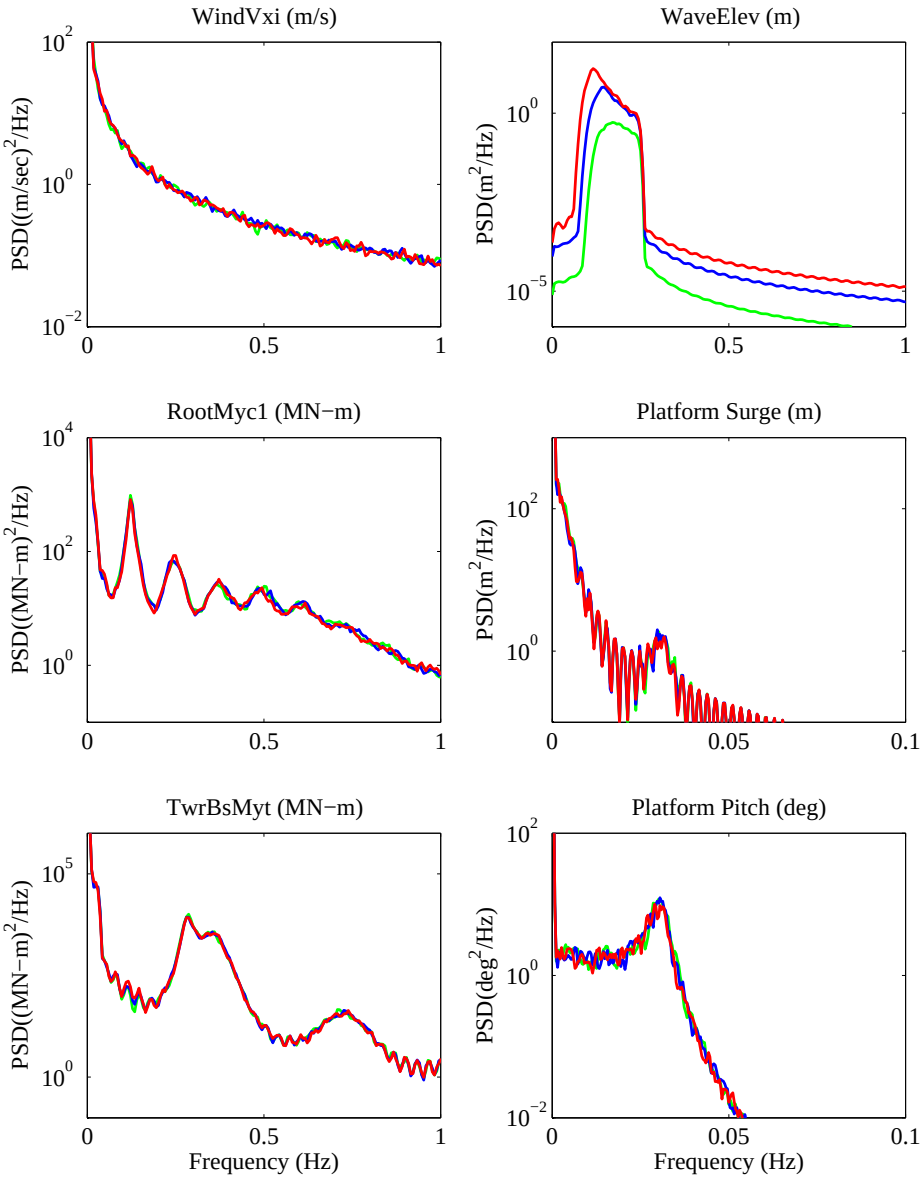


Figure 3.18: Variation in power spectral density functions of the hub-height longitudinal wind speed, wave elevation, and various other system response variables as the significant wave height is changed for a fixed one-hour average hub-height longitudinal wind speed of 12 m/s (green: $H_S$=1 m, blue: $H_S$=2.5 m, red: $H_S$=4.0 m)

# Chapter 4

# Additional Comparison Studies with the Integrated Turbine-Platform-Mooring System

The Sandia 13.2 MW wind turbine is a very large turbine that is best suited for operation in an offshore environment. To understand the behavior of this integrated offshore wind turbine system with semi-submersible platform and mooring lines, it is important to compare its behavior with other established models of wind turbine systems. It is also useful to study its behavior when changes in some system parameters or in the loading are introduced . This chapter presents comparisons based on stochastic simulations of the 13.2 MW offshore wind turbine with (i) a land-based 13.2 MW turbine installation [9]; and (ii) the same 13.2 MW offshore wind turbine system but with controller turned off. Additionally, for steady non-turbulent wind fields, two studies are undertaken—one, for a sea state with significantly higher waves than were analyzed for the selected site; the other, a direct comparison with the OC4 5 MW offshore wind turbine system.

These comparison studies can help understand key response variables whose behavior might greatly influence the performance of the integrated wind

turbine system. The comparison with the land-based turbine highlights the influence of the offshore environment. The comparison with the same system with controller turned off highlights the role of the control system. Simulation studies for a more severe sea state help test the integrated system design in more demanding environmental conditions. Finally, comparisons with the smaller OC4 5 MW offshore wind turbine system [8] serve to illustrate the influence of scaling and model size.

These comparison studies also help us to gain an understanding of the various system vibration modes and their interaction with incident wind and wave loading which, in turn, can help us better understand overall system behavior and make model refinements.

## 4.1 Comparison Studies involving Stochastic Simulations

Stochastic simulations are performed for the 13.2 MW offshore wind turbine to compare its response with: (i) a land-based 13.2 MW land-based turbine; and (ii) the same 13.2 MW offshore system but with controller turned off. We discuss these comparison studies next.

### 4.1.1 Influence of the Offshore Environment versus Land

As we move from land to offshore, it is expected that the offshore system will experience higher loads. Figure 4.1 shows various simulated time series for the 13.2 MW offshore wind turbine system compared with the land-based

13.2 MW wind turbine, assuming the same incident wind fields. The average hub-height longitudinal wind speed is 12 m/s while no waves are incident at the offshore turbine. It can observed that the behavior of the blades and the tower is similar in both cases. The blade tip out-of-plane deflection and blade root out-of-plane bending moment show only with very small differences due to introduction of the platform in the offshore case. The tower-top fore-aft displacement and tower-base fore-aft bending moment also show similar behavior; the response is higher in the offshore environment. This is due to the introduction of additional degrees of freedom at the base of the tower, by virtue of the floating platform, which causes the tower response to increase as the platform pitches.

Figure 4.2 shows power spectral density function plots for the blade root out-of-plane bending moment and the tower-base fore-aft bending moment for the 13.2 MW offshore and the same land-based turbine. Peaks at natural frequencies of the turbine system can be identified in the spectra. The natural frequencies associated with blade bending are the same for both the cases, while tower frequencies are slightly on land versus offshore. This is due to the additional flexibility at the base of the tower introduced in the offshore case, which also changes the mode shapes of the tower. In both the power spectra plots, the overall energy content is quite similar due to the identical incident wind fields.

Table 4.1 shows mean and maximum values of the blade tip out-of-plane deflection, the tower-top fore-aft displacement, the blade root out-of-

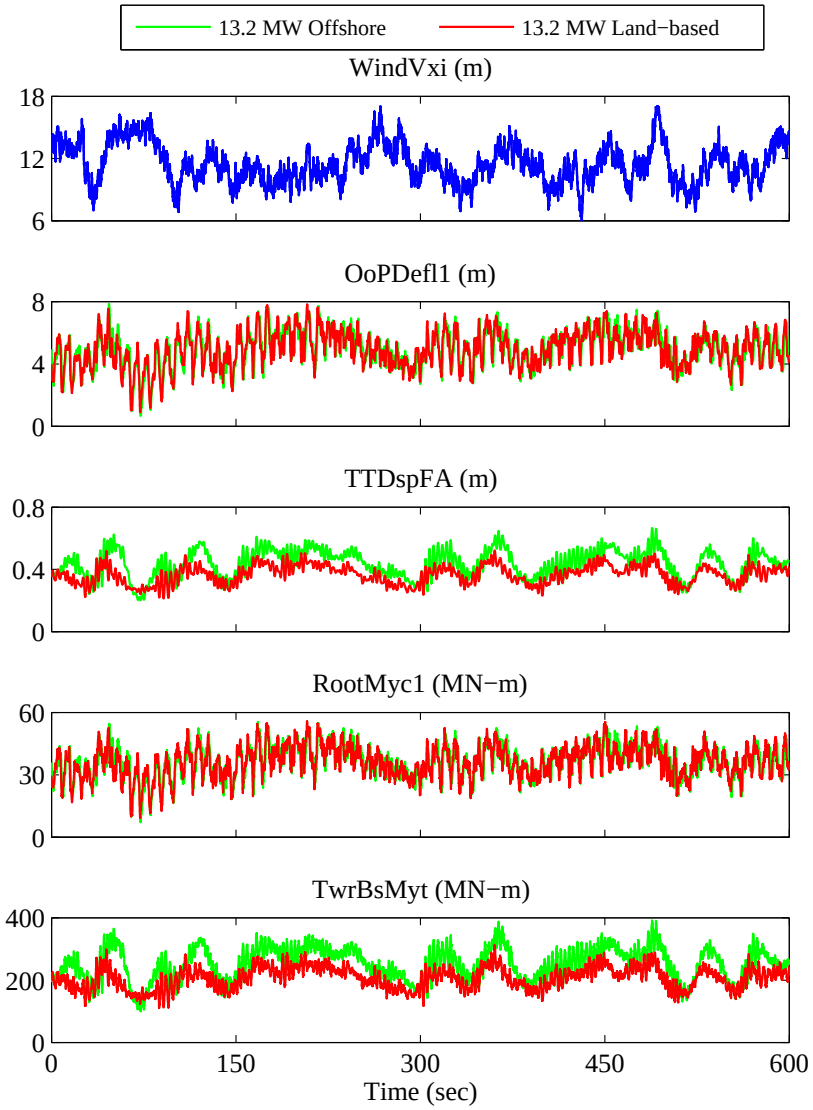


Figure 4.1: Representative 10-minute segments of simulated time series of the hub-height wind speed, blade tip out-of-plane deflection, tower-top fore-aft deflection, blade root out-of-plane bending moment, and tower base fore-aft bending moment ($V$=12 m/s).

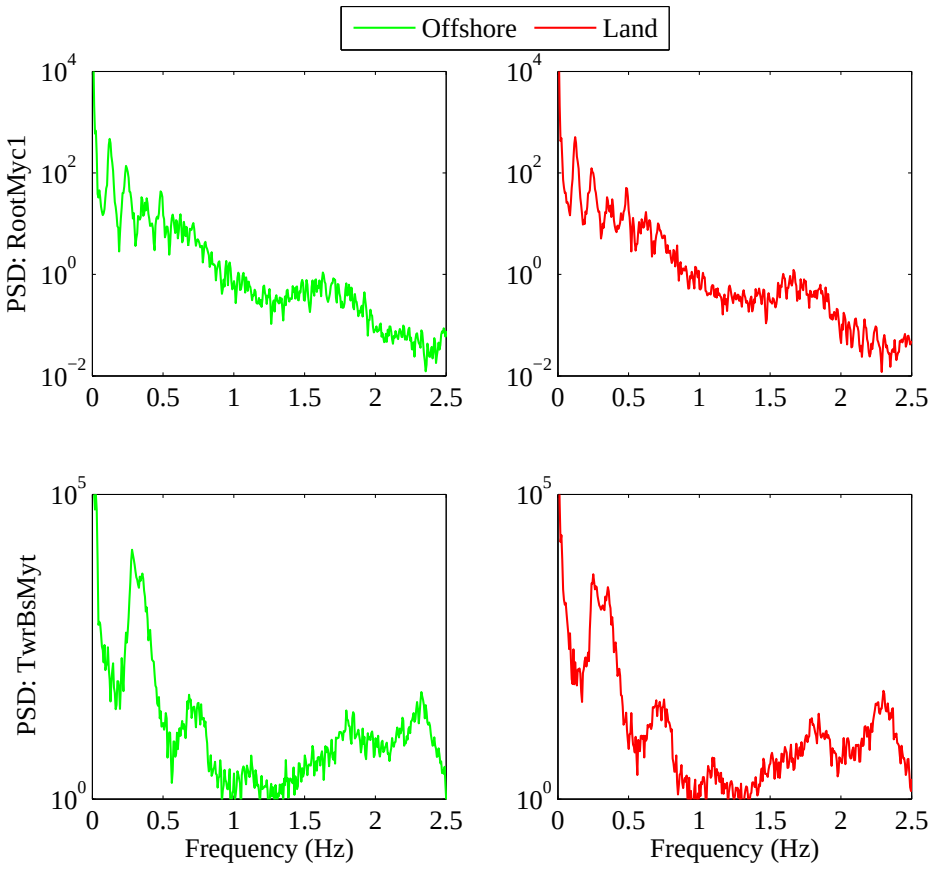


Figure 4.2: Power spectral density functions for the blade root out-of-plane bending moment and the tower base fore-aft bending moment for the 13.2 MW offshore and land-based wind turbines ($V$=12 m/s).

Table 4.1: Comparison of the 13.2 MW offshore and land-based turbines ($V$=12 m/s).

| Response | Mean | | Std. Dev. | | Maximum | |
|---|---|---|---|---|---|---|
| | Offshore | Land | Offshore | Land | Offshore | Land |
| OoPDefl1 (m) | 4.72 | 4.68 | 1.18 | 1.18 | 8.49 | 8.52 |
| TTDspFA (m) | 0.42 | 0.35 | 0.09 | 0.06 | 0.70 | 0.56 |
| RootMyc1 (MN-m) | 35.15 | 34.78 | 7.62 | 7.54 | 61.06 | 61.02 |
| TwrBsMyt (MN-m) | 242.66 | 198.53 | 52.58 | 36.79 | 412.05 | 325.39 |

plane bending moment, and the tower base fore-aft bending moment for the 13.2 MW offshore turbine and the 13.2 MW land-based turbine, based on fifteen simulations. The mean and maximum blade tip out-of-plane deflection increases slightly in the offshore case. The mean blade root bending moment increases slightly, while the maxima are comparable. The tower top fore-aft displacement increases significantly in the offshore environment; the mean increases by 11% and the maximum increases by 28%. The tower base fore-aft bending moment also increases significantly; the mean increases by 22% and the maximum by 29%. For the blade responses and the tower top displacement, standard deviation values are similar for the offshore and land cases. For the tower base bending moment, the standard deviation increases suggesting larger variation in the tower bending moment in the offshore environment.

It is evident that moving from a land-based site to the offshore environment has a greater effect on the tower response than on the blades. This is an important finding with regard to refining the design the tower of

the wind turbine for its planned use offshore.

### 4.1.2 Influence of the Turbine Control System

In a wind turbine, power production is managed by two control systems: a generator-torque controller and a blade-pitch controller [13]. The generator-torque controller maximizes the power below the rated operation point, while the blade-pitch controller regulates the generator speed above the rated operation point and feathers the blade to control the structural loads on wind turbine. When these controllers are turned off, the wind turbine experiences higher loads and the power output is not regulated. The rated wind speed for the 13.2 MW wind turbine is 11.3 m/s, after which the blades start to pitch.

To understand the importance of the control systems in wind turbines, the 13.2 MW offshore wind turbine is analyzed with both the controllers turned off, and then various response variables are studied. Figures 4.3 and 4.4 show simulated response time series for the 13.2 MW offshore wind turbine compared with the same turbine with the controller turned off. Both systems are subjected to same incident wind field and sea surface elevation. It is evident that the turbine with the controller turned experiences much higher response levels than the one with control actions allowed to take place. The general behavior is, however, quite similar, except over periods where blade pitch control is clearly needed.

Figure 4.5 and 4.6 show power spectral density function plots for the

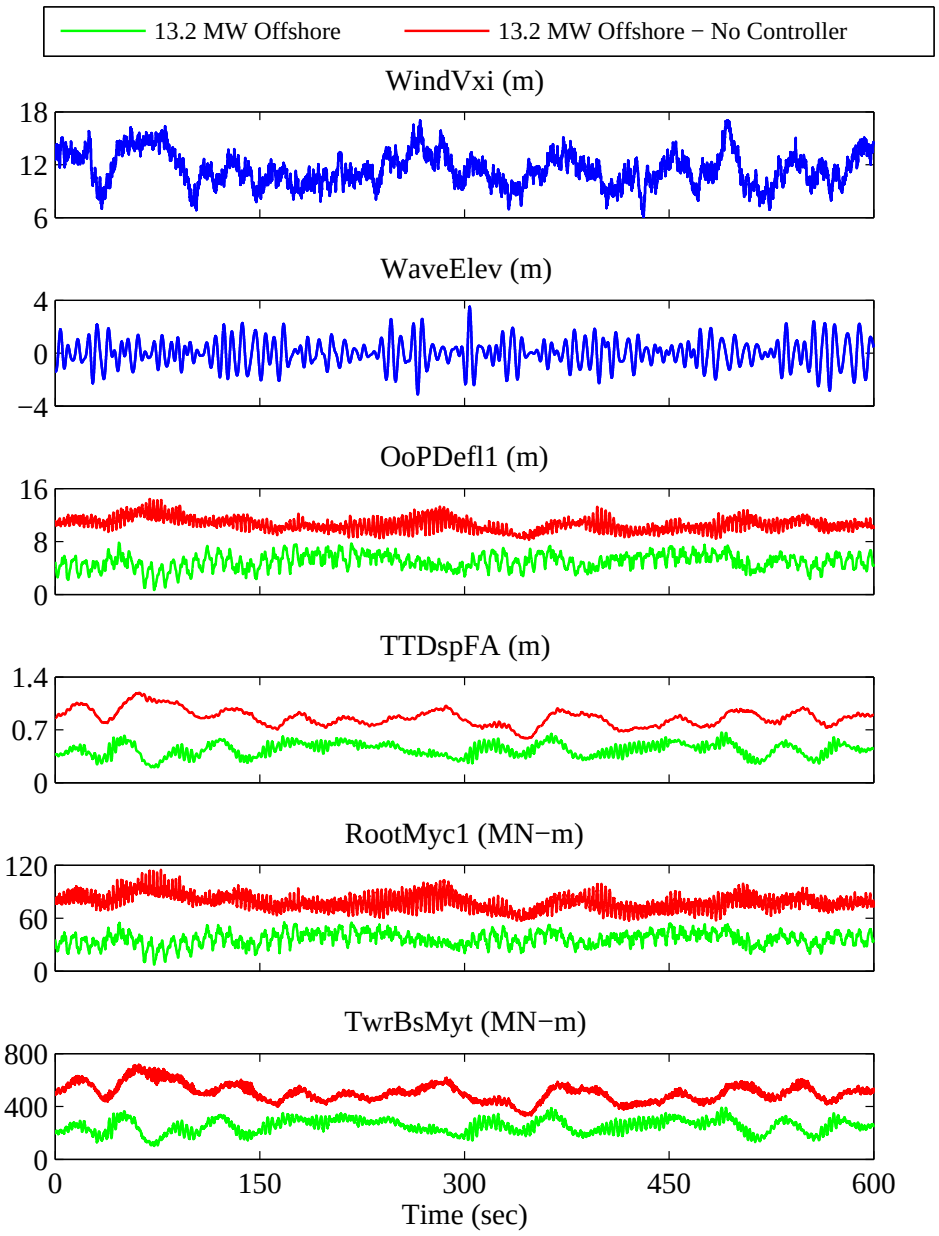


Figure 4.3: Representative 10-minute segments of simulated time series of the hub-height wind speed, sea surface elevation, blade tip out-of-plane deflection, tower-top fore-aft deflection, blade root out-of-plane bending moment, and tower base fore-aft bending moment ($V$=12 m/s, $H_S$=4 m, $T_P$=8.5 sec).

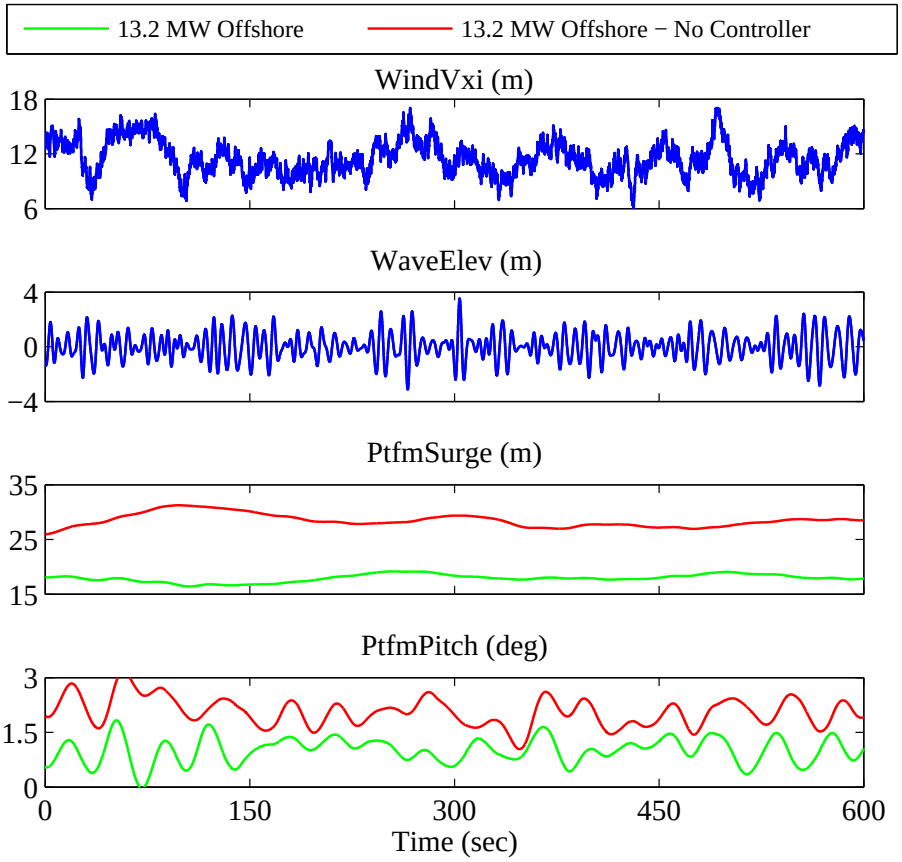


Figure 4.4: Representative 10-minute segments of simulated time series of the hub-height wind speed, sea surface elevation, platform surge, and platform pitch ($V$=12 m/s, $H_S$=4 m, $T_P$=8.5 sec).

13.2 MW wind turbine with controller turned on and off. It can be observed that, due to the blade pitching action when the controller is on, the power spectra show different peaks since the blade assumes a different profile each time the blade pitches. The energy content, however, is quite similar in the two cases. Tower response power spectra are changed slightly in the two cases. The platform motion spectra show very slight changes in the two cases—with and without control.

Table 4.2 shows mean and maximum values of the blade tip out-of-plane deflection, the tower top fore-aft displacement, the blade root out-of-plane bending moment, the tower base fore-aft bending moment, the platform surge, and the platform pitch, for the 13.2 MW offshore wind turbine with controller turned on and off, based on fifteen one-hour simulations. Ensemble statistics for all the response variables show significant increase when the controller is turned off. The blade tip out-of-plane deflection and the tower-top fore-aft displacement have a two-fold increase, the blade and tower bending moments have about a three-fold increase, and the platform surge and pitch motions are almost doubled. The standard deviation values for all the responses variables increase with the controller turned off suggesting greater variation in the response processes.

In summary, it is evident that the control system in this offshore wind turbine is very important to alleviate structural loads on the turbine and motions of the platform as well as to manage the output power generated.

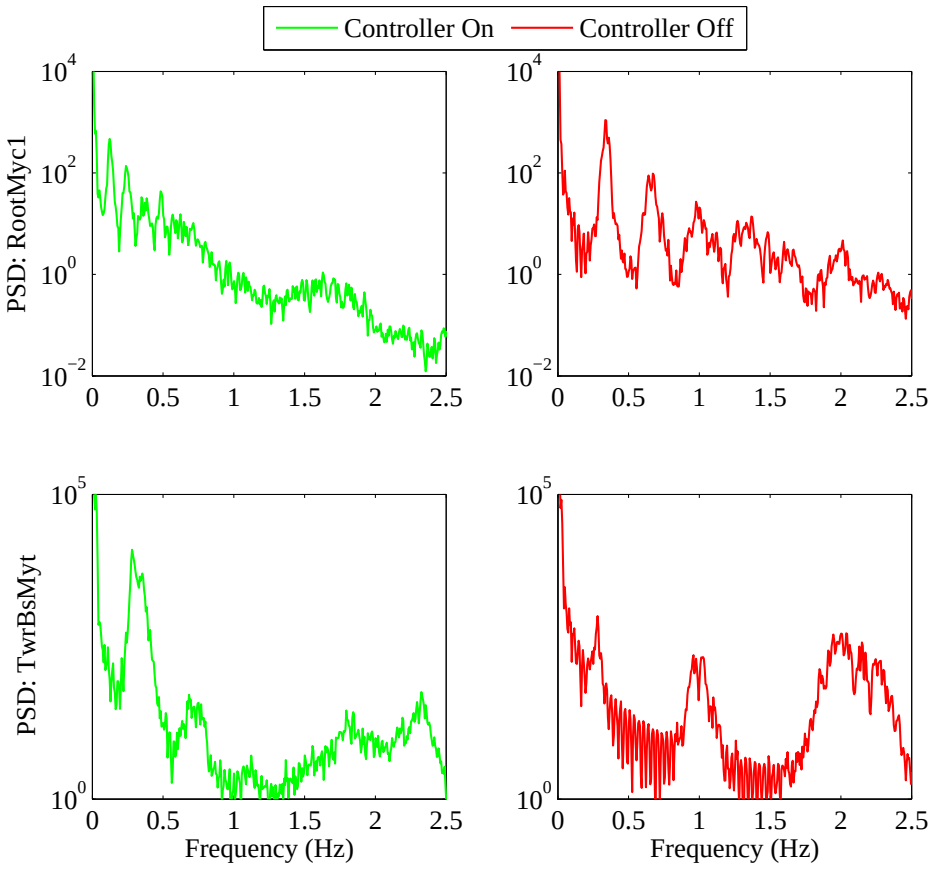


Figure 4.5: Power spectral density functions for the blade root out-of-plane bending moment and the tower base fore-aft bending moment for the 13.2 MW wind turbine with and without controller ($V$=12 m/s, $H_S$=4 m, $T_P$=8.5 sec).

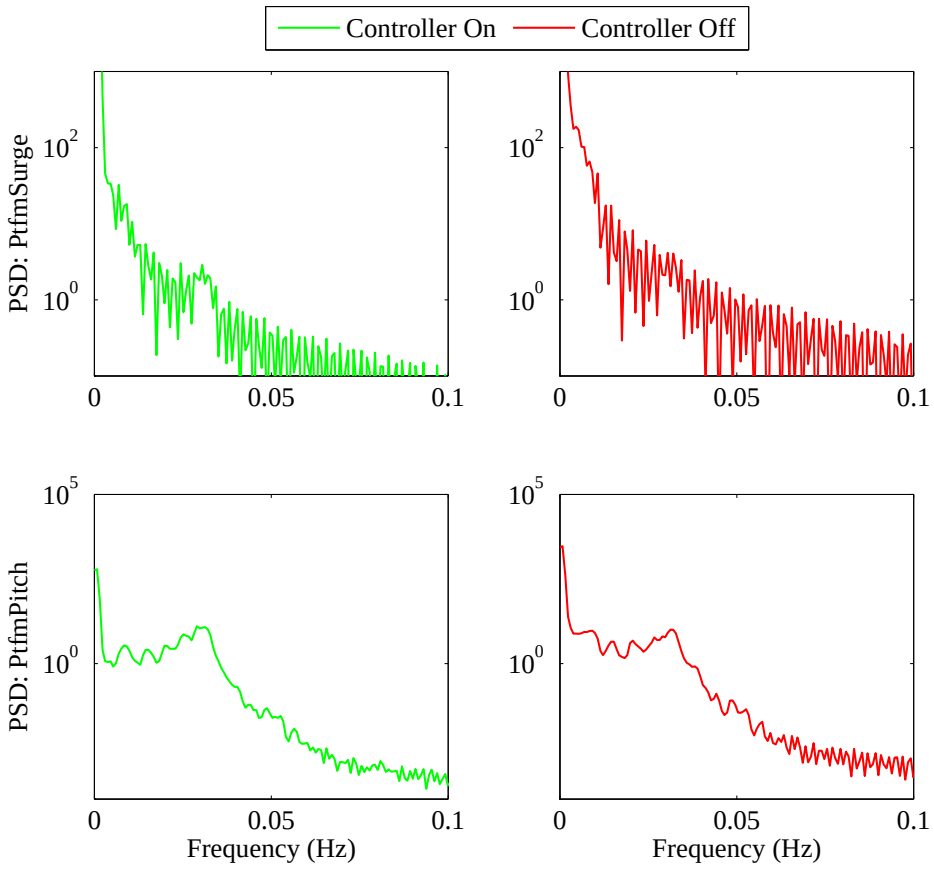


Figure 4.6: Power Spectral Density functions for platform surge and pitch motions for the 13.2 MW wind turbine with and without controller ($V$=12 m/s, $H_S$=4 m, $T_P$=8.5 sec).

Table 4.2: Comparison of 13.2 MW turbine variables with and without controller ($V$=12 m/s, $H_S$=4 m, $T_P$=8.5 sec).

| Parameter | Mean | | Std. Dev. | | Maximum | |
|---|---|---|---|---|---|---|
| | On | Off | On | Off | On | Off |
| OoPDefl1 (m) | 4.72 | 10.83 | 1.18 | 1.20 | 8.49 | 15.77 |
| TTDspFA (m) | 0.42 | 0.90 | 0.09 | 0.15 | 0.70 | 1.38 |
| RootMyc1 (MN-m) | 35.15 | 81.05 | 7.62 | 11.13 | 61.06 | 130.96 |
| TwrBsMyt (MN-m) | 242.66 | 527.37 | 52.58 | 87.03 | 412.05 | 843.67 |
| PtfmSurge (m) | 17.43 | 29.37 | 0.89 | 1.94 | 19.36 | 34.33 |
| PtfmPitch (deg) | 0.98 | 2.15 | 0.33 | 0.46 | 1.89 | 3.75 |

## 4.2 Comparison Studies with Non-Turbulent Steady Wind Fields

To assess the performance of the 13.2 MW turbine in a severe sea state and to understand the influence of model scale, we perform simulations based on steady incident wind (with shear but no turbulence) with the same hub-height wind speed for all the cases, and with waves simulated based on JONSWAP spectra [38].

### 4.2.1 Response in a Severe Sea State

It can be observed from Section 3.4.2 that the turbine and platform responses show little variation with wave height. This is because the reference site chosen here (Section 3.2) experiences very low wave heights. There are many sites around the world with comparable water depths that experience much higher waves. Understanding the response of the platform and turbine

at such sites where the system might experience high waves is also important. To assess the system performance at such sites, we assume a steady wind speed of 12 m/s with irregular waves with a significant wave height of 12 m and wave period of 16 sec, which represents a more severe sea state which we will refer to as the "High Wave" sea state. The response at this site will be compared with that at a "Low Wave" sea state for which conditions are similar to those at our selected site.

Figures 4.7 and 4.8 show the turbine and platform response of the 13.2 MW offshore wind turbine for the "Low Wave" sea state ($H_S$=4 m, $T_P$=8.5 sec) and the "High Wave" sea state ($H_S$=12 m, $T_P$=16 sec) with a steady hub-height wind speed of $V$=12 m/s. Since the significant wave height increases from 4 m to 12 m and the associated peak spectral wave period increases from 8.5 sec to 16 sec, the sea surface elevation time series (WaveElev) shows an increase in the amplitude of the waves as well as in the separation of the peaks. The blade tip out-of-plane deflection (OoPDefl1) shows little variation with wave elevation because it mostly depends on the incident wind speed. With a steady wind of 12 m/s, the blade tip deflection is largely due to the wind, and the increasing wave height only increases it by a small amount. The blade root out-of-plane bending moment (RootMyc1) also shows similar behavior to that of the blade tip deflection, with small effects due to changes in the wave height. The tower responses—tower-top fore-aft displacement (TTDspFA) and tower-base fore-aft bending moment (TwrBsMyt)—follow the same behavior as the sea surface elevation

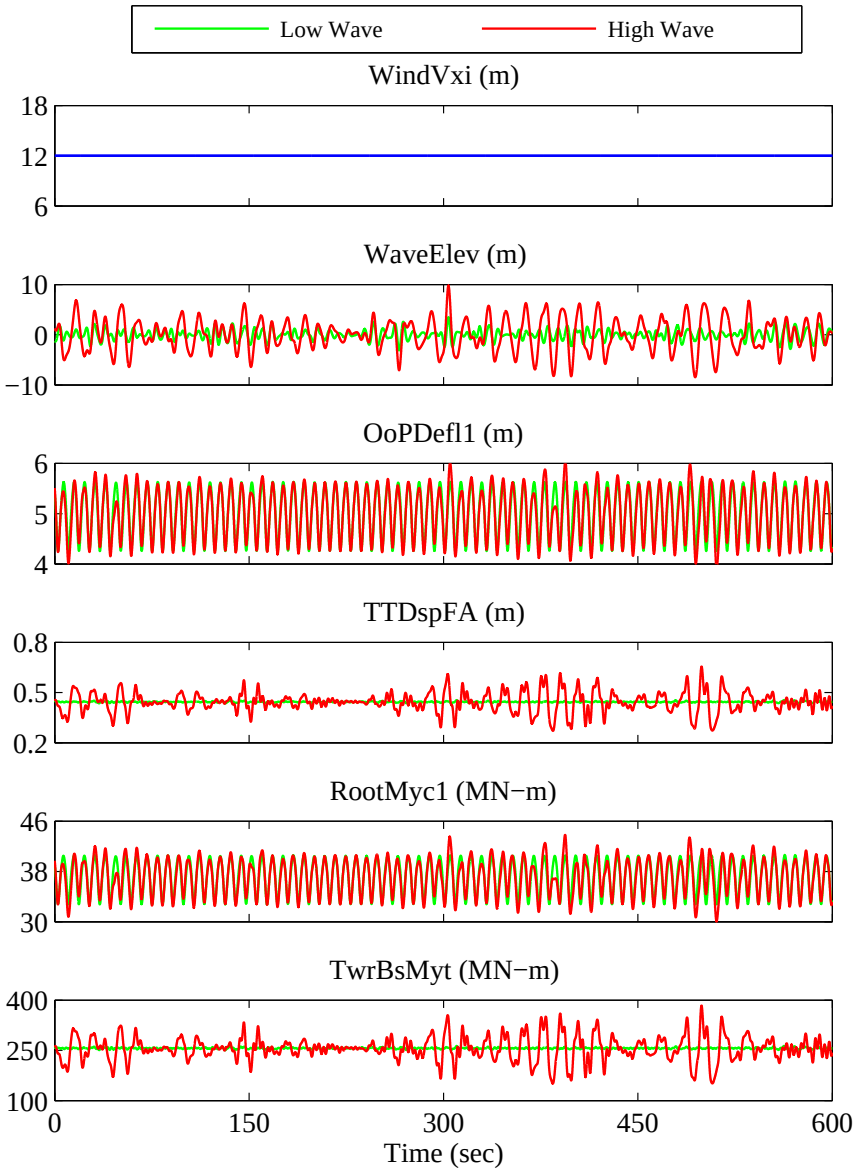


Figure 4.7: Representative 10-minute segments of simulated time series of the hub-height wind speed, sea surface elevation, blade tip out-of-plane deflection, tower-top fore-aft deflection, blade root out-of-plane bending moment, and tower base fore-aft bending moment for a "Low Wave" sea state ($H_S$=4 m, $T_P$=8.5 sec) and a "High Wave" sea state ($H_S$=12 m, $T_P$=16 sec) assuming a hub-height steady wind speed of $V$=12 m/s.

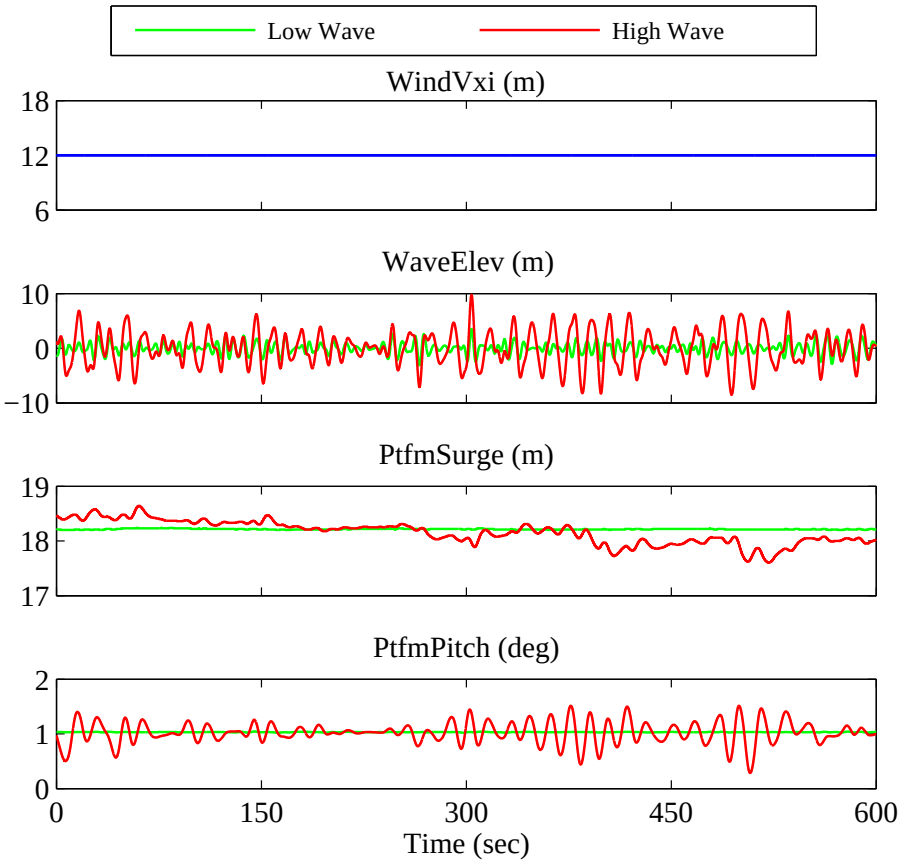


Figure 4.8: Representative 10-minute segments of simulated time series of the hub-height wind speed, sea surface elevation, platform surge, and platform pitch for a "Low Wave" sea state ($H_S$=4 m, $T_P$=8.5 sec) and a "High Wave" sea state ($H_S$=12 m, $T_P$=16 sec) assuming a hub-height steady wind speed of $V$=12 m/s.

(WaveElev). The response with the lower waves shows very little variation compared to that with the higher waves. Since the significant wave height and peak spectral wave period are almost doubled in the "High Wave" sea state, the tower response shows a significant increase. The mean for the low and high waves is almost same since the mean sea surface elevation is still zero. Maximum and standard deviation values of the tower response variables show the effect of an increase in wave heights. The platform response variables—platform surge (PtfmSurge) and platform pitch (PtfmPitch)—show similar behavior as the tower response. The platform pitch response closely follows the sea surface elevation, with the mean still the same for low and high waves while the maximum increases significantly. The platform surge shows small variations with wave height; this is mainly due to the coupling effects of the surge and pitch degrees of freedom.

Power spectral density function plots of the blade and tower bending moments and platform motions are presented in Figures 4.9 and 4.10 for the 13.2 MW wind turbine with incident low and high waves. The blade root bending moment power spectra are quite similar for both the cases because the incident wind field is the same. In the tower base bending moment and platform pitch spectra, the wave energy peak is quite evident. This is due to the fact that both the tower and platform response are strongly influenced by the waves. Platform surge, however, shows no large wave energy contribution. The tower response power spectra show peaks at 3P (3-per-rev frequency) for both the cases with low and high waves.

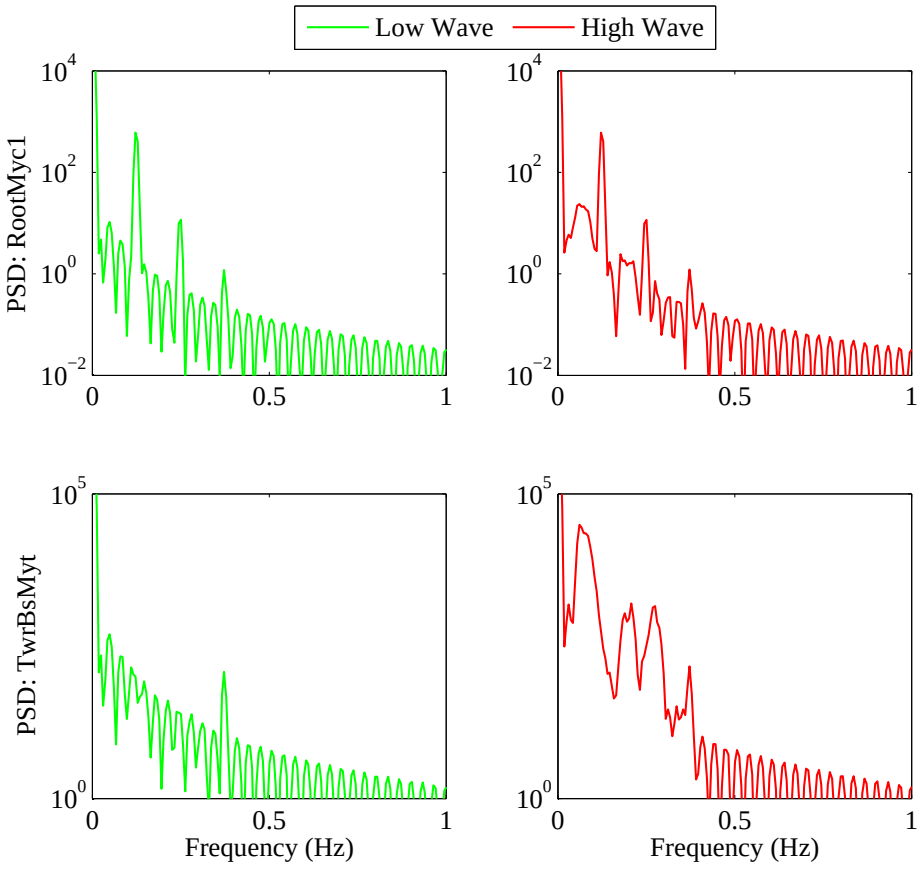


Figure 4.9: Power spectral density functions for the blade root out-of-plane bending moment and the tower base fore-aft bending moment for the 13.2 MW wind turbine in a "Low Wave" sea state ($H_S$=4 m, $T_P$=8.5 sec) and a "High Wave" sea state ($H_S$=12 m, $T_P$=16 sec) assuming a hub-height steady wind speed of $V$=12 m/s.

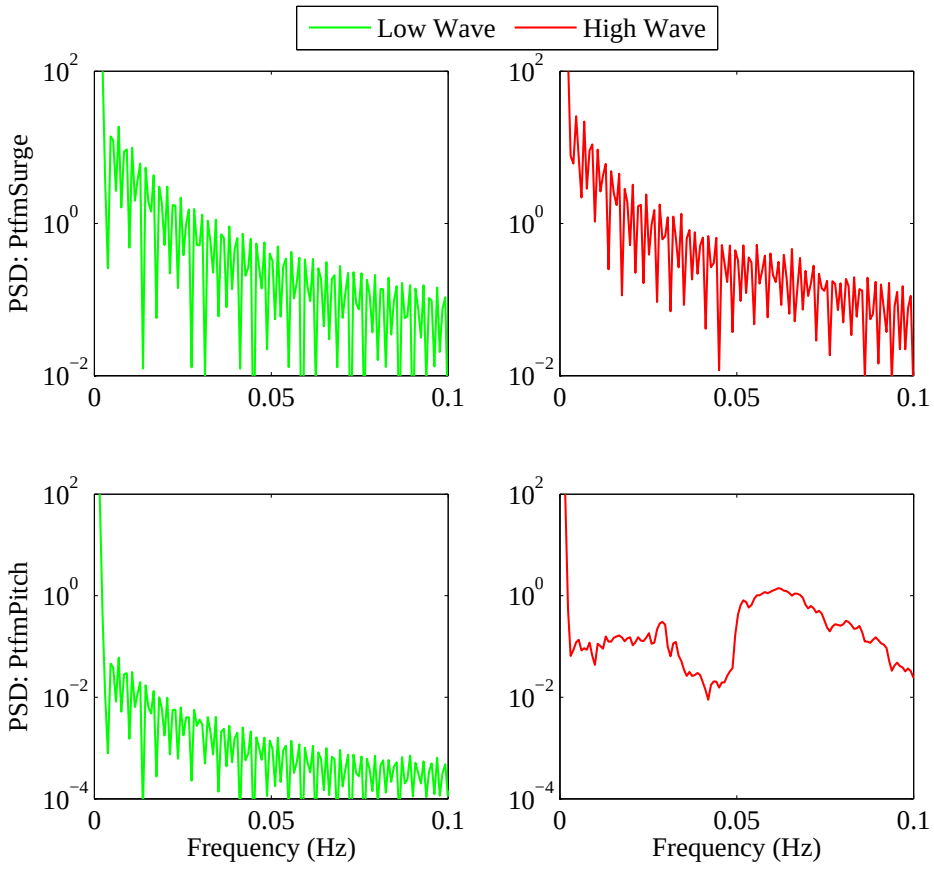


Figure 4.10: Power spectral density functions for platform surge and pitch motions for the 13.2 MW wind turbine in a "Low Wave" sea state ($H_S$=4 m, $T_P$=8.5 sec) and a "High Wave" sea state ($H_S$=12 m, $T_P$=16 sec) assuming a hub-height steady wind speed of $V$=12 m/s.

It is evident that siting an offshore wind turbine at a site where it might experience high waves will increase loads and deflections of the turbine and platform. This becomes important when the design of an integrated turbine-platform-mooring system is to be established for specific water depths, such that it can withstand various combinations of winds and waves that it might experience at different offshore locations.

### 4.2.2 Influence of Scaling

The 13.2 MW wind turbine's platform and other components were scaled up from the NREL 5 MW wind turbine; new 100-m blades were developed also following some scaling studies. The offshore platform developed in this study for SNL 13.2 MW wind turbine is scaled up from OC4 5 MW offshore semi-submersible platform [8]. The scale factor used was 1.8. To understand the effect of scaling, a comparison between the response of the 13.2 MW wind turbine and the OC4 5 MW wind turbine is presented in this section. For both the cases, a steady hub-height longitudinal wind speed of 12 m/s is employed. The hub-height of the 5 MW wind turbine is 90 m, while that of the 13.2 MW wind turbine is 146 m. This means that the incident wind fields (with shear but no turbulence) are not exactly the same for the cases but they are quite similar. The 126-meter rotor diameter for the 5 MW wind turbine is much less than the 205-meter rotor diameter of the 13.2 MW wind turbine. Due to these differences, for the same steady hub-height wind speed, the larger turbine experiences much greater

aerodynamic forces. Figures 4.11 and 4.12 show simulated response time series for the 13.2 MW offshore wind turbine compared with the OC4 5 MW offshore wind turbine for a high sea state where $V$=12 m/s, $H_S$=12 m, $T_P$=16 sec as was selected in the previous section.

From Figure 4.11, it can be seen that for the same incident sea surface elevation time series, the blade tip deflection (OoPDefl1) shows a slight increase for the 13.2 MW turbine. Since the 100-m blades of the 13.2 MW wind turbine are much larger than the 61.5 m bladed of the 5 MW turbine, these 100-m blades are more flexible and experience comparatively larger deflections. The blade root out-of-plane bending moment (RootMyc1) shows similar behavior to the blade tip deflection, with the time-varying characteristics of the response of the 13.2 MW turbine being similar in general to 5 MW turbine, but with a mean value significantly larger due to higher aerodynamic forces on the 13.2 MW turbine. The tower responses—tower-top fore-aft displacement (TTDspFA) and tower-base fore-aft bending moment (TwrBsMyt)—follow the sea surface elevation response quite well. Again, the 13.2 MW wind turbine shows higher tower response, a result of the large rotor area.

Figure 4.12 shows that the mean platform surge for the 13.2 MW turbine of 18 meters is much higher than that of the 5 MW wind turbine (7 meters). This is due to the larger aerodynamic forces on the larger turbine, which in turn, puts greater demands on the system than is the case with the smaller turbine. As a result, a higher surge offset results. The platform

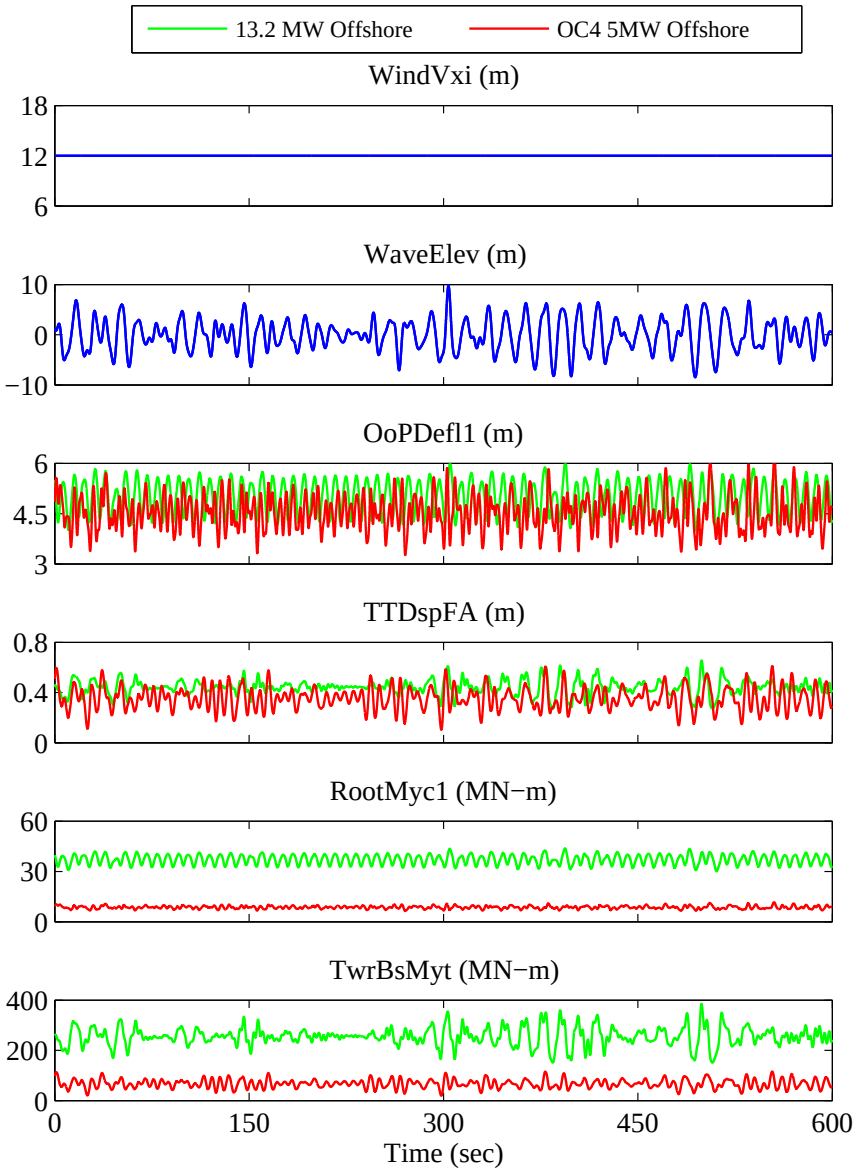


Figure 4.11: Representative 10-minute segments of simulated time series of the hub-height wind speed, sea surface elevation, blade tip out-of-plane deflection, tower-top fore-aft deflection, blade root out-of-plane bending moment, and tower base fore-aft bending moment for the Sandia 13.2 MW and OC4 5 MW turbine systems (for a sea state with $H_S$=12 m, $T_P$=16 sec and assuming a hub-height steady wind speed of $V$=12 m/s).

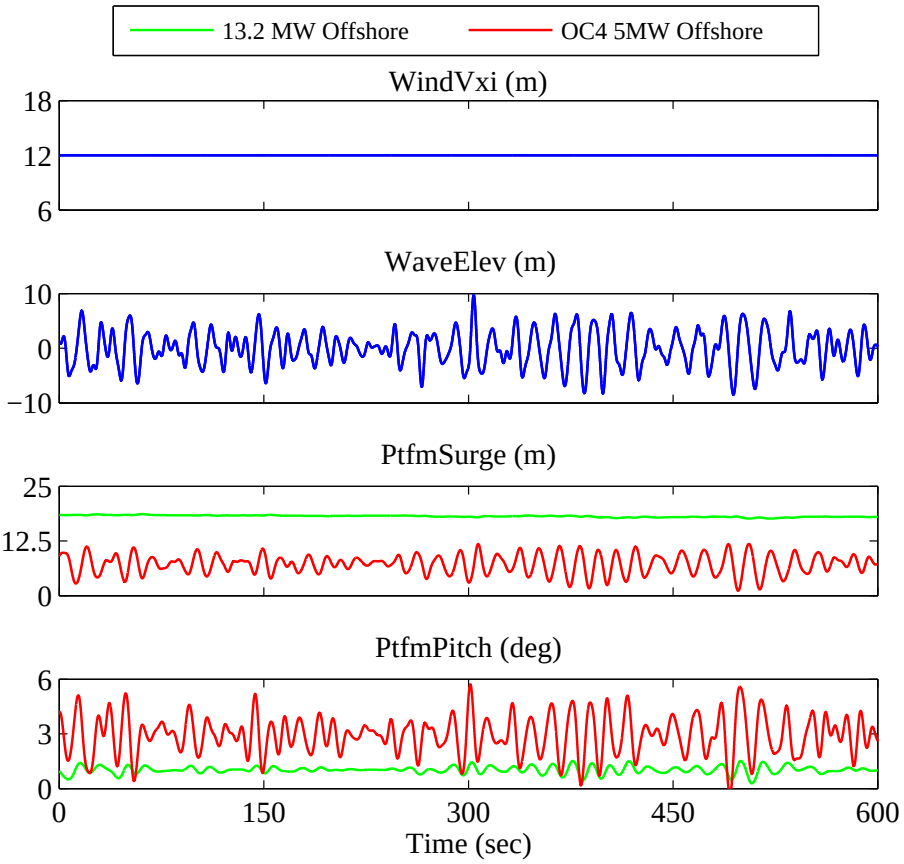


Figure 4.12: Representative 10-minute segments of simulated time series of the hub-height wind speed, sea surface elevation, platform surge, and platform pitch for the Sandia 13.2 MW and OC4 5 MW turbine systems (for a sea state with $H_S$=12 m, $T_P$=16 sec and assuming a hub-height steady wind speed of $V$=12 m/s).

pitch, however, behaves in a different manner; the pitch motions are larger for the 5 MW turbine than for the 13.2 MW turbine. Due to scaling of the platform by a factor of 1.8, the base columns of the platform, which act as heave plates, offer much higher resistance to platform pitch motion. This results in lower pitch response for the larger platform. Platform surge and pitch motions for the 13.2 MW turbine show smaller variation with the wave elevation time series compared to the 5 MW turbine due to the fact that, being significantly larger, the 13.2 MW turbine platform offers high resistance to motions in surge than the smaller platform. Both the turbines, however, closely follow the sea surface elevation process, suggesting that the platform motions are greatly affected by the sea surface elevation (waves).

In Figures 4.13 and 4.14, the power spectral density function plots of the blade, tower and platform responses are presented for the 13.2 MW and 5 MW offshore wind turbines. It can be observed that the 1P frequency and multiples of it are different for both the cases. The 13.2 MW wind turbine has a rated rotor rotation rate of 7.44 rpm, which corresponds to a 1P frequency of 0.124 Hz, while the 5 MW turbine has a rated rotor rotation rate of 12.1 rpm, which corresponds to a 1P frequency of 0.20 Hz. The 3P frequency peaks for both cases are seen in the tower base bending moment response. Also, due to the high waves, the energy from the waves at 0.0625 Hz can be seen in the response of the tower and platform.

Overall, it can be seen that the scaling up of a turbine and platform is an acceptable process for generating new models. However, care should be

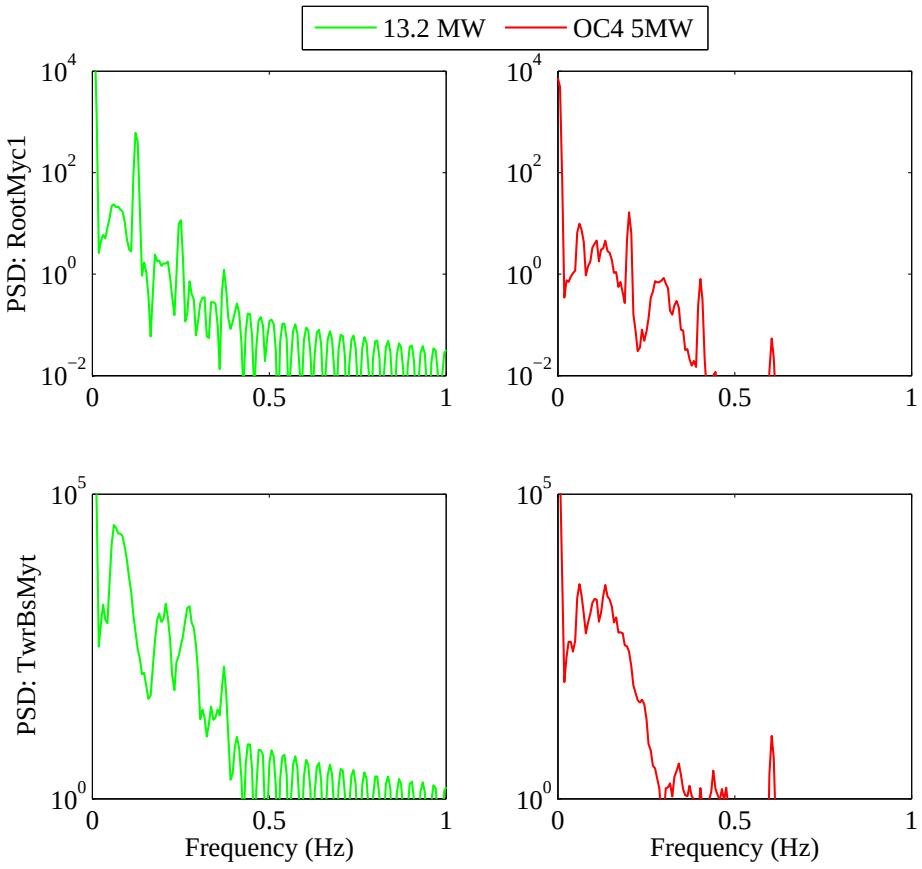


Figure 4.13: Power spectral density functions for the blade root out-of-plane bending moment and the tower base fore-aft bending moment for the Sandia 13.2 MW and OC4 5 MW turbine systems (for a sea state with $H_S$=12 m, $T_P$=16 sec and assuming a hub-height steady wind speed of $V$=12 m/s)

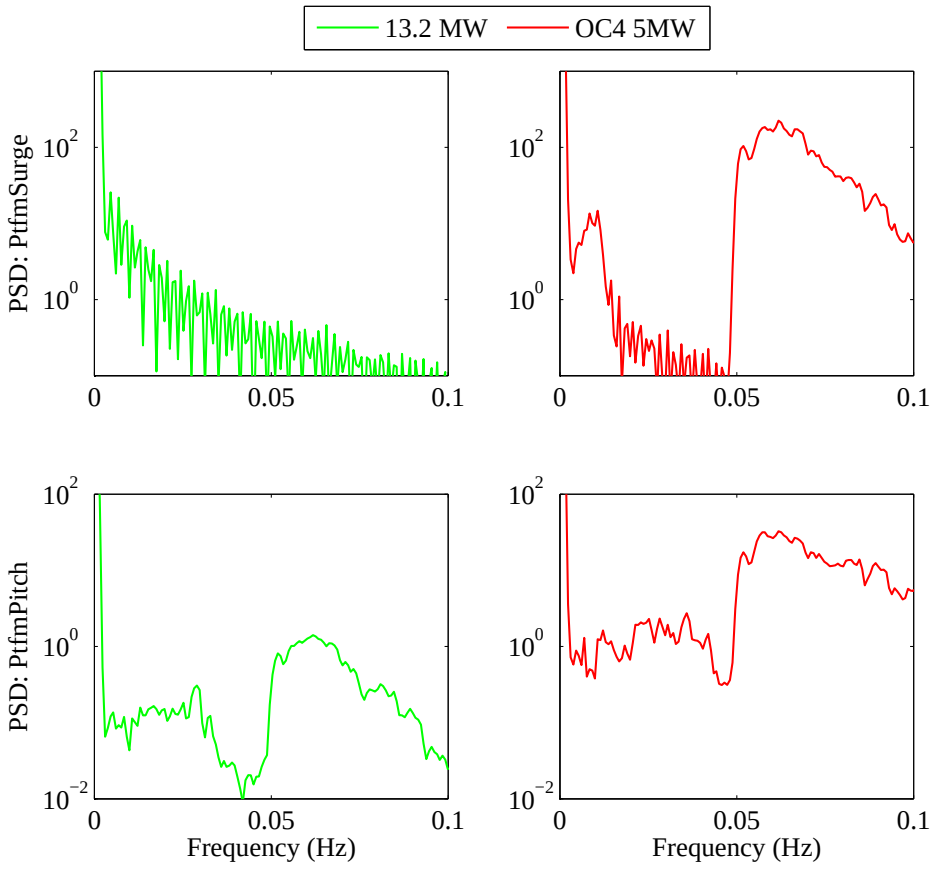


Figure 4.14: Power spectral density functions for platform surge and pitch motions for the Sandia 13.2 MW and OC4 5 MW turbine systems (for a sea state with $H_S$=12 m, $T_P$=16 sec and assuming a hub-height steady wind speed of $V$=12 m/s)

exercised in adopting a scaled-up model when dealing with details such as controller settings in order to optimize performance. Finally, components of the turbine and platform might need to be redesigned to account for increased loads and deflections after preliminary up-scaling from existing smaller models as was done in this study.

# Chapter 5

# Conclusions

## 5.1 Summary of Research Objectives

In recent times, there is a growing interest in establishing offshore wind turbines for effective and low-cost power generation. Offshore sites provide favorable conditions for wind power generation—offshore winds are stronger and less turbulent. Most of the offshore wind turbines in operation, to date, have been confined to shallow waters. For deepwater sites that are beginning to be considered, floating platforms need to be developed to support the wind turbines. Wind turbines with large rotors have the capacity to generate significant output power economically; therefore, the combination of very large wind turbines supported on floating platforms at deepwater sites appears promising for energy generation.

The floating platform studied here is a moored semi-submersible platform, designed to support a large 13.2 MW wind turbine. Models for the 13.2 MW wind turbine as well as for the semi-submersible platform have been developed in recent studies. Environmental data from a selected reference site (where the water depth is 200 meters) were used in the simulations discussed in this study. These simulations were performed to

understand the dynamic behavior of the integrated turbine-platform-mooring system. Statistics of various response variables were studied; important combinations of wind and waves were identified. Also, comparison studies considering performance in the offshore environment versus at a land site, the effect of scaling, and the influence of the control system were understood. As well, different mild and severe sea states were considered to assess performance under different environmental conditions.

## 5.2 Conclusions

A model for the SNL 13.2 MW wind turbine and the supporting semi-submersible platform was developed and analyzed for particular sea states at a reference site. From the study, we draw the following conclusions:

- For the various blade versions developed by Sandia National Laboratories for the 100-meter blades, the lightest SNL100-02 blade is the most suitable and leads to reduced loads on the system.

- Scaling a platform model is an effective way of utilizing a pre-established model to generate models for larger turbines.

- For developing a wind turbine-platform system model and analyzing it, various tools are needed from ones for modeling the platform, blades, and tower to simulation tools for aerodynamic and hydrodynamic calculations. Additional simulation tools such as TurbSim and FAST

provided by NREL are effective in overall assessment of the response of the integrated turbine system.

- In a coupled turbine-platform response analysis, blade deflections and loads are influenced greatly by the incident wind process; tower loads and platform motions are influenced by the sea surface elevation process (waves). Platform motions have very long resonance periods, while blade and tower response variables have comparatively high-frequency resonance modes.

- Due to the non-zero mean wind speed on the rotor, there is a significant mean platform surge offset of the semi-submersible platform supporting the 13.2 MW wind turbine.

- The wind speed is the most important environmental variable that influences loads on the turbine and tower; it also greatly influences platform motions. The integrated system response is highest around the rated wind speed.

- Wave loading on the system has relatively little effect on the turbine/rotor loads. Blade and tower structural loads tend to increase very slightly with increasing wave heights. Platform motions, however, show comparatively higher response, the increases though are still quite small with increasing wave heights.

- As we move from an onshore to an offshore environment, the tower

natural frequencies change due to additional flexibility at its base resulting from the supporting platform.

- Surge and pitch motions of the platform, due to its large size, show very slowly varying response in time compared to the blades and tower.

- If wave height is kept constant, while the wind speed is varied, the blade and tower loads show an increase when the wind speed is increased. Platform motions also increase significantly with increasing wind speed.

- If wind speed is kept constant, while the wave height is gradually increased, the response of the turbine blades and tower little change. Platform motions, however, show a small increase with increasing wave height.

- In comparison studies of the 13.2 MW turbine at a land site versus in an offshore environment, it is found that supporting floating platform offshore causes an increase in tower loads. Blade loads are only increased only very slightly.

- A control system in a wind turbine plays a very important role in reducing the structural loads. If the controller is turned off, when wind speeds are high, structural loads and platform motions increase considerably.

- At a site where the integrated turbine system experiences high waves, the response of the system increases significantly with increasing wave

heights.

- Scaling up a wind turbine system can cause significant increases in the system response; tower loads and platform motions are affected the most with the scaled-up semi-submersible platform from the smaller OC4 model.

## 5.3 Suggestions for Future Research

This research study was focused on developing a preliminary model for a large offshore wind turbine supported by a floating semi-submersible platform. Analysis was done for limited number of combinations of wind speeds and wave heights at one particular site. The conclusions in this study are based on various assumptions made throughout to simplify the modeling and analysis. In light of these assumptions, the model may not be adequately optimized for performance. These assumptions need to be examined closely to in further refinements of the model. Also, this study focuses on a single wind turbine model and floating platform combination; additional studies with alternative floating platform models to support the turbine are recommended.

By carrying out analysis with different combinations of wind and waves at various sites around the world, a range of estimates of loads and motions can be derived so that different extreme environmental conditions will have been tested. The models developed for the wind turbine and platform need to be studied carefully to reduce costs; this was outside the scope of the present

study.

Once an optimized model for such a turbine-platform-mooring system is available, a detailed assessment of design load cases for fatigue and ultimate limit states is recommended. Reliability studies of the integrated system are also recommended.

# Bibliography

[1] Renewable Energy and Alternate Use Program (U.S.). *Technology white paper on wind energy potential on the U.S. Outer Continental Shelf [electronic resource].* U.S. Dept. of the Interior, Minerals Management Service, Renewable Energy and Alternate Use Program, Washington, D.C., 2006.

[2] K John and D Zafirakis. The wind energy revolution: A short review of a long history. *Renewable Energy*, 36(7):1887 – 1901, 2011.

[3] European Wind Energy Association. Wind in power, 2013 European Statistics. Technical report, 2014.

[4] European Wind Energy Association. Statistics and Targets. Technical report.

[5] American Wind Energy Association. U.S. Wind Industry Fourth Quarter 2013 Market Report. Technical report, 2014.

[6] N Schwartz, D Heimiller, S Haymes, and W Musial. *Assessment of Offshore Wind Energy Resources for the United States.* Citeseer, 2010.

[7] U.S. Department of Energy. 20% Wind Energy by 2030: Increasing Wind Energy's Contribution to U.S. Electricity Supply. Technical report, 2008.

[8] A Robertson, J Jonkman, M Masciola, H Song, A Goupee, A Coulling, and C Luan. Definition of the semisubmersible floating system for Phase II of OC4. *IEA OC4 Report*, 2012.

[9] D Griffith, D Ashwill, and B Resor. Large offshore rotor development: Design and analysis of the Sandia 100-meter wind turbine blade. In *53rd AIAA Structures, Structural Dynamics, and Materials Conference, Honolulu, HI*, 2012.

[10] D Griffith and B Resor. Description of model data for SNL13.2-00-Land: A 13.2 MW land-based turbine model with SNL100-00 blades. *Sandia National Laboratories Technical Report, SAND2011-9310P*, 2011.

[11] D Griffith and D Ashwill. The Sandia 100-meter all-glass baseline wind turbine blade: SNL100-00. *SAND2011-3779, Sandia National Laboratories, Albuquerque, June*, 2011.

[12] W Sahasakkul. Model Development for an Offshore Wind Turbine Supported by a Moored Semi-Submersible Platform. Master's thesis, University of Texas at Austin, 2014.

[13] J Jonkman. *Dynamics Modeling and Loads Analysis of an Offshore Floating Wind Turbine*. PhD thesis, University of Colorado at Boulder, 2007.

[14] J Jonkman and L Buhl Jr. FAST user's guide. *National Renewable Energy Laboratory*, 2005.

[15] B Jonkman. *TurbSim user's guide: Version 1.50*. National Renewable Energy Laboratory Colorado, 2009.

[16] G Bir. Multiblade coordinate transformation and its application to wind turbine analysis. In *Proceedings of 2008 ASME Wind Energy Symposium, Reno, Nevada, USA, Jan. 7*, volume 10, page 2008, 2008.

[17] NWTC Design Codes (MBC by Gunjit Bir). http://wind.nrel.gov/designcodes/postprocessors/mbc/. Last modified 28-June-2012; accessed 28-June-2012.

[18] J Jonkman. Campbelldiagram (excel sheet). https://wind.nrel.gov/forum/wind/viewtopic.php?p=1679#p1679.

[19] P Agarwal. *Structural Reliability of Offshore Wind Turbines*. PhD thesis, University of Texas at Austin, 2008.

[20] D Griffith. The SNL100-01 Blade: Carbon Design Studies for the Sandia 100-meter Blade. *Sandia National Laboratories Technical Report, SAND2013-1178*, 1, 2013.

[21] D Griffith, B Resor, and D Ashwill. Challenges and opportunities in large offshore rotor development: Sandia 100-meter blade research. In *AWEA WINDPOWER 2012 Conference and Exhibition, Scientific Track Paper, Atlanta, GA, USA*, 2012.

[22] J Jonkman. Definition of the Floating System for Phase IV of OC3. *National Renewable Energy Laboratory*, 2010.

[23] A Coulling, A Goupee, A Robertson, J Jonkman, and H Dagher. Validation of a FAST semi-submersible floating wind turbine numerical model with DeepCwind test data. *Journal of Renewable and Sustainable Energy*, 5(2):023116, 2013.

[24] J Jonkman, A Robertson, and G Hayman. *HydroDyn Users Guide and Theory Manual*. National Renewable Energy Laboratory Colorado, 2014.

[25] A Sultania. Reliability analysis of a spar buoy-supported floating offshore wind turbine. Master's thesis, University of Texas at Austin, 2010.

[26] T Ishihara, P Phuc, H Sukegawa, K Shimada, and T Ohyama. A study on the dynamic response of a semi-submersible floating offshore wind turbine system Part 1: A water tank test. In *Proceedings of the 12th International Conference*, pages 2511–2518, 2007.

[27] P Phuc and T Ishihara. A study on the dynamic response of a semi-submersible floating offshore wind turbine system Part 2: numerical simulation. *ICWE12. Cairns, Australia*, pages 959–966, 2007.

[28] C Lee. *WAMIT theory manual*. Massachusetts Institute of Technology, Department of Ocean Engineering, 1995.

[29] NWTC Computer-Aided Engineering Tools (FAST by Jason Jonkman, Ph.D.). http://wind.nrel.gov/designcodes/simulators/fast/. Last modified 2-July-2014; accessed 28-July-2014.

[30] NWTC Computer-Aided Engineering Tools (TurbSim by Neil Kelley, Bonnie Jonkman). http://wind.nrel.gov/designcodes/preprocessors/turbsim/. Last modified 30-May-2013; accessed 28-July-2014.

[31] International Electrotechnical Commission. IEC 61400-1. *Wind Turbines. Part 1: Design Requirements*, 2007.

[32] AeroHydro Inc. *MultiSurf for WAMIT 8.0 Manual*. 2011.

[33] NWTC Computer-Aided Engineering Tools (FAST v8 by Jason Jonkman, Ph.D. and Bonnie Jonkman). http://wind.nrel.gov/designcodes/simulators/FAST8/. Last modified 9-July-2014; accessed 28-July-2014.

[34] P Agarwal and L Manuel. Extreme Loads for an Offshore Wind Turbine using Statistical Extrapolation from Limited Field Data. *Wind Energy*, 2008.

[35] NWTC Computer-Aided Engineering Tools (MAP by Marco D. Masciola, Ph.D.). http://wind.nrel.gov/designcodes/simulators/map/. Last modified 17-July-2014; accessed 28-July-2014.

[36] International Electrotechnical Commission. IEC 61400-3. *Wind Turbines. Part 3: Design Requirements for Offshore Wind Turbines*, 2009.

[37] NDBC Station 46012 (LLNR 325) - Half Moon Bay - 24NM SSW of San Francisco, CA.

http://www.ndbc.noaa.gov/station_page.php?station=46012.
Owned and maintained by National Data Buoy Center.

[38] K Hasselmann, T Barnett, E Bouws, H Carlson, D Cartwright, K Enke, J Ewing, H Gienapp, D Hasselmann, P Kruseman, et al. Measurements of wind-wave growth and swell decay during the Joint North Sea Wave Project (JONSWAP). 1973.

# Vita

Mohit Soni was born in Bhopal, M.P., India on 08 June 1990, the son of Mr. Kishore Kumar Soni and Mrs. Madhubala Verma. He received the Bachelor of Technology degree in Civil Engineering from Indian Institute of Technology Roorkee in 2012. He entered the Master's program in the Department of Civil, Architectural and Environmental Engineering at the University of Texas at Austin in 2012.

Email address: mohitsoni@utexas.edu

This thesis was typeset with LaTeX[†] by the author.

[†]LaTeX is a document preparation system developed by Leslie Lamport as a special version of Donald Knuth's TeX Program.